The Effects of Shear Deformation in Rectangular and Wide Flange Sections

By:

Hariharan Iyer

Thesis submitted to the Faculty of the Virginia Polytechnic Institute and State University

in partial fulfillment of the requirements for the degree of

MASTER OF SCIENCE

In

CIVIL ENGINEERING

Approved:

_____

Dr. Finley A. Charney

Committee Chairman

_____ _____

Dr. Raymond H. Plaut

Committee Member

Dr. Carin L. Roberts-Wollmann

Committee Member

February 24, 2005

Blacksburg, Virginia

Keywords: Steel Moment Resisting Frames, Shear Deformations, Shear Area, Form Factor, Displacement Participation Factor, Rectangular Section, Wide Flange Section

The Effect of Shear Deformation in Rectangular and Wide Flange Sections

By:

Hariharan Iyer

Committee Chairman: Dr. Finley A. Charney

(ABSTRACT)

Shear deformations are, generally, not considered in structural analysis of beams and frames. But shear deformations in members with low clear span-to-member depth ratio will be higher than normally expected, thus adversely affecting the stiffness of these members. Inclusion of shear deformation in analysis requires the values of shear modulus (modulus of rigidity, *G*) and the shear area of the member. The shear area of the member is a cross-sectional property and is defined as the area of the section which is effective in resisting shear deformation. This value is always less than the gross area of the section and is also referred to as the form factor. The form factor is the ratio of the gross area of the section to its shear area. There are a number of expressions available in the literature for the form factors of rectangular and wide flange sections. However, preliminary analysis revealed a high variation in the values given by them. The variation was attributed to the different assumptions made, regarding the stress distribution and section behavior. This necessitated the use of three-dimensional finite element analysis of rectangular and wide flange sections to resolve the issue.

The purpose of finite element analysis was to determine which, if any, of the expressions in the literature provided correct answers. A new method of finite element

analysis based on the principle of virtual work is used for analyzing rectangular and wide flange sections. The validity of the new method was established by analyzing rectangular sections for which closed form solutions for form factor were available. The form factors of various wide flange sections in the AISC database were calculated from finite element analysis and an empirical relationship was formulated for easy calculation of the form factor. It was also found that an empirical formula provided good results for form factors of wide flange sections.

Beam-column joint sub-assemblies were modeled and analyzed to understand the contribution of various components to the total drift. This was not very successful since the values obtained from the finite element analysis did not match the values calculated using virtual work. This discrepancy points to inaccuracies in modeling and, possibly, analysis of beam-column joints. This issue needs to be resolved before proceeding further with the analysis.

Dedication

The completion of my graduate studies is a culmination of expectations of many people and marks the beginning of a new phase in my life. My success would not have been possible without my family, whose unflinching support and guidance throughout my life have enabled me to focus on my goals and achieve them. My parents have always strived to provide the best for their children to be knowledgeable and successful in their lives. I regret my inability to share this joy with my grandparents, who dearly wished to see me complete my graduate studies. Their blessings have always been a source of strength in pursuit of my endeavors. In recognition for their efforts, I dedicate this thesis to:

Shivkumar Iyer
(Father)

Gowri Iyer
(Mother)

Sindhuja Iyer
(Sister)

Saraswathi Iyer (Deceased)
(Paternal Grandmother)

B.S. Ramakrishnan (Deceased)
(Maternal Grandfather)

Saraswathi Ramakrishnan
(Maternal Grandmother)

Acknowledgements

My efforts at Virginia Tech have earned me a Master's degree in Civil Engineering. I take this opportunity to thank all the people who have helped through my studies and my stay in Blacksburg for the last twenty months.

I would like to thank Dr. Finley A. Charney for his support and guidance throughout my studies and research. His knowledge and understanding of the subject never cease to amaze me. I enjoyed my time working with him and hope to have gained some of that knowledge. I would also like thank Dr. Raymond H. Plaut and Dr. Carin L. Roberts-Wollmann for serving on my committee. Their help and guidance are highly appreciated.

I greatly appreciate the efforts of Paul W. Spears in helping me understand the research problem and taking time off his busy schedule to clarify my doubts. Without his efforts, I would have been hard pressed to complete my research in such a short time. Thanks are also due to my fellow graduate students Anantha, Hardik, Gordon, Rakesh and Yasser who helped me at various stages of my studies and research.

Lastly I would like to thank all my friends in Blacksburg for making my stay a very pleasant and memorable experience.

Table of Contents

List of Tables

List of Figures

Chapter 1 Introduction

1.1 Shear Deflection

Structural design is based on the forces developed in the members due to the applied loads. The member forces are developed primarily due to deformations in the structures caused by these loads. Thus it is very important to accurately determine the deformations for the design to be adequate. Flexural and axial deformations in structures can be determined to a high level of accuracy. Deformations in multi-story structures are affected by shear deformations in the members. However, shear deformations in structures are, typically, a very low percentage of the total deformation, allowing them to be neglected in most cases. A good amount of research has been done on modeling and predicting the value of shear deformations, but the issue is still far from being resolved. This is because the determination of shear deformation requires the calculation of a quantity referred to as 'Shear Area' of the member cross section. 'Shear Area' is generally understood to be the effective area of the section participating in the shear deformation and as such is a nebulous value ranging from the gross cross-sectional area to the area of the web for a wide flange section. For structures involving members having low clear span to member depth ratio, shear deformations could be responsible for as high as 20% of the total drift (Charney, 1990). This necessitates a better understanding of shear deformations. The traditional method of including the effects of shear deformation is also not accurate. Consider a cantilever beam of length L. The deflection of the tip, Δ, under a point load P including the shear deformation is given by the Equation 1.1.

$$\Delta = \frac{PL^3}{3EI} + \frac{PL}{GA_v} \quad \text{..... (1.1)}$$

where E is the modulus of elasticity, G is the shear modulus, I is the moment of inertia of the section about the bending axis and A_v is the shear area of the section. The first term in Equation 1.1 represents the flexural deformation and the shear deformation is denoted by the second term. It is clear that the flexural term will dominate the deflection for increasing values of member length if the other quantities are held constant. Figure 1.1 shows the contribution of flexural and shear deformations for a W24x335 section for different span to depth ratios. The shear area, A_v, was taken as the web thickness times the depth between the centers of the flanges for this exercise.

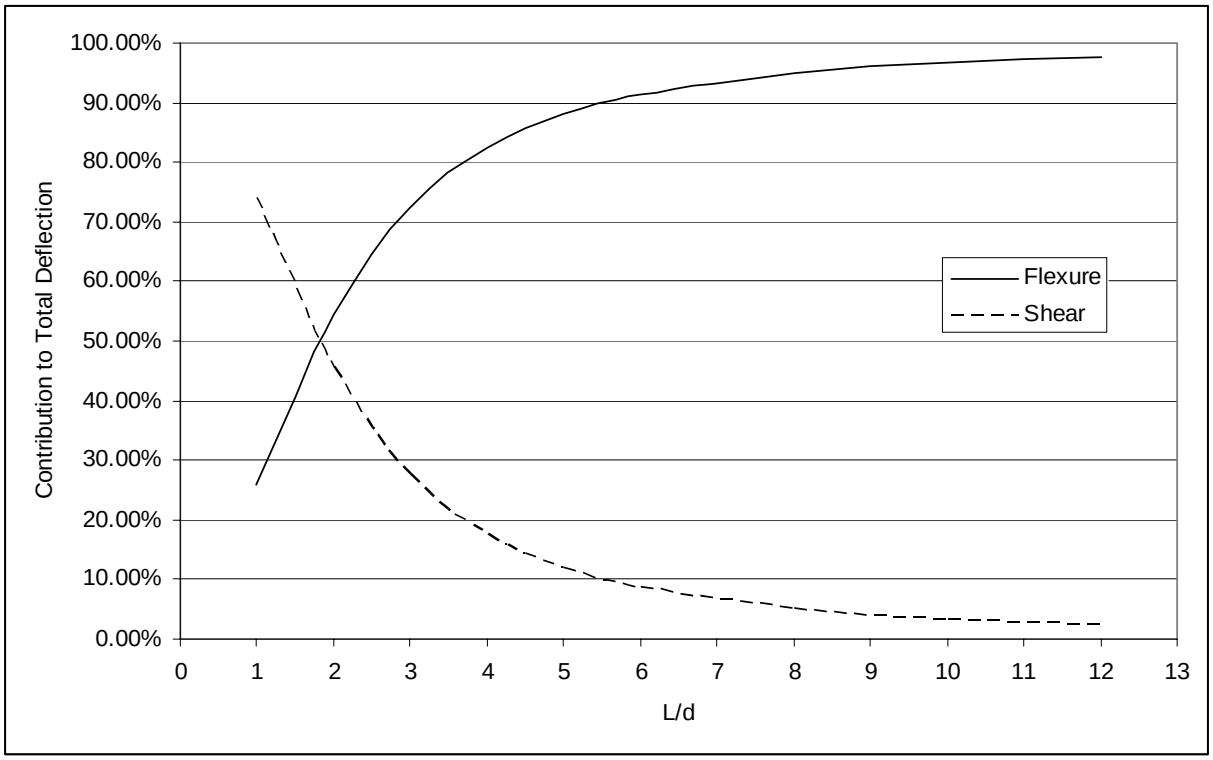

Figure 1.1– Flexure and shear contribution to the total deflection of a cantilevered W24x335

Equation 1.1 has two separate terms for flexural and shear deformation of the beam. This indicates that the flexural and shear deformations are uncoupled and can be calculated independent of each other. This will be shown to be true in Chapter 2 of this thesis.

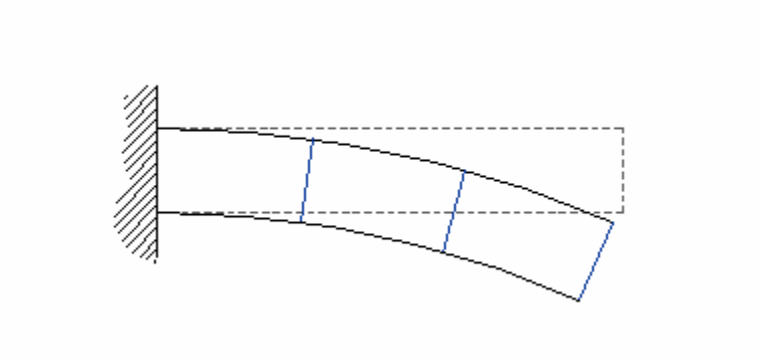

a) without cross sectional warping

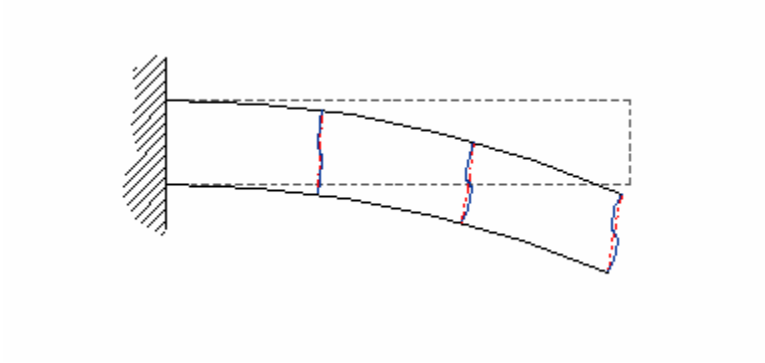

b) with cross sectional warping

Figure 1.2 – Deflection of beam under shear load at the tip of cantilever beam

Figure 1.2 demonstrates the differences between the assumed shape of the section and the real distorted shape. Figure 1.2a shows the sections deforming under the assumption of plane sections remaining plane during bending. Thus the points lying in a plane of the section before bending remain so after bending also. In Figure 1.2b, it is seen that the points lying in the plane of the section do not remain in the plane after bending. This is due to the effect of

cross-sectional warping. Also the sections distort increasingly towards the tip of the cantilever. For any section, the shear strain is zero at the extreme fibers and maximum at the neutral axis. This follows the distorted shape of the section, where the warping is minimum at the extreme fibers and maximum at the neutral axis. Since shear stress is directly proportional to shear strain, shear stress is maximum at the neutral axis of the section.

Since a significant amount of structural design utilizes wide flange sections, the focus of this thesis will be to better understand shear deformations in these sections and to analyze their behavior in the beam-column joint of steel moment resisting frames. Deformations in the Panel Zone (PZ) of a beam-column joint of steel moment resisting frames contribute significantly towards total drift of the subassemblies. But the amount of flexural and shear deformation in the PZ is still not easy to determine due to the complex distribution of stresses in the PZ (Downs, 2002). This can lead to serious errors in the calculations, if neglected or inaccurately determined.

A survey of existing expressions for calculating the shear area of wide flange sections results in values for shear area, which differ by up to forty percent between themselves. This discrepancy has necessitated the calculation of the 'exact' shear area of wide flange sections. The determination of the 'exact' shear area of wide flange sections is done using three-dimensional finite element analysis. The value of shear area so obtained is 'exact' within the limitations of the finite element analysis. This study focuses on the application of a method of Finite Element Analysis (FEA) based on the principle of virtual work. The method, herein referred to as the Displacement Participation Factor (DPF) method, calculates the

contributions of individual components of the structure or the elements of the finite element model towards the total displacement. This allows for greater accuracy since no assumptions are made regarding the behavior of sections. The shear area is also presented in the form of shear deformation coefficient, shear correction factor or form factor in the available literature. The shear coefficients and the form factor are defined as the ratio of the gross area of the section to the shear area of the section. Thus

$$\kappa = \frac{A}{A_v} \quad \text{..... (1.2)}$$

where κ is the form factor, shear correction factor or shear deformation coefficient, A is the gross sectional area and A_v is the shear area of the section.

1.2 Organization of the Thesis

Chapter Two of this thesis begins by reviewing available literature dealing with shear deformations. This is necessary to get an idea of the amount of work done on shear deformations and also to know the various approaches used by researchers. It is found that there were mainly two approaches to obtain the shear area or the coefficients; one based on the principle of virtual work and the other based on the mathematical theory of elasticity. The results from the literature are presented and analyzed. The development of the DPF method is then explained in detail. Chapter Three discusses the study of rectangular sections. The modeling and analysis of rectangular sections is discussed in detail and results of the DPF analysis are presented. Rectangular sections are analyzed to establish the validity of the DPF method because closed form solutions for shear area of rectangular sections are available in the literature. This exercise also helps in calibration of the various parameters of the model for

finite element analysis. Chapter Four concerns the study of wide flange sections. Once the finite element models are calibrated and the values from DPF method are verified for the rectangular sections, the wide flange sections are modeled and analyzed. The form factor is determined with respect to strong and weak axes of the section. Based on these values, trend line analysis is performed using suitable parameters to develop a simplified expression for shear area. Lastly beam–column subassemblies are modeled and analyzed in Chapter Five and the contributions of the individual components to the total drift of the subassembly is determined. This helps to achieve a better understanding of their behavior. The results obtained from the preceding chapters are summarized and conclusions are drawn from them in Chapter Six. Recommendations for further research are also made in Chapter Six.

Chapter 2 Method of Analysis

2.1 Literature Review

There are many closed form solutions in the literature for calculation of shear area of rectangular and wide flange beams. Newlin and Trayer (1924) (NT) present a formula for calculation of shear area based on the principle of virtual work. The expression can be divided into flange and web components of the form factor. Cowper (1966) has developed expressions for form factors for a variety of sections. The Cowper expression is a strain energy solution of the three-dimensional theory of elasticity equation using shear stress functions given in Love (1944) for the various cross sections. Schramm et al. (1994) develop a tensor of 'shear deformation coefficients' using the energy solution of the two-dimensional theory of elasticity equation. The non-diagonal terms are zero when the coefficients are computed for the principal axes of the section. Timoshenko and Goodier (1970) introduced compatibility conditions for shear stress distributions in beams, resulting in the shear stress distribution along the width of a section to be a function of Poisson's ratio and the shape of the cross section. This affects the calculations of form factor, and Renton (1991) presents a closed form solution for the form factor of rectangular sections incorporating the compatibility conditions of Timoshenko and Goodier (1970). This is also an energy solution of the elasticity equation. Timoshenko (1940) defines form factor as the ratio of maximum stress in the section at the neutral axis to the average stress across the section. Thus, the form factor for rectangular sections is 1.5 according to Timoshenko (1940). Pilkey (2003) develops a finite element analysis based solution similar to Schramm et al. (1994) and provides a computer program for calculation of shear deformation coefficients of any arbitrary cross section. The values for

rectangular sections are nearly identical to those of Renton (1991). Young and Budynas (2002) have presented the simplified expression found in Newlin and Trayer (1924) and McGuire et al (2002) have presented the expression in Timoshenko (1940) as the shear area of the wide flange sections. The following sections will discuss in detail some of the solutions mentioned above.

2.1.1 Rectangular Sections

The form factor of the section depends on the shear stress distribution assumed along the section. The stresses obtained from simple beam theory are different from those obtained from the theory of elasticity. The rectangular section considered for discussion in this thesis is shown in Figure 2.1.

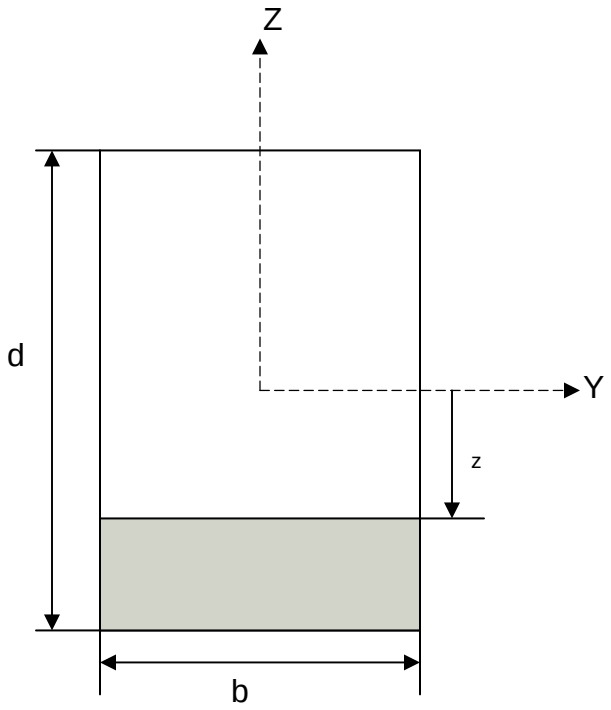

Figure 2.1 – Typical rectangular section

Applying the simple beam theory to a rectangular section with width b and depth d, the moment of inertia of the section about the neutral axis is $bd^3/12$ and the first moment of area of the material at some distance z about the neutral axis, represented by the shaded portion in the figure, is

$$Q(z) = 0.5b(0.5d - z)(0.5d + z) \quad \text{..... (2.1)}$$

Based on this, the shear stress τ_{zx} at any depth z is calculated as follows:

$$\tau_{zx} = \frac{PQ(z)}{It(z)} \quad \text{..... (2.2)}$$

where P is the transverse shear at the cross section, Q is the first moment of the area (the darker shaded portion of the section in Figure 2.1 at some distance z, taken about the neutral axis, and $t(z)$ is the width of the cross section at z. The shear stress computed by Equation 2.2 is constant across the width at any depth z. It should be noted that the shear stresses computed using Equation 2.2 are not a function of Poisson's ratio. Using Equation 2.2, the maximum shear stress τ_{zx} is obtained at the neutral axis as $1.5P/A$. It is zero at the extreme fibers (i.e. $z=\pm d/2$) and constant along the width b. It also indicates that the τ_{yx} stresses are zero since there are no surface loads on the vertical sides of the section to cause complementary shear stresses.

The stress by Equation 2.2 is determined on the basis of equilibrium only. Compatibility conditions are not enforced. This is not consistent with the solution provided by

Timoshenko and Goodier (1970), where compatibility conditions are introduced to show that the shear stress distribution across the width of the section is not constant. The variation of stress across the width is a function of the shape of the section, and of Poisson's ratio. However, the average τ_{zx} stress across the width is the same as predicted by Equation 2.2. It is also shown that nonzero τ_{yx} stresses exist within the cross section (Timoshenko and Goodier, 1970). It is interesting to note that the normal stresses, given by My/I, are independent of the shear stresses, regardless of the use of simple beam theory or the more advanced theory of elasticity. This is paradoxical because the presence of the shear stresses causes cross-sectional warping, which would appear to contradict the plane section hypothesis on which My/I and PQ/It are based. However, if a length segment of a beam is in a region of constant shear (as in the end-loaded cantilever beam), the warping at the two ends of the segment is the same and the warping will not affect the longitudinal stresses in the beam (Hingdon et al., 1985).

Using the stress functions developed by Timoshenko and Goodier (1970) based on the theory of elasticity, the shear stress distributions are much more complicated. The 'exact' shear stress distribution is obtained after adding corrective stresses to the stresses obtained by simple beam theory. The corrective stresses, which are a function of Poisson's ratio and the width of the section, act along the *zx* and the *yx* directions. This effect has to be incorporated in the solution for finding the shear area of the rectangular sections. Love (1944) has also developed similar compatibility conditions for stresses but his formulation is more difficult to apply than Timoshenko and Goodier (1970). Chapter 3 on rectangular sections has details of the stress function and its effect on the shear stress distributions.

Timoshenko (1940) calculated the form factor for a rectangular section as 1.5. It was based on physical interpretation of the deformed shape of the cross-section using the concept of effective strain at the neutral axis of the section. A detailed discussion on the basis of obtaining the form factor based on physical interpretation of the deformed shape is presented in Charney et al. (2005).

Cowper (1966) provided a formula for the form factor of rectangular sections using the energy solution of the theory of elasticity equation. The stress functions provided by Love (1944) were used to develop the solution. But surprisingly, the solution is a function of Poisson's ratio only. It does not include the aspect ratio of the section, which is defined as the ratio of the width of the section to the depth of the section. The shear area has to be a function of the shape of the section since cross-sectional warping depends on the shape of the section and it affects the shear deformations. The formula given by Cowper is as follows:

$$\kappa = \frac{12 + 11\nu}{10(1+\nu)} \quad \text{..... (2.3)}$$

It is observed that for increasing values of Poisson's ratio, the value of form factor for rectangular would be decreasing. This trend was found to be incorrect.

Renton (1991) provided a closed form solution for shear area of rectangular sections using the stress functions given by Timoshenko and Goodier (1970). The shear area given by the solution is a function of the Poisson's ratio and also the aspect ratio of the section. Thus

the results are likely to be more accurate than those by Cowper. The formula is shown in Equation 2.4.

$$\kappa = 1.2 + \left(\frac{\nu}{1+\nu}\right)^2 \sum_{i=0}^{\infty}\sum_{j=1}^{\infty} \frac{144(b/d)^4}{\pi^6 (2i+1)^2 j^2 [(2i+1)^2 (b/2d)^2 + j^2]} \quad \ldots\ldots\ldots\ldots\ldots\ldots (2.4)$$

It is important to note that the value of 1.2 in Equation 2.4 is similar to the value obtained using virtual work. The second term in the equation arises due to the stress function used in theory of elasticity. The second term reduces to a negligible value when the aspect ratio of the section is very high. It reduces to zero when the Poisson's ratio is zero. Figure 2.2 shows the variation of form factors for rectangular sections for various aspect ratios and different values of Poisson's ratio.

Schramm et al. (1994) and Pilkey (2003) have provided a finite element solution to the two-dimensional theory of elasticity equation for deformation under transverse load using the principle of strain energy equilibrium. The solution provides form factors similar to those from Renton (1991).

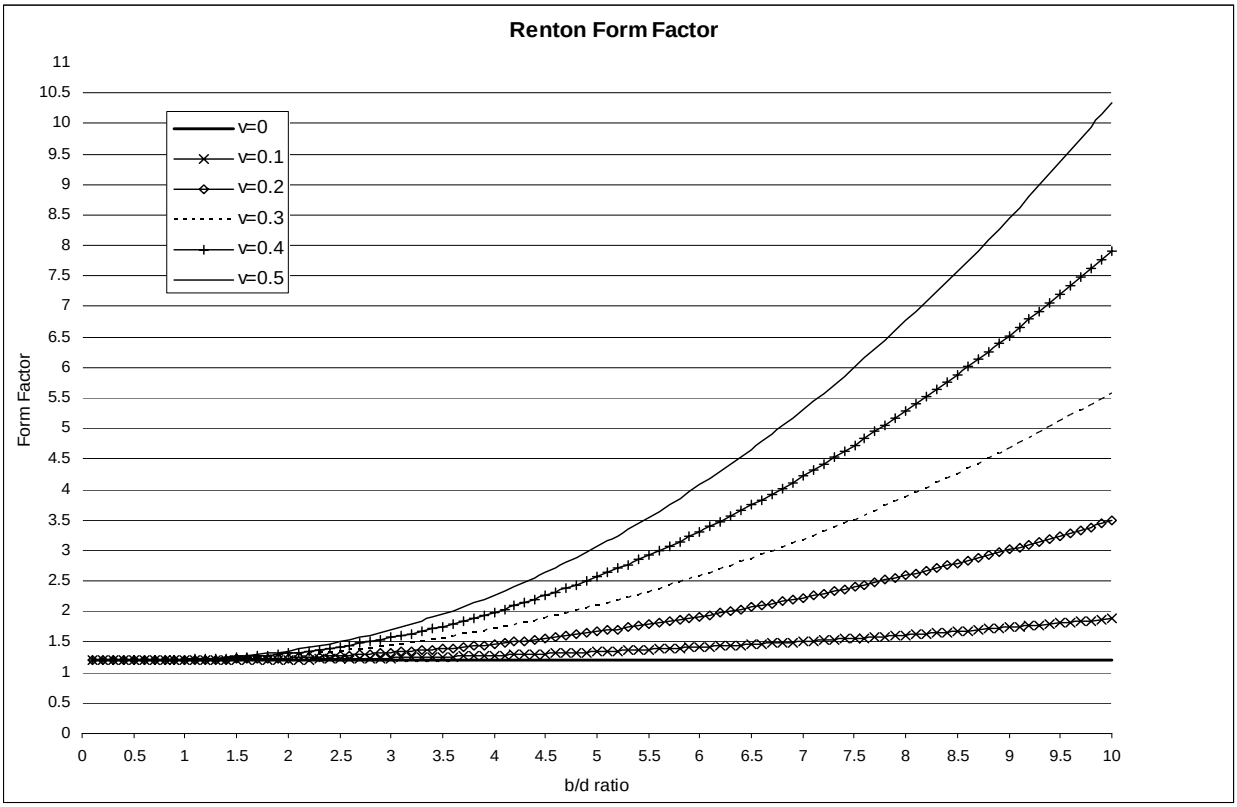

Figure 2.2 – Variation of form factor for rectangular section using Renton's formula

2.1.2 Wide Flange Sections

The form factor of wide flange sections has been widely investigated, resulting in a number of formulas. The formulas are based on the principle of virtual work or the mathematical theory of elasticity. Some of the formulas are empirically developed based on assumed behavior of the sections. Figure 2.3 shows the typical cross section of a wide flange section and the assumed shear stress distribution along the vertical centerline of the section. This stress distribution is generally used for the calculation of shear area using the principle of virtual work. It is interesting to note that the different solutions for shear area are obtained due to the varying assumptions made regarding the stress distribution across the section.

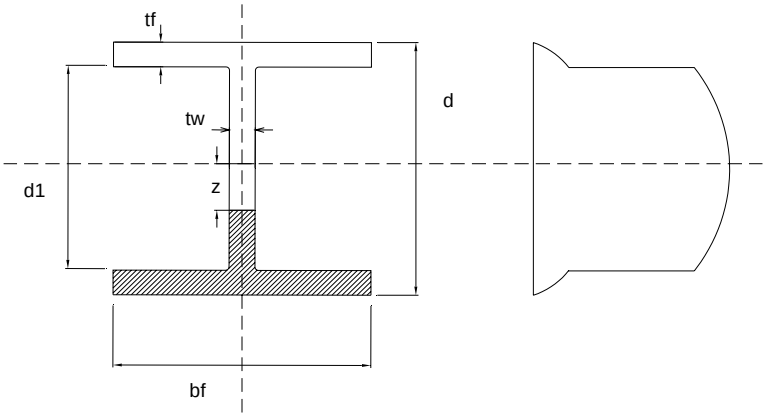

Figure 2.3 – Typical wide flange section and shear stress distribution along the center of the web

For the wide-flange section shown in Figure 2.3, two expressions are required for Q. When z is less than 0.5 d_1, the plane of interest is in the web, producing

$$Q_w(z) = 0.25 b_f t_f (d + d_1) + 0.5 t_w (0.5 d_1 - z)(0.5 d_1 + z) \quad \text{..... (2.5a)}$$

When z is greater than $0.5 d_1$, the plane of interest is in the flange, and

$$Q_f(z) = 0.5 b_f (0.5 d - z)(0.5 d + z) \quad \text{..... (2.5b)}$$

By the principal of virtual work, the internal work due to shear deformation is defined as the product of the shear stress, τ, and the shear strain, γ, integrated over the volume of the beam. Thus

$$W_{Internal} = \int_{volume} (\tau \cdot \gamma) dV \quad \text{..... (2.6)}$$

The shear strain can be expressed in terms of the shear stress and the modulus of rigidity, G, and the volume integral can be separated into a length integral and an area integral.

$$W_{Internal} = \iint \frac{\tau^2}{G} dA dx \quad \text{..... (2.7)}$$

The shear stress at a distance z from the neutral axis is $\tau(z) = \frac{VQ(z)}{It(z)}$. The area integral must be processed in two parts because the width of the cross section is constant except for the web-flange intersection where it changes from b_f to t_w. One integral will be processed from the neutral axis to the bottom of the flange. This integral will be called the web integral. The other integral will be called the flange integral and will be processed from the bottom of the flange to the extreme fiber. Also the length integral will yield the length of the beam since the beam is prismatic. Thus, the internal work equation becomes

$$W_{Internal} = \frac{V^2 L}{GI^2} \int \frac{Q(z)^2}{t(z)^2} dz \quad \text{..... (2.8)}$$

where $Q(z)$ = First moment of area above or below z about the neutral axis

V = Transverse shear load applied to the section at the shear center

I = Moment of inertia about the axis of bending

$t(z)$ = Width of the section at depth z

L = Length of the beam

The external work done due to shear deformations is given by:

$$W_{External} = V\delta_{\gamma} \quad \text{..... (2.9)}$$

where δ_{γ} = shear deflection of the beam. According to virtual work, the external work must equal the internal work. From Equations 2.8 and 2.9, we get

$$\delta_{\gamma} = \frac{VL}{GI^2}\int \frac{Q(z)^2}{t(z)^2}dA \quad \text{..... (2.10)}$$

Comparing the above Equations 1.1 and 2.10, we get

$$A_v = \left[\frac{1}{I^2}\int_y \frac{Q^2(z)}{t(z)}dz\right]^{-1} \quad \text{.....(2.11)}$$

From Equations 1.2 and 2.11, we have

$$\kappa = \frac{A}{I^2}\int_y \frac{Q^2(z)}{t(z)}dz \quad \text{..... (2.12)}$$

The next step is to process the integrals. Using Equations 2.5a and 2.5b in 2.11, we get

$$A_v = \left[\frac{2}{I^2} \left[\int_0^{\frac{d_1}{2}} \frac{\left(0.25 b_f t_f (d + d_1) + 0.5 t_w (0.5 d_1 - z)(0.5 d_1 + z)\right)^2}{{t_w}^2} dz + \int_{\frac{d_1}{2}}^{\frac{d}{2}} \frac{(0.5 b_f (0.5 d - z)(0.5 d + z))^2}{{b_f}^2} dz \right] \right]^{-1}$$

(2.13)

Newlin and Trayer (1924) provide two expressions for the shear area of wide flange sections developed during their research focused on wooden airplane wings. The first of these expressions was developed using the principle of virtual work, while the other was semi-empirical based on the equivalent area of the rectangular section. The shear stress distribution assumed was similar to that shown in Figure 2.3. The first expression by Newlin and Trayer is obtained by simplifying equation 2.13 as follows:

$$A_v = 8 {I_z}^2 \left[b_f \left(\frac{8}{15} d^5 - d^4 d_1 + 2 d^2 {d_1}^3 - \frac{23}{15} {d_1}^5 \right) + \frac{{b_f}^2}{t_w} \left(d^4 d_1 - 2 d^2 {d_1}^3 + {d_1}^5 \right) + t_w \left(\frac{8}{15} {d_1}^5 \right) \right]^{-1}$$

(2.14)

where I_z = Moment of inertia of the cross section about the strong axis.

It is seen that Equation 2.12 can be split into two parts; one for the flange and the other for the web. Newlin and Trayer (1924) do not split the expression but this facilitates the study of contribution of the web and flange to the form factor of the section. Thus splitting equation 2.12, we get

$$\kappa = \kappa_w + \kappa_f \quad \text{..... (2.15)}$$

where

$$\kappa_w = \frac{2A}{b_f I^2}\int_0^{d_1/2} Q_f(z)^2 dz = \frac{Ab_f}{64I^2}\left[d_1{}^5\left(\frac{8t_w}{15b_f}+\frac{b_f}{t_w}-\frac{4}{3}\right) - d_1^3 d^2\left(\frac{2b_f}{t_w}-\frac{4}{3}\right) + d_1 d^4\left(\frac{b_f}{tw}\right)\right] \quad \ldots (2.15a)$$

and

$$\kappa_f = \frac{2A}{t_w I^2}\int_{d_1/2}^{d/2} Q_w(z)^2 dz = \frac{Ab_f}{64I^2}\left(-\frac{1}{5}d_1^5 + \frac{2}{3}d_1^3 d^2 - d_1 d^4 + \frac{8}{15}d^5\right) \quad \ldots\ldots\ldots\ldots (2.15b)$$

The second expression by Newlin and Trayer was developed due to the perceived complexity of their first expression. The simplified expression is based on the assumption that the shear deflection in any two beams of the same length, depth, and moment of inertia, which are similarly loaded, is proportional to the sum of the shear stresses on the vertical section. Thus the wide flange section is effectively transformed into an equivalent rectangular section, for which the shear stress distribution is more accurately known. The simplified expression developed by Newlin and Trayer using the concept of equivalent rectangular area is as follows:

$$A_v = \frac{A_g}{\left[1+\frac{3(d-d_1)d_1}{2d^3}\left(\frac{b_f}{t_w}-1\right)\right]\frac{4d^2}{10{r_z}^2}} \quad \ldots\ldots\ldots\ldots\ldots\ldots\ldots\ldots\ldots\ldots (2.16)$$

where r_z = radius of gyration of the cross section about the strong axis. The denominator in the above equation is cited as the form factor for wide flange sections in Young and Budynas (2002).

Timoshenko (1940) provided an expression for the shear area of wide flange sections based on the theory that the effective shear strain is *1/G* times the shear stress at the mid-depth of the section obtained using simple beam theory. This resulted in the expression given as follows:

$$A_v = \frac{8 t_w I_z}{b_f d - d_1^{\,2}(b_f - t_w)} \quad \text{..... (2.17)}$$

This formula has been cited by McGuire et al. (2002) as the shear area of wide flange sections.

Cowper (1966) used the strain energy based approach to develop an expression for the shear area of wide flange sections. The shear stress distributions used in the solution are given in Love (1944). The expression is a function of Poisson's ratio, the ratio of area of flanges to the gross area and the ratio of web area to the gross area of the section. This expression is based on a rather complex two-dimensional distribution of shear stresses across the section. Cowper (1966), Schramm et al. (1994) and Pilkey (1994) provide more detailed explanation for further background. Cowper's form factor for I-shaped sections is

$$\kappa = \frac{(12 + 72m + 150m^2 + 90m^3) + \nu(11 + 66m + 135m^2 + 90m^3) + 30n^2(m + m^2) + 5\nu n^2(8m + 9m^2)}{10(1+\nu)(1+3m)^2} \quad \text{(2.18)}$$

where $m = \frac{2 b_f t_f}{d t_w}$, $n = \frac{b_f}{d}$, and ν = Poisson's ratio.

Both *m* and *n* are dimensionless parameters which depend on the size of the cross section. It is interesting to note that the original Cowper's formula showed *d* as the effective depth between the flanges. But it will be shown in Chapter 4 that using the full depth of the section for *d* provides better answers.

Empirical formulas for shear area of the wide flange sections will also be investigated. The most common of these are of the form

$$A_v = d_{eff} * t_w \quad \text{..... (2.19)}$$

where d_{eff} = effective depth of the wide flange section. Various choices for the effective depth of the section are,

$d_{eff} = d$ or

$d_{eff} = (d-t_f)$ or

$d_{eff} = (d-2t_f)$

The effective depth of the section could be any of the three values listed above. The above formulas are generally preferred due to the complexity of the other expressions discussed earlier in calculating the form factor.

As stated earlier, the various existing expressions for calculating shear area provide differing values. This is illustrated in Figures 2.4 and 2.5.

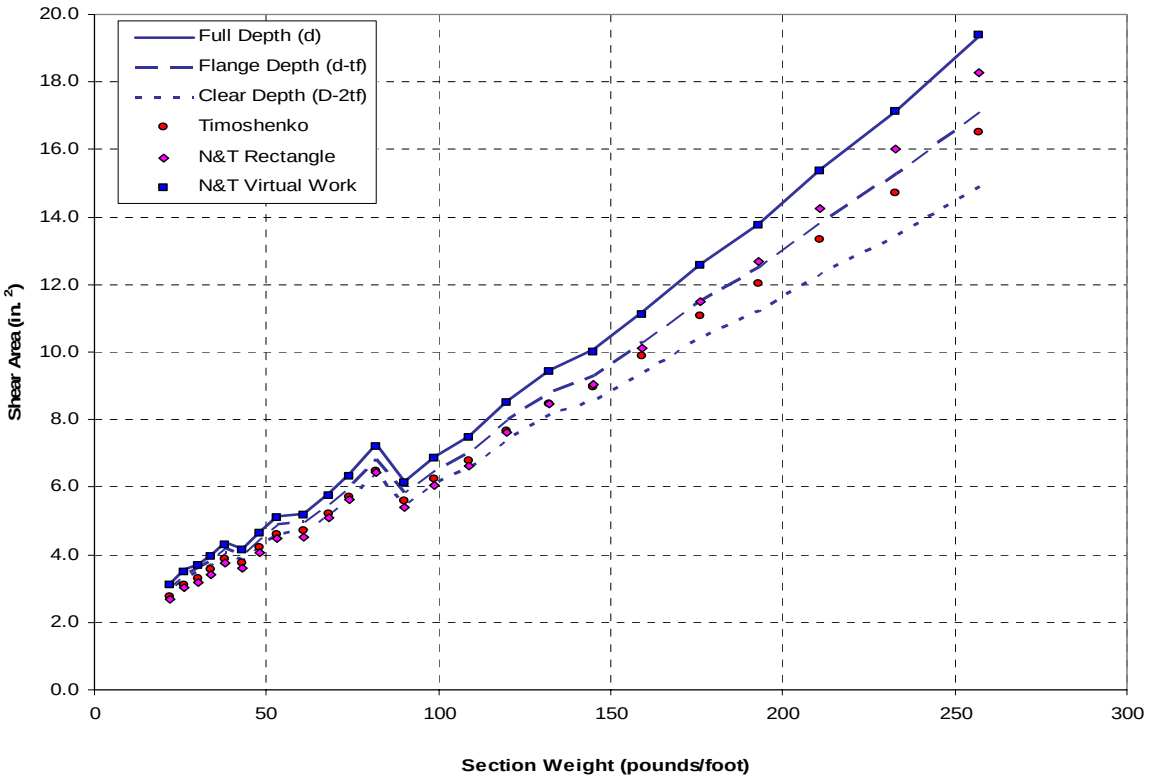

Figure 2.4a – Various shear area values for lighter W14 sections

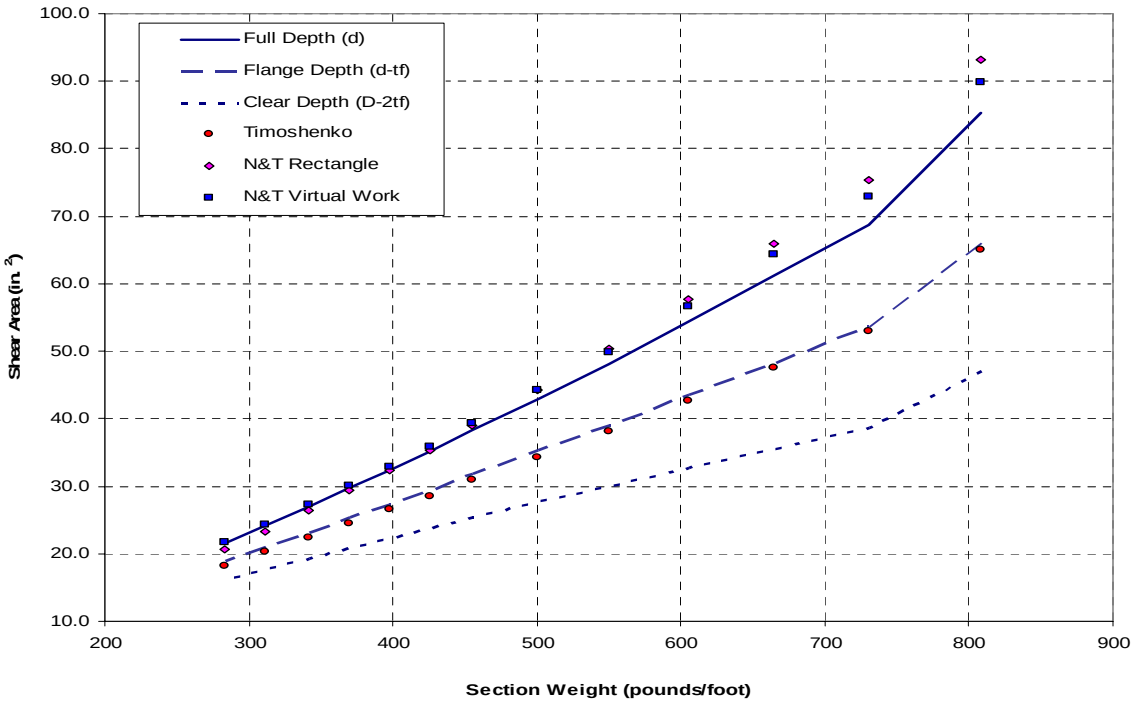

Figure 2.4b – Various shear area values for heavier W14 sections

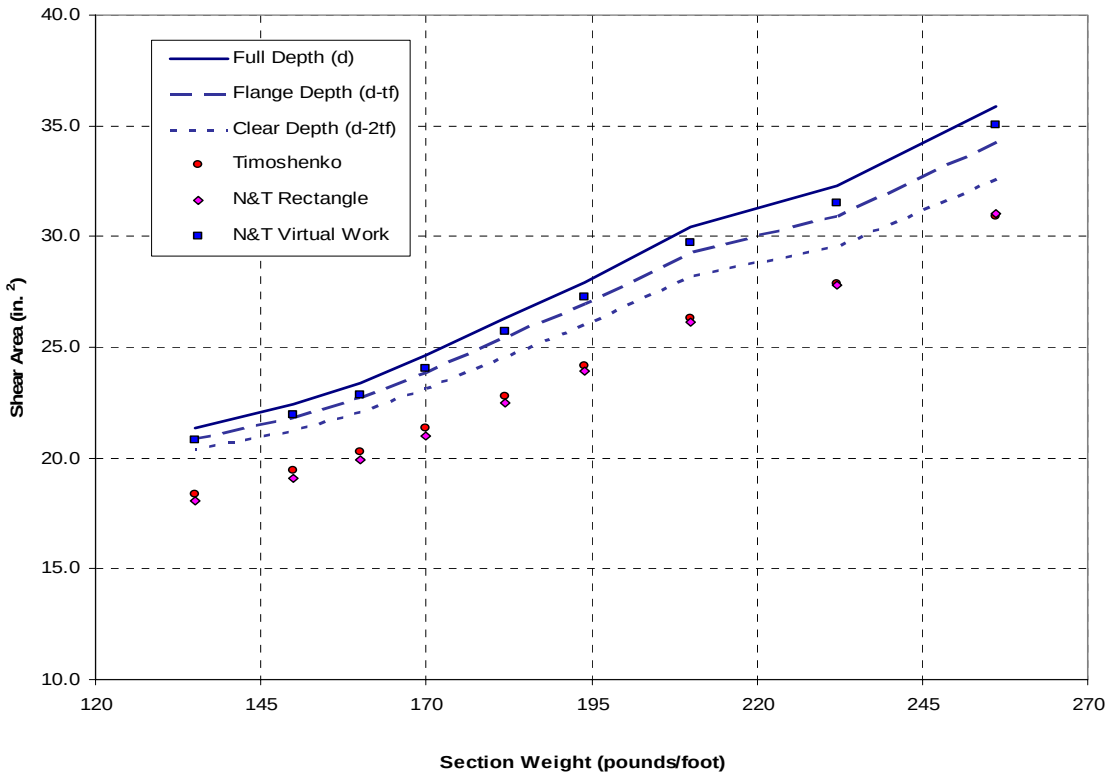

Figure 2.5a – Various shear area values for lighter W36 Sections

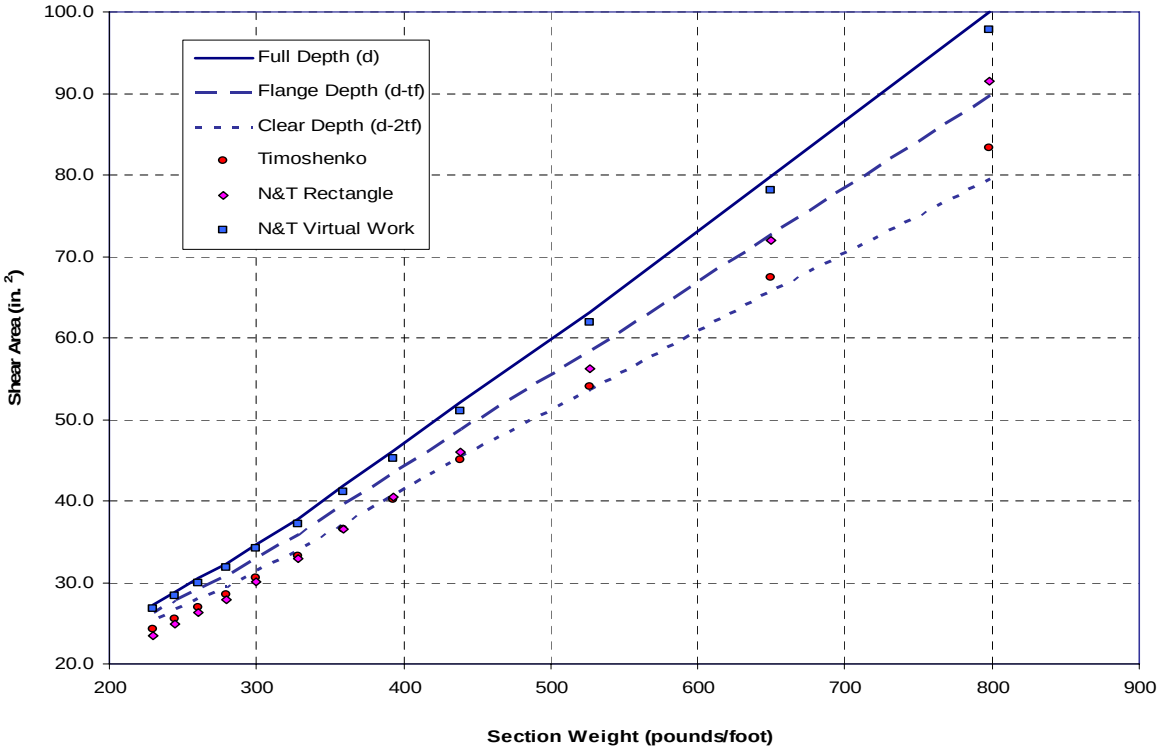

Figure 2.5b – Various shear area values for heavier W36 Sections

Figures 2.4 and 2.5 show the variation of shear area with regard to section weight. Note that the variation in shear area values increases as the member weights increase. The disparity between the formulas is greatest for the heaviest beams. There is, for example, a maximum difference of 66% between shear area values for a W14x808. The maximum shear area value for the W14x808 is 93.16 $in.^2$ and is calculated by the N&T Rectangle formula. The minimum is 46.97 $in.^2$ and results from $(d-2t_f).t_w$. Furthermore, the extreme values for W36x798 are 79.54 $in.^2$ and 113.51 $in.^2$, which results in a maximum difference in shear areas of 31%.

Although existing shear area formulas provide varying values for shear area, it must be shown that this variance leads to significant error in deflection calculation. To show this, it is necessary to have a point of reference. For the purpose of this discussion, it was assumed that the true shear area was at least in the range of the existing formulas. The true shear area was assumed to be the average of the existing formulas. This was considered the "true" shear area. Then, with a point of reference, increments of error were imposed on the "true" shear area value and the deflection results were recorded. The results of this exercise for the W14x808 are plotted in Figure 2.6.

As expected, the shorter beams are more affected by errors in shear area. Also, the deflection error increases rapidly with increasing shear area error. For a W14x808 beam with an L/d ratio of 3 (thus length, L is 68.4 in.), a 10% error in shear area results in approximately a 3% error in total deflection. Furthermore, a 25% error in calculation of shear area corresponds to an 8% error in total deflection. Recall that for a W14x808, the maximum

variation in shear area values using existing formulas is 66%. Thus, it is clear that the choice of shear area formula greatly impacts deflection calculations. The differences encountered in the shear area formulas, exemplified in Figures 2.3 and 2.4, and enumerated in Figure 2.6, necessitate the use of three-dimensional finite element analysis to resolve the issue.

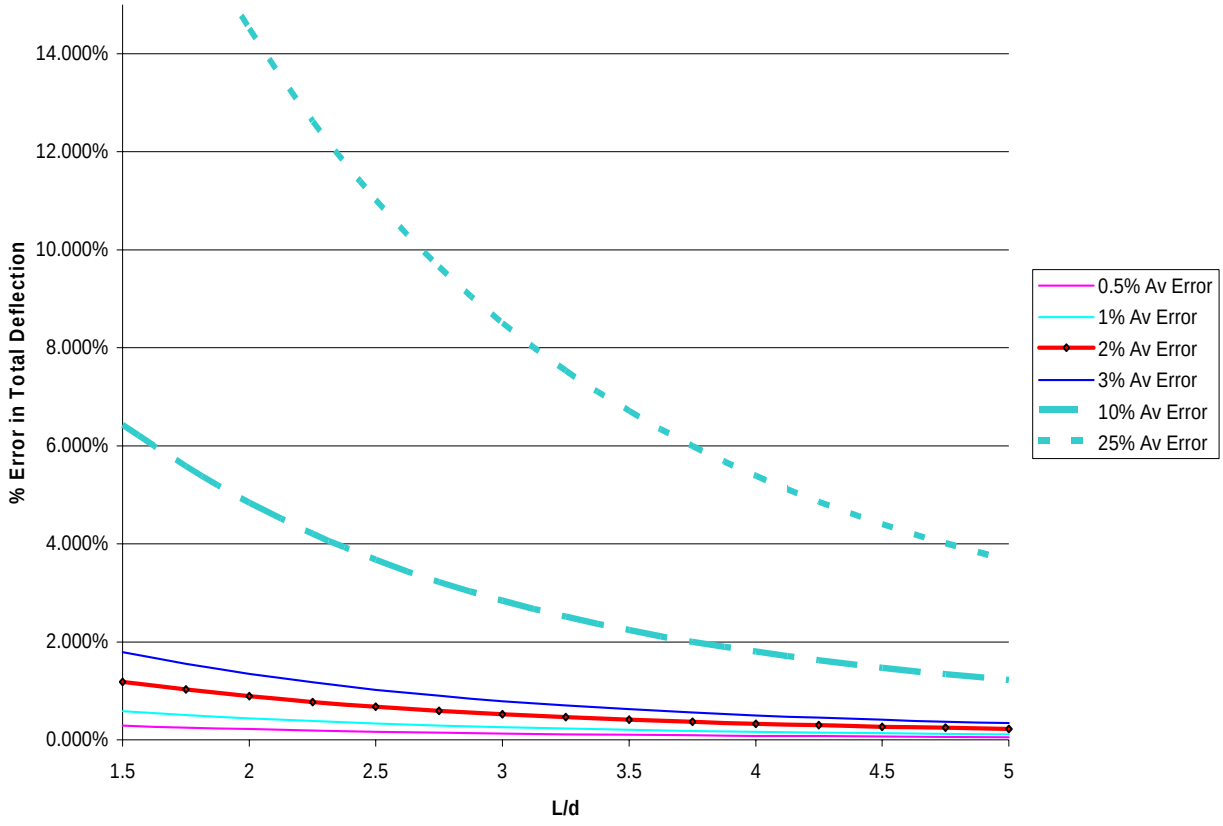

Figure 2.6 – Error in total deflection of a cantilever W14x808 beam at varying lengths and varying amounts of error in shear Area.

2.2 Methodology for Analysis of Beams

The finite element analysis of cantilever beams required much refinement throughout the process. Boundary conditions, loading methods, and element sizes all caused variations in the results. In the end, however, two different methods, one which used deflections and the other which used stresses, provided consistent results. The first method which used deflections will be called the Finite Element Deflection (FED) Method for discussion purposes. The stress method which uses stresses and virtual work will be called the Displacement Participation Factor (DPF) Method.

2.2.1 Finite Element Deflection (FED) Method - Back Calculate Av from deflection equations and FEA analysis deflection output.

In this method, deflections obtained from the three-dimensional finite element analysis were used to determine shear areas. The FED method employs the conventional two-dimensional beam equations to back calculate moments of inertia and shear areas. A full description of the calculation process involved is provided in Appendix A.

The first step in this method was to apply a pure moment to the end of the beam, thus causing constant moment and no shear. The absence of shear force in the beam meant the deflection was caused by flexure only. By using the deflection resulting from the application of moment at the end, the moment of inertia could be calculated with a high degree of accuracy. Even so, the moment of inertia determined by FED method values varied with the

length-to-depth ratio (L/d) as Figure 2.7 illustrates. Several cross sections are shown in the figure. They are plotted in a nondimensional form, that is, the moments of inertia from the FED method were divided by the hand calculated moments of inertia of the sections without the fillets. Note that the moments of inertia from FED method were always greater than the calculated values. Moreover, note that deviation from the calculated values depended to some extent on the stockiness of the cross-section profile. The heavier and stockier sections tended to deviate further from unity than the more slender profiles. For the most part, the moment of inertia values from the FED method were within 0.50% of the actual calculated values. It is important to note that, in the cases where the variation exceeded 0.50%, the length-to-depth (L/d) ratios were typically below 2.5 or the cross-sections were fairly stocky. Conversely, the variation was generally in the vicinity of 0.30% as the L/d ratios increased beyond 3.5 and when the cross-sections were more slender.

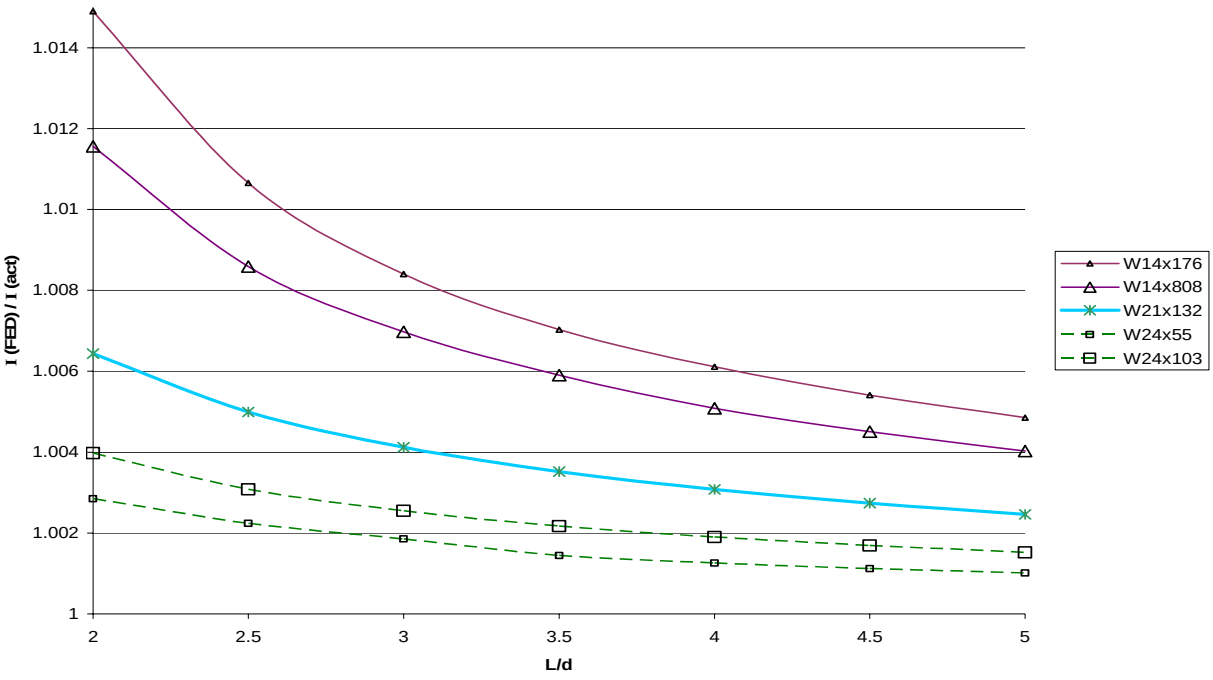

Figure 2.7 – Variation in nondimensional moment of inertia with respect to length

The next step was to determine the sensitivity of the shear area value with respect to the accuracy in calculation of moment of inertia. This was done by changing the value of moment of inertia in small increments. This resulted in different values of shear area for a given L/d ratio. Figure 2.8 illustrates the sensitivity of shear area calculation to the error in determination of moment of inertia. The knowledge of sensitivity of shear area helps in deciding if the finite element analysis of a particular model is satisfactory. This is done by comparing the error in moment of inertia calculated from the procedure with Figure 2.8 to determine the probable amount of error in shear area.

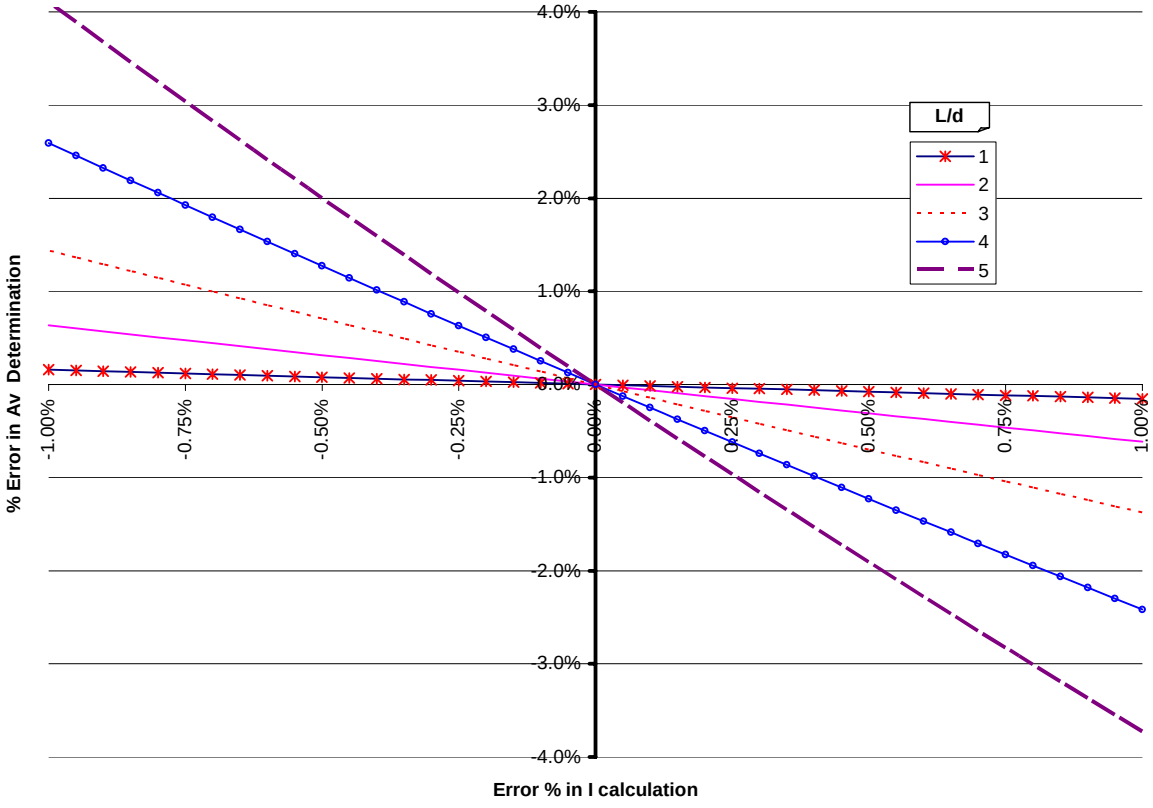

Figure 2.8 – Sensitivity of shear area to error in determination of moment of inertia.

With the moment of inertia values obtained from FED method, the next step was to consider the same model except with a single shear load applied at the tip of the free end. The deflections resulting from the shear load model along with the moment of inertia enabled the determination of the experimental shear areas. The shear areas calculated by FED method, like the moments of inertia, were dependent on the L/d ratio. For L/d ratios less than approximately 2.5, shear area values increased at varying rates as the L/d ratio decreased. For L/d ratios greater than approximately 3.5, the shear area values increased slightly at approximately equal rates as the L/d ratio increased.

Knowing that the shear area values were not uniform for varying L/d ratios, the value of shear area was taken as the average of shear areas when L/d varies from 2.5 to 4. It is important to note that for the FED method, all deflection measurements were taken at the centerline of the beam. This is because plane sections did not remain plane and so the vertical deflection at the tip of the cantilever was not constant. The cross sectional warping due to shear stresses caused the middle of the beam to deflect less than the extreme fibers.

2.2.2 Displacement Participation Factor (DPF) Method - Calculate Av using virtual work and FEA stress output.

While the FED method produced fairly reliable results, a second method was sought to calculate the shear areas. The second method of shear area determination used the three-dimensional stress output from SAP and virtual work. A comprehensive derivation of this method is provided in the next section

A major benefit of this method is that each element's contribution to deflection is calculated. Moreover, the elemental contributions can be broken down into components due to normal stress and shear stress. These contributions, called displacement participation factors (DPF), can be combined to produce meaningful results. For example, with this method, one can determine the amount of deflection caused by the web due to shear or the deflection caused by the flanges due to flexure. Since shear contributions to deflection are directly determined using the DPF method, it enables the direct calculation of shear area. The process of calculation is fairly simple as the principle of virtual work is employed. With this method, a real vertical point load is applied at the tip of the cantilever and the elemental stresses are measured. Then, a set of vertical virtual point loads are applied at interior points at equal distances from the ends. Once again, all of the elemental stresses are measured. Since energy is conserved, the internal work is equal to the external work and so the virtual set of forces moving through a real displacement is equal to the virtual internal stresses moving through real strains. The virtual strains can be obtained by employing a three-dimensional constitutive relationship. The resulting generic formula is

$$1 \times \delta = \sigma_r C \sigma_v \quad \ldots\ldots\ldots\ldots\ldots\ldots\ldots\ldots\ldots\ldots \quad \ldots\ldots. \quad (2.20)$$

where δ= displacement under real load,

σ_r = vector of real stress

σ_v = vector of virtual stress

C = constitutive material matrix

The shear and flexure terms can be uncoupled in the Equation 2.20 and the resulting equation is

$$1 \times \delta_s = \tau_r \frac{\tau_v}{G} \quad \text{.......................................} \ (2.21)$$

where δ_s = deflection due to shear

τ_r = shear stresses due to real load

τ_v = shear stresses due to virtual load

G = shear modulus of the material.

It is important to note that any finite element analysis software provides nodal stresses, which need to be averaged in order to be used in the aforementioned equation. One weakness of the DPF method is that it uses element stresses for calculations, which are typically less accurate than deflections when using FEA. This is due to the fact that the stresses are calculated at the Gauss points of the element which are inside the element. The stresses are then extrapolated to the nodes of the element. Even so, for this exercise, the results seemed to be acceptable. The results were very reasonable and close, compared to those of the FED method above. Like the FED method above, the shear area values computed using the DPF method were dependent on the L/d ratio. Unlike the FED method though, the DPF values followed a different pattern. Whereas the FED values of shear area tended to increase with increasing L/d ratios, the DPF values decreased as the L/d ratios increased. Both methods produced similar results, that is, the shear area determined using the DPF method was approximately equal to the value obtained using the FED method. Moreover, the average of the DPF and FED methods produced values that were independent of L/d when evaluated for L/d ratios greater than 3.

2.3 Derivation of DPF Method

Consider the cantilever beam shown in Figure 2.9. The vertical deflection at the tip of the beam, measured at the neutral axis, is given by the expression

$$\delta = \delta_{\varepsilon} + \delta_{\gamma} \quad \text{..... (2.22)}$$

where δ_{ε} = deflection due to normal strains, typically induced through flexure, and

δ_{γ} =deflection due to shear strains.

In equation 2.9 above, no assumptions are made with regards to the distribution of stresses across the given cross section. Thus the cross sections are free to warp and all the components of deformation are considered.

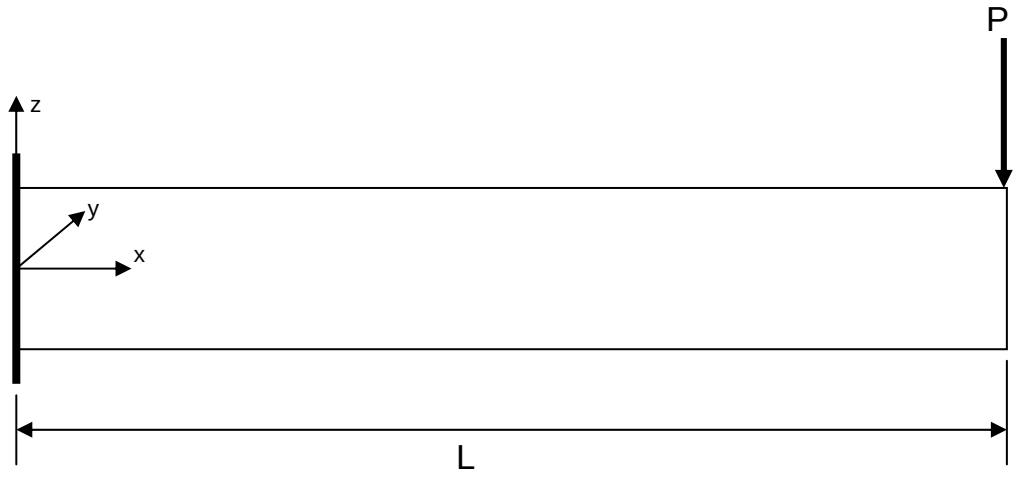

Figure 2.9 – Typical orientation and loading of the cantilever beam.

The fact that the displacements due to flexure and shear are uncoupled and hence separable may be shown through the principle of virtual work. If a virtual load $\hat{p}$ is applied at the location and orientation of the real load *P*, the total deflection δ due to *P* may be found from

$$\delta \times \hat{p} = \int_V \hat{\sigma}^T \varepsilon dV \quad \text{..... (2.23)}$$

where the stresses due to the virtual load are given by

$$\hat{\sigma} = \begin{Bmatrix} \hat{\sigma}_{xx} \\ \hat{\sigma}_{yy} \\ \hat{\sigma}_{zz} \\ \hat{\tau}_{yx} \\ \hat{\tau}_{yz} \\ \hat{\tau}_{zx} \end{Bmatrix} \quad \text{..... (2.24)}$$

the strains associated with the real load *P* are

$$\varepsilon = \begin{Bmatrix} \varepsilon_{xx} \\ \varepsilon_{yy} \\ \varepsilon_{zz} \\ \gamma_{yx} \\ \gamma_{yz} \\ \gamma_{zx} \end{Bmatrix} \quad \text{..... (2.25)}$$

and *V* and *dV* are the total volume of the beam and the volume of a differential element of the beam, respectively. Now let the virtual load equal unity (1.0). Therefore $\hat{p} = 1.0$. As it is easier to use stresses than strains, the real strains are transformed to real stresses using Hooke's law for an isotropic material:

$$\varepsilon = C\sigma \quad \text{..... (2.26)}$$

where C = constitutive material matrix given by

$$C = \frac{1}{E}\begin{bmatrix} 1 & -\nu & -\nu & 0 & 0 & 0 \\ -\nu & 1 & -\nu & 0 & 0 & 0 \\ -\nu & -\nu & 1 & 0 & 0 & 0 \\ 0 & 0 & 0 & 2(1+\nu) & 0 & 0 \\ 0 & 0 & 0 & 0 & 2(1+\nu) & 0 \\ 0 & 0 & 0 & 0 & 0 & 2(1+\nu) \end{bmatrix} \quad \text{..... (2.27)}$$

E = Modulus of elasticity, and

ν = Poisson's ratio.

It is important to note that the constitutive matrix is uncoupled with regards to normal and shear stresses. Thus, shear stresses can only be transformed to shear strain and normal stresses can only be transformed to normal strains. But normal stresses in a given direction are dependent on the normal stresses produced in other directions due to the effect of Poisson's ratio. The shear stresses however are independent of the stresses in the other direction. The beam in Figure 2.8 exhibits a complex stress distribution pattern therefore it is difficult to discern the above behavior of stresses by mere observation.

Equations (2.24) – (2.27) are substituted in equation (2.23), and noting the shear modulus $G = E/2(1+\nu)$, the equation can be split into two parts:

$$\delta_\varepsilon = \frac{1}{E}\int_V \left(\{\hat{\sigma}_{xx} \quad \hat{\sigma}_{yy} \quad \hat{\sigma}_{zz}\} \begin{bmatrix} 1 & -\nu & -\nu \\ -\nu & 1 & -\nu \\ -\nu & -\nu & 1 \end{bmatrix} \begin{Bmatrix} \sigma_{xx} \\ \sigma_{yy} \\ \sigma_{zz} \end{Bmatrix} \right) dV \quad \text{..... (2.28a)}$$

$$\delta_\gamma = \frac{1}{G}\int_V \left(\{\hat{\tau}_{yx} \quad \hat{\tau}_{yz} \quad \hat{\tau}_{zx}\} \begin{bmatrix} 1 & 0 & 0 \\ 0 & 1 & 0 \\ 0 & 0 & 1 \end{bmatrix} \begin{Bmatrix} \tau_{yx} \\ \tau_{yz} \\ \tau_{zx} \end{Bmatrix} \right) dV \quad \text{..... (2.28b)}$$

The above equations clearly show that the normal stresses and shear stresses are completely separable. There are basically three ways to compute the shear stresses in equations 2.28b: simple beam theory, the mathematical theory of elasticity, and finite element analysis. If simple beam theory is used to compute the stresses, all normal stresses are zero except for σ_{xx}, and all shear stresses are zero except for τ_{zx}. In this case, the total displacement becomes

$$\delta = \delta_\varepsilon + \delta_\gamma = \frac{1}{E}\int_V \hat{\sigma}_{xx}\sigma_{xx}dV + \frac{1}{G}\int_V \hat{\tau}_{yx}\tau_{yx}dV \qquad (2.29)$$

If simple beam theory is adopted, virtual stresses $\hat{\tau}(y)$ are obtained from equation 2.2 by replacing the real load P by the unit virtual load $\hat{p}$. Using equation 2.18 and simplifying it after proper substitutions, the total displacement is now

$$\delta = \frac{PL^3}{3EI} + \frac{PL}{I^2 G}\int_y \frac{Q^2(y)}{t(y)}dy \quad \text{..... (2.30)}$$

The more traditional form of equation 2.19 is

$$\delta = \frac{PL^3}{3EI} + \frac{PL}{GA_v} \quad \text{..... (2.31)}$$

where A_v = effective shear area and is given by

$$A_v = \left[\frac{1}{I^2} \int_y \frac{Q^2(y)}{t(y)} dy \right]^{-1} \quad \text{..... (2.32)}$$

Equation 2.21 is used in later chapters to derive expressions for the effective shear area of both rectangular and wide flange sections.

An alternate form of equation 2.20 is

$$\delta = \frac{PL^3}{3EI} + \frac{\kappa PL}{GA} \quad \text{..... (2.33)}$$

where κ = form factor or shear correction factor

A = gross cross sectional area of the member.

From equations 1.2, 2.21 and 2.22 it is clear that

$$\kappa = \frac{A}{I^2} \int_y \frac{Q^2(y)}{t(y)} dy \quad \text{..... (2.34)}$$

From a physical perspective, it may be seen that the shear displacement at the end of the cantilever is due to an *effective shear strain*, γ_e, times the length of the cantilever. The effective shear strain is

$$\gamma_e = \frac{\kappa(P/A)}{G} \quad \text{..... (2.35)}$$

where the effective shear stress is

$$\tau_e = \kappa\left(P/A\right) \quad \text{..... (2.36)}$$

and P/A is defined as the average shear stress over the cross section. The use of κ as a multiplier for the average shear stress has led to the use of the term shear correction factor in lieu of form factor. In structural analysis, though, it is common to use the effective shear area, as this represents a cross sectional property analogous to the true area, or moment of inertia. The term form factor is used in this thesis because it is a dimensionless number related to the shape, not the physical size of the member.

Simple beam theory has been used in the above development because the real and virtual stresses are easy to compute for any cross section. While the theory of elasticity provides shear stress distributions which may be used to compute more accurate form factors for many cross sections, it is more convenient to compute the stresses using three-dimensional finite element analysis. In this case, the stresses are provided as discrete values reported at integration points inside each element which are then interpolated and averaged as stresses acting at the nodes of the elements. Using the stresses from a real and virtual load, the flexural component of deflection is computed as

$$\delta_\varepsilon = \frac{1}{E}\sum_{i=1}^{nels} \{\hat{\sigma}_{xx,i} \quad \hat{\sigma}_{yy,i} \quad \hat{\sigma}_{zz,i}\} \begin{bmatrix} 1 & -\nu & -\nu \\ -\nu & 1 & -\nu \\ -\nu & -\nu & 1 \end{bmatrix} \begin{Bmatrix} \sigma_{xx,i} \\ \sigma_{yy,i} \\ \sigma_{zz,i} \end{Bmatrix} V_i \quad \text{..... (2.37}a\text{)}$$

and the shear deflection is computed as

$$\delta_\lambda = \frac{1}{G}\sum_{i=1}^{nels} \{\hat{\tau}_{xy,i} \quad \hat{\tau}_{yz,i} \quad \hat{\tau}_{zx,i}\} \begin{bmatrix} 1 & 0 & 0 \\ 0 & 1 & 0 \\ 0 & 0 & 1 \end{bmatrix} \begin{Bmatrix} \tau_{xy,i} \\ \tau_{yz,i} \\ \tau_{zx,i} \end{Bmatrix} V_i \quad \text{..... (2.37b)}$$

In equations 2.37, i is the element number, V_i is the volume of the 'i'th element, and *nels* is the total number of elements. By summing only over the appropriate volumes, the deflections given by equations 2.37a or 2.37b may be broken into components associated with the web or the flanges of the section. These components of displacement are the DPF's.

If, using equation 2.37*a*, the deflection δ_ε has been computed from the results of a finite element analysis and if it is assumed that the same deflection of the idealized beam is equal to $PL^3/3EI$, the *effective moment of inertia* of the beam may be recovered. Similarly, if equation 2.37*b* has been used to compute the shear deflection in the cantilever beam and if the shear deflection for the cantilever is taken as PL/GA_v, the effective shear area (or form factor) may be recovered. When using a finite element analysis to compute the section properties, it is important to avoid the influence of end conditions, where local stress concentrations may lead to inaccuracies. When end effects are avoided, the shear area or form factor obtained

will be “exact” within the limitations of the finite element analysis solution. Details of the implementation of the finite element procedure are given in Appendix B of this thesis.

Chapter 3 Rectangular Sections

The rectangular sections were modeled and analyzed to calculate the shear area, since closed form solutions for shear area were available. Also studying the behavior of rectangular sections provides a better understanding of the behavior of wide flange section. Thus cantilever beam models were created for the purpose of testing the accuracy of the methods adopted for calculation of shear area.

3.1 Development of Finite Element Model

The software package SAP 2000 v7.44 (CSI, 2002) was used for the analysis. Linear static analysis was performed using SAP2000. The cantilever beams were modeled using the eight-node brick element available in SAP2000. The brick element has three translational degrees of freedom per node, resulting in twenty-four degrees of freedom per element. The brick element was chosen over a shell element because it allows for more elements through the width and depth of the section. All six components of the stress tensor are calculated without any assumption regarding behavior of the cross section. A special program was written for generating the input files for SAP2000.

Only half of the cross-section of the beams was modeled to increase computational efficiency and permit higher mesh density across the model. Beams were oriented such that the beam length extended in the X direction, the cross-section strong axis was along the Y

direction and the weak axis was along the Z direction. The applicable boundary conditions are as follows:

- Restraints were placed in the Y direction at the plane where the beams were cut in half. This set of restraints ensured that the half model behaved like the full model.
- Restraints were placed at the support end in the X direction at all nodes. Only the node along the horizontal neutral axis of the cross-section lying in the plane of symmetry of the model is restrained in the Y direction. All the nodes on the horizontal neutral axis of the cross-section are restrained in the Z direction.

This set of restraints ensured that the cross-section was free to expand and contract due to Poisson's effects, but behaved like a fixed connection for the loads applied. It is important to note that the fixed end restraints just described had to be coupled with applied support forces to accurately create the fixed condition.

Early in the testing program, it was discovered that a true fixed boundary condition, where every node was restrained in the X, Y and Z directions at the support, caused tension field action in some beams at certain lengths. This phenomenon is shown in the Figure 3.1. The beam in the Figure 3.1 is a 10 ft long W36x798 with a 10,000 kip load applied at the tip of the cantilever. The lightly colored areas denote compression and the dark colored areas denote tension. The stress contours should have shown compression in the bottom half of the beam along the entire length and tension in the top of the beam.

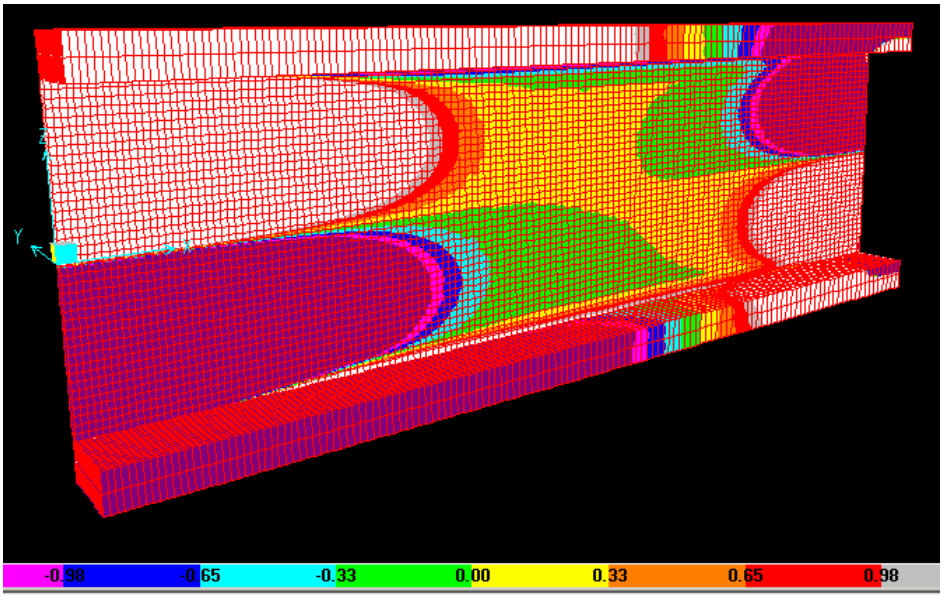

Figure 3.1 – Tension field action due to fixed boundary condition

To combat this problem, two steps were taken. First, the fixed boundary conditions were modified as previously mentioned. Second, the load at the tip was applied differently and equal and opposite loads were added at the support. The loads were modified to more closely resemble the shear stress distribution in a rectangular section. For a rectangular section, the shear stress diagram is parabolic, reaching a maximum at the neutral axis. Since the applied loads could only be nodal, they were scaled to resemble the shear stress distribution. Also, the equal but opposite loads, with the same distribution, were applied at the fixed boundary condition. This was done to create an ideal shear stress distribution at the support as at the free end. As stated earlier, the new restraints coupled with the applied support forces at the fixed boundary condition aided in creating an ideal stress distribution.

Another source of error was size of the solid elements and their aspect ratios. To minimize errors of this sort, the maximum aspect ratio of the elements was kept close to 1.0

and the element sizes were kept below 0.75 in. It was not difficult to maintain an aspect ratio nearly equal to 1.0 in the rectangular sections. The number of elements across the sections was increased to keep the size of the elements less than 0.75 in. To further minimize error, deflection values were measured at interior points in the beam span. At the fixed boundary and at the end of the beam where the load was applied, the stress contours were not smooth and consistent. They were greatly improved due to the variable loads and improved support conditions, but they were still not totally smooth and consistent. Therefore, deflection values were measured at a distance of 20% and 30% of the total span within the beam from the ends. The two percentages were chosen over others because, at the outset, it was not clear how far the points needed to be moved in from the ends to effectively remove end effects. By trial and error, it was found that these two values provided consistent answers and also allowed for a maximum portion of the beam to be used in the calculation of the shear area.

In the incipient stages of analyzing the rectangular sections, it was found that the FED method was not giving accurate answers. The values of shear area were reasonably accurate only when the Poisson's ratio was set nearly equal to zero. The models were refined to a great extent and many combinations of boundary conditions, loading conditions and element sizes were used to improve the accuracy but to no avail. It was surprising that the FED method provided answers of high accuracy for wide flange sections. This was surprising as well as perplexing as no satisfactory explanation could be found the discrepancy. Eventually the FED method was abandoned for rectangular sections. Further, it was used for wide flange sections only as a means of checking the answers from the DPF method.

3.2 3-D Finite Element Analysis of Rectangular Section

The finite element analysis procedure described in Appendix B was used to compute the moments of inertia and the form factors for a variety of cantilever beams with rectangular cross sections. Analysis was performed for beams with span-to-depth ratios of 2, 3, and 4, and with width to depth ratios of 0.25, 0.5, 1.0, and 2.0. It should be noted that the finite element analyses were run with element aspect ratios as close as possible to 1.0 and a mesh of sufficient density was used to provide a convergent solution. The loads at the ends were applied uniformly across the width of the section in a manner which minimized the stress concentrations at the loaded and supported end.

3.2.1 Effect of Stress Function on Shear Stress Distribution for Rectangular Sections

Before discussing the results for shear area from the finite element analyses, it is interesting to discuss the τ_{zx} shear stresses reported for sections with various width to depth ratios for different values of Poisson's ratio. The stress function, ϕ, provided in Timoshenko and Goodier (1970), is a function of the width and the depth of the section. It is in the form of an infinite series and is used to determine the correction to be applied to the stresses obtained by elementary beam theory. It is developed for any given section by solving the equilibrium conditions and compatibility conditions on the boundary of the section. The correction to the stresses is provided for τ_{zx} stresses and also for τ_{yx} stresses. But since the τ_{yx} stresses are zero from the elementary beam theory, the corrections are the net resultant τ_{yx} stresses in the section. Figure 3.2 shows the rectangular section used for determining the stress function. The

corrective stresses are applied accordingly since the nomenclature and orientation of the rectangular section considered are different from those adopted for this thesis.

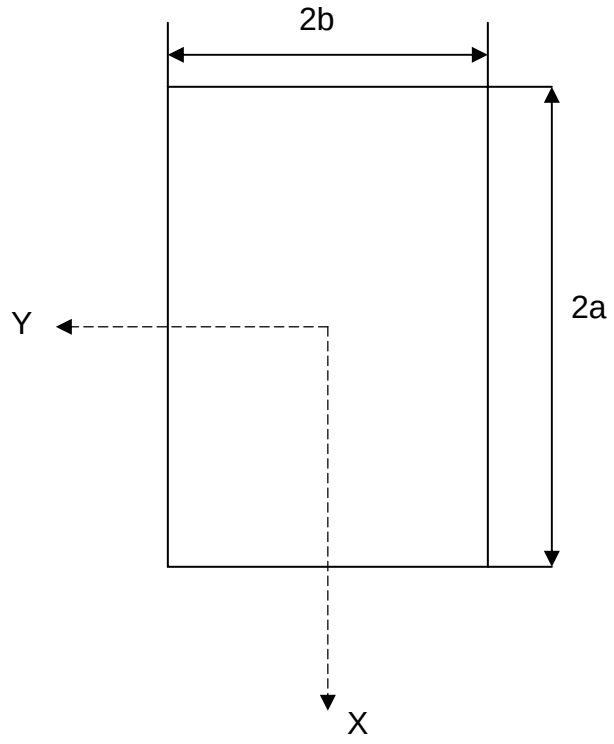

Figure 3.2 – Rectangular cross section used for stress function

For a rectangular section, the stress function, ϕ, given by Timoshenko and Goodier (1970), is

$$\phi = \frac{-\nu}{1+\nu}\frac{P}{I}\frac{8b^3}{\pi^4}\sum_{m=0}^{\infty}\sum_{n=1}^{\infty}\frac{(-1)^{m+n-1}\cos\dfrac{(2m+1)\pi x}{2a}\sin\dfrac{n\pi y}{b}}{(2m+1)n\left[(2m+1)^2\dfrac{b^2}{4a^2}+n^2\right]} \quad \text{..... (3.1)}$$

The parabolic stress distribution from the elementary beam theory is given as follows:

$$\tau_{xz}' = \frac{P}{2I}\left(a^2 - x^2\right) \text{ and } \tau_{yz}' = 0 \quad \text{.. (3.2)}$$

The correction to the stresses from elementary beam theory is given by

$$\tau_{xz}'' = \frac{\partial \phi}{\partial y} \text{ and } \tau_{yz}'' = -\frac{\partial \phi}{\partial x} \quad \text{..(3.3)}$$

Thus, from equations 3.1 and 3.3

$$\tau_{xz}'' = \frac{-\nu}{1+\nu}\frac{P}{I}\frac{8b^2}{\pi^3}\sum_{m=0}^{\infty}\sum_{n=1}^{\infty}\frac{(-1)^{m+n-1}\cos\frac{(2m+1)\pi x}{2a}\cos\frac{n\pi y}{b}}{(2m+1)\left[(2m+1)^2\frac{b^2}{4a^2}+n^2\right]} \quad \text{.......................... (3.4)}$$

and

$$\tau_{yz}'' = \frac{-\nu}{1+\nu}\frac{P}{I}\frac{4b^3}{a\pi^3}\sum_{m=0}^{\infty}\sum_{n=1}^{\infty}\frac{(-1)^{m+n}\sin\frac{(2m+1)\pi x}{2a}\sin\frac{n\pi y}{b}}{n\left[(2m+1)^2\frac{b^2}{4a^2}+n^2\right]} \quad \text{.......................... (3.5)}$$

Hence

$$\tau_{xz} = \tau_{xz}' + \tau_{xz}'' \quad \text{.. (3.6)}$$

$$\tau_{yz} = \tau_{yz}' + \tau_{yz}'' \quad \text{.. (3.7)}$$

Table 3.1 shows the values of correction to be added to the stress obtained by elementary beam theory at the neutral axis for sections of varying *b/d* ratios. The values are calculated for a section with *b=5* inches and *v*=0.3. Note that the values have been normalized with respect to the average stress across the section. These values shall be added to *1.5* to obtain the total stress at the neutral axis of the section in terms of the average stress across the section.

Table 3.1 – Variation of correction to stresses at neutral axis of section

b/d	Distance along the width of the section (inch)										
	2.5	**2**	**1.5**	**1**	**0.5**	**0**	**-0.5**	**-1**	**-1.5**	**-2**	**-2.5**
0.25	0.014	0.007	0.001	-0.004	-0.006	-0.007	-0.006	-0.004	0.001	0.007	0.014
0.5	0.056	0.026	0.002	-0.015	-0.025	-0.029	-0.025	-0.015	0.002	0.026	0.056
1	0.213	0.096	0.006	-0.056	-0.092	-0.104	-0.092	-0.056	0.006	0.096	0.213
2	0.664	0.240	-0.021	-0.162	-0.229	-0.249	-0.229	-0.162	-0.021	0.240	0.664
4	1.622	0.286	-0.163	-0.296	-0.329	-0.339	-0.329	-0.296	-0.163	0.286	1.622

Figure 3.3 shows the total stress at the neutral axis of the section for the sections considered in Table 3.1. The stress values have been normalized with respect to the average stress across the section.

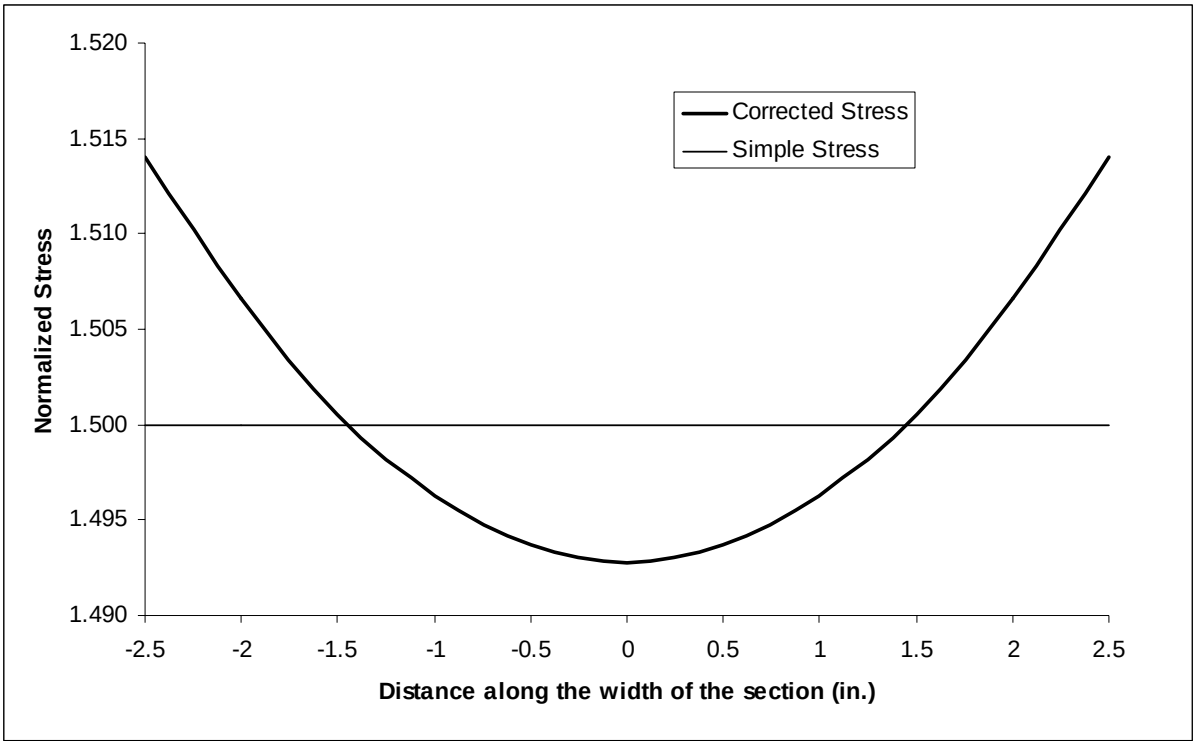

a) b/d = 0.25

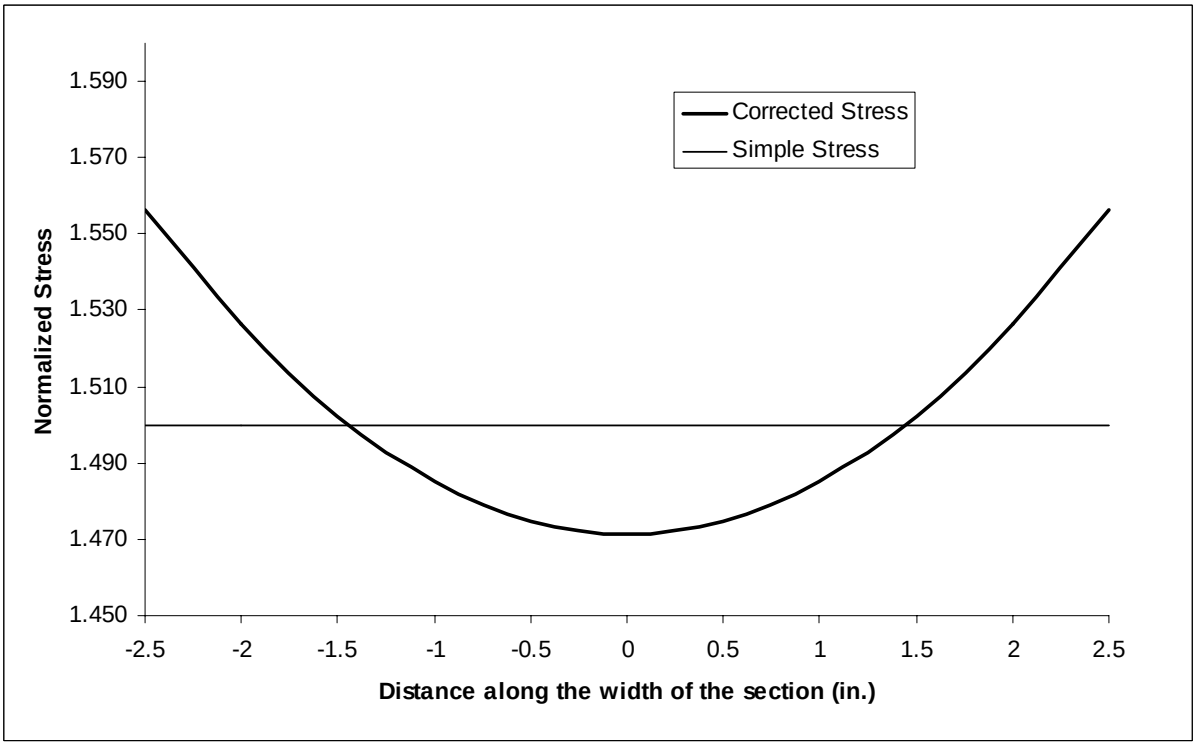

b) b/d = 0.5

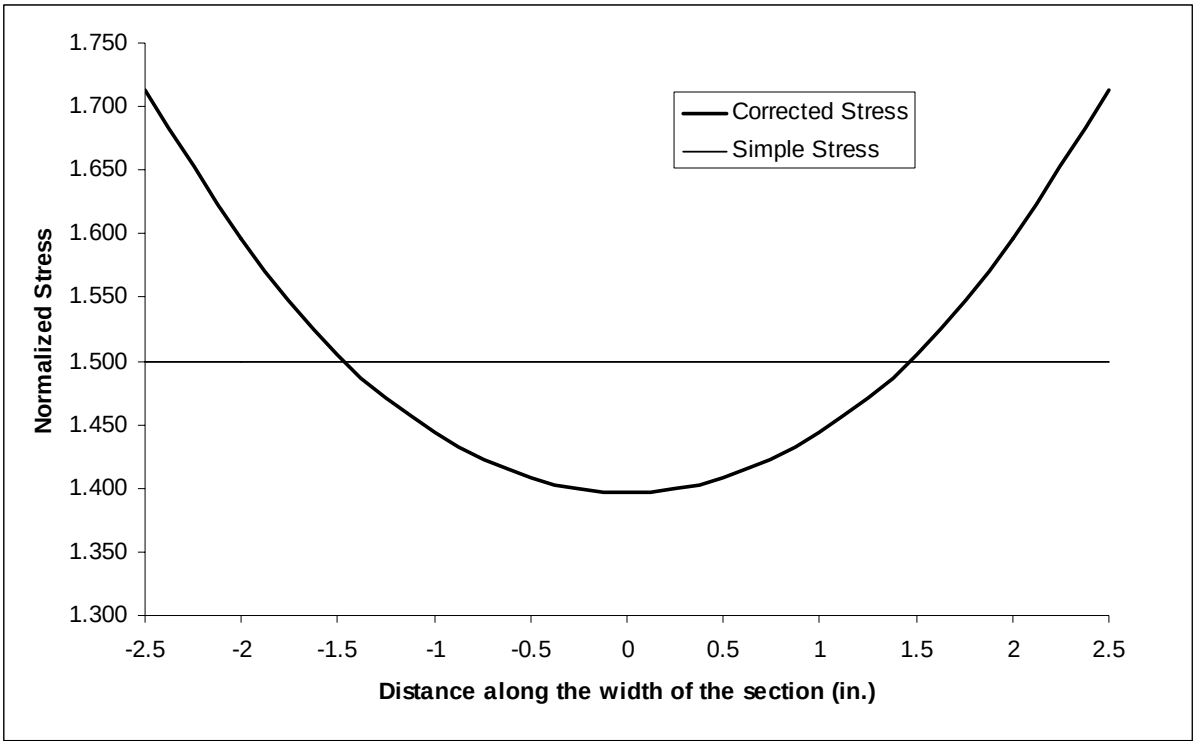
1.750
1.700
1.650
1.600
1.550
1.500
1.450
1.400
1.350
1.300
Normalized Stress
Corrected Stress
Simple Stress
-2.5
-2
-1.5
-1
-0.5
0
0.5
1
1.5
2
2.5
Distance along the width of the section (in.)

c) b/d = 1

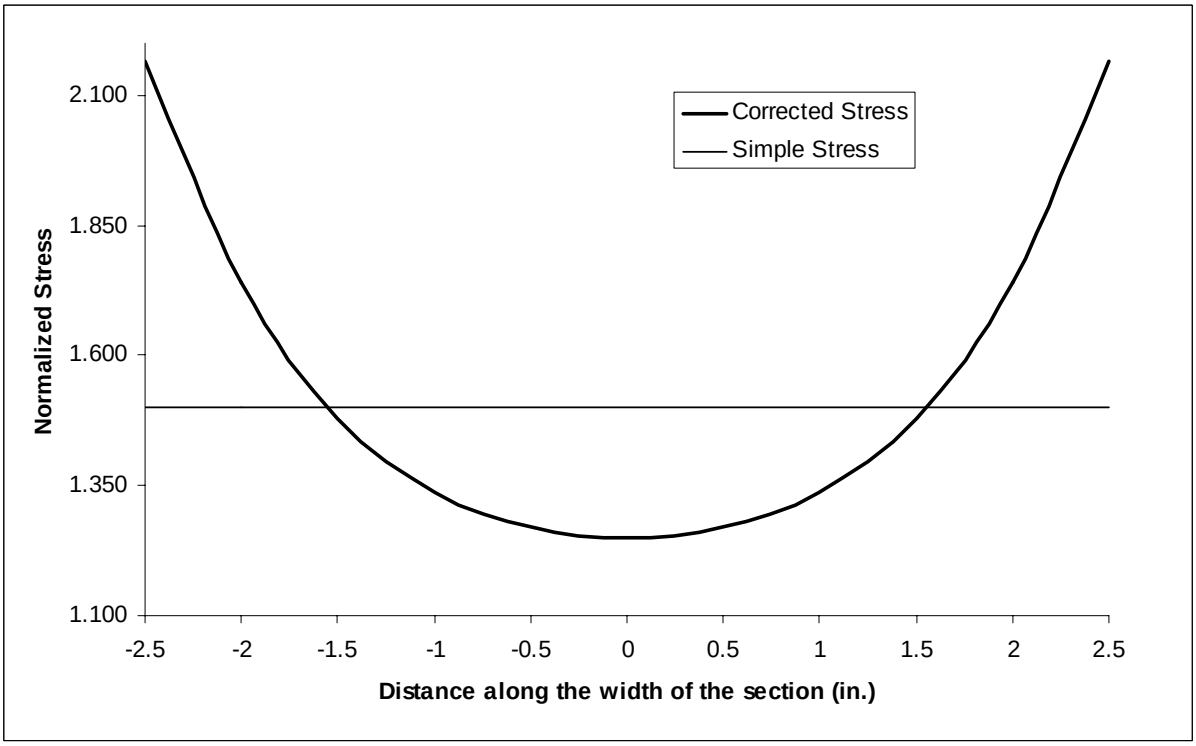
2.100
1.850
1.600
1.350
1.100
Normalized Stress
Corrected Stress
Simple Stress
-2.5
-2
-1.5
-1
-0.5
0
0.5
1
1.5
2
2.5
Distance along the width of the section (in.)

d) b/d = 2

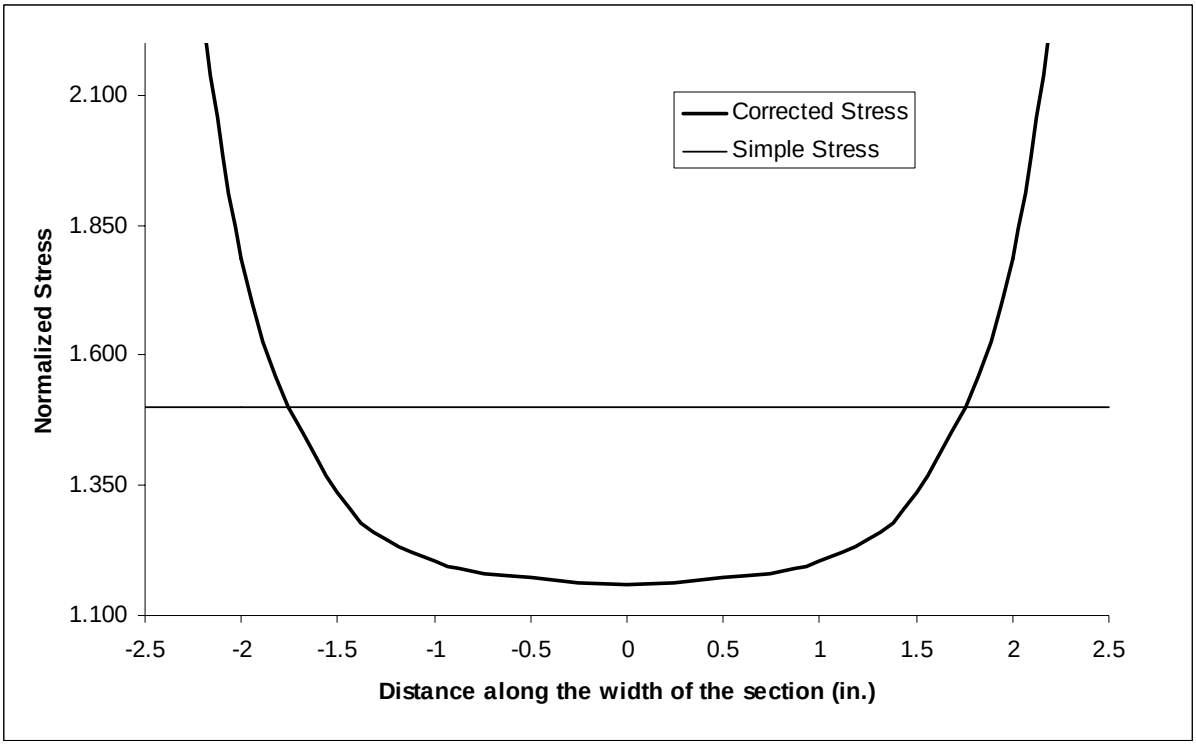

e) b/d = 4

Figure 3.3 – Shear stress values for rectangular sections with various aspect ratios. (*ν=0.3*)

Based on Table 3.1 and Figure 3.3, the following observations can be made about the corrective stresses and the stress distribution:

1) The exact shear stress at any point on a cross section consists of two terms, the stress from simple beam theory plus a correction that depends on Poisson's ratio and on the width to depth ratio of the section.
2) The correction applies to τ_{yx} stresses and also to the τ_{zx} stresses.
3) The sum of the corrective shear stresses across the width is exactly zero.

4) The average shear stress, inclusive of the corrective stress, across the width of the section at the neutral axis is 1.5*P*/*A*.
5) The corrective stresses approach zero for sections with width to depth ratios much less than one, but can dominate the solution when the width to depth ratio is much greater than one.
6) The corrective stresses have maxima at the edges of the neutral axis of the section.
7) The corrective stresses are zero when Poisson's ratio approaches zero.

Figure 3.4 shows these stresses as contours on the full cross section. The results are shown for beams with a span to depth ratio of 4. Contours for other span to depth ratios were similar. It should be noted that the stresses are normalized by dividing the computed stress by the average shear stress. Simple beam theory predicts a stress ratio of 1.5 across the full width at the neutral axis of each section, zero stress at the extreme fibers, and a parabolic distribution between the extreme fiber and the neutral axis.

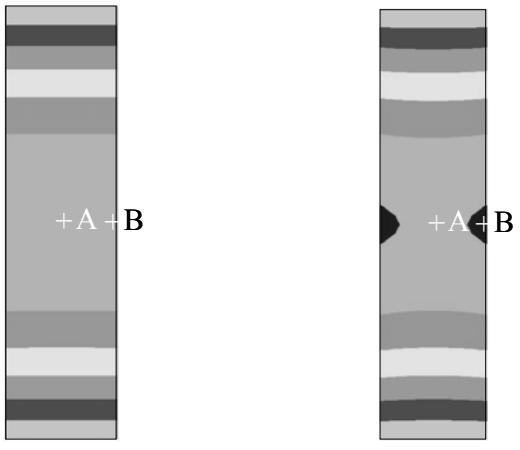

$\nu = 0.01$ $\nu = 0.30$

a) *b*/*d* = 0.25

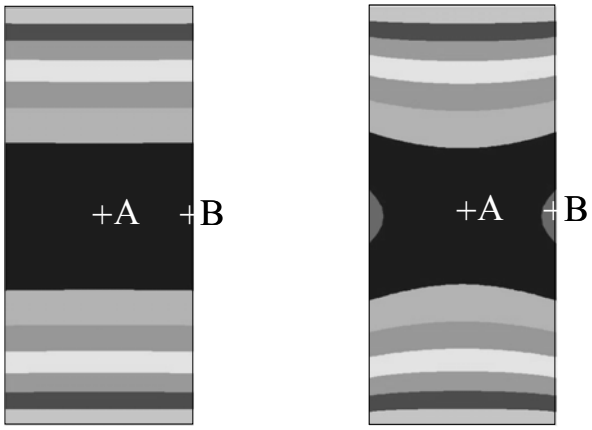

$v = 0.01$ $v = 0.30$

b) $b/d = 0.5$

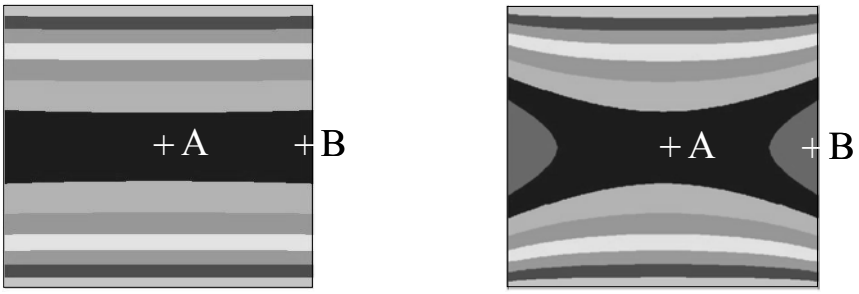

$v = 0.01$ $v = 0.30$

c) $b/d = 1$

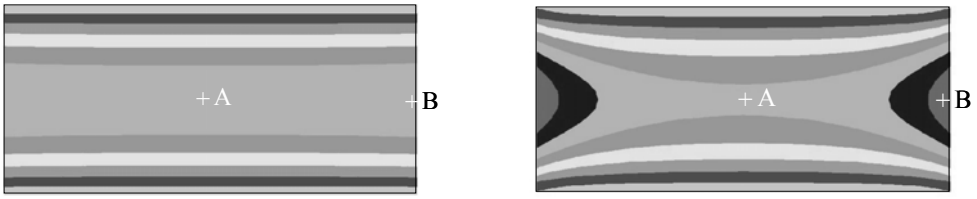

$v = 0.01$ $v = 0.30$

d) $b/d = 2$

Figure 3.4 – Shear stress contours from finite element analysis of rectangular sections (L/d=4)

In Figure 3.4a, where b/d=0.25, it is seen that there are slight differences in the contours of stress ratio when v=0.01 or v=0.30. The analysis was run with v=0.01 instead of v=0.0 because SAP2000 does not allow v to be exactly zero. For v=0.01, the bands of shear stress are horizontal and correspond exactly to the values calculated by simple beam theory. When v=0.30, the shear stress pattern is more complex and was similar to the distribution obtained using the stress function from the theory of elasticity. This agreement is seen in Table 3.2 which shows stress ratios computed at points A and B of each cross section. As with Figure 3.4, Table 3.2 is based on the analysis of beams with a span to depth ratio of 4.

Table 3.2 – Stress Ratios from Finite Element Analysis and from Theory of Elasticity (L/d=4)

b/d Ratio	Location in Section	v=0.01		v=0.30	
		FEA	Theory	FEA	Theory
0.25	A	1.500	1.500	1.491	1.493
	B	1.500	1.501	1.513	1.514
0.50	A	1.498	1.499	1.470	1.471
	B	1.502	1.502	1.557	1.558
1.00	A	1.495	1.496	1.400	1.397
	B	1.507	1.509	1.716	1.718
2.0	A	1.489	1.489	1.310	1.251
	B	1.519	1.529	2.093	2.185

3.3. Results from DPF Analysis

Results from analyses with relatively wider sections indicate increasingly larger differences in the resulting stress ratios with v=0.01 and 0.30. The comparison of the computed stress ratios at points A and B indicates that the stress patterns closely follow those predicted by theory, but also shows that the correlation is poorer when the width to depth ratio increases. In no case, however, do the differences in computed stress ratios versus theoretical

stress ratios differ by more than 0.5 percent. While it is not shown in Figure 3.3 or in Table 3.2, the comparison between the computed and theoretical stress ratios degraded to an appreciable extent when beams with smaller span to depth ratios were analyzed. This is likely due to the difficulty of eliminating the end effects in the beams of shorter span.

Tables 3.3 and 3.4 present the moments of inertia and the form factors that have been recovered from the finite element analysis. Moments of inertia are presented in terms of generic length units. These tables are based on analyses with Poisson's ratio of 0.01 and 0.3. From Table 3.3, where Poisson's ratio is 0.01, it may be observed that the finite element analysis was able to recover the moment of inertia with great accuracy in all cases. The form factors computed by finite element analysis were very close to the solutions provided by Cowper (1966) and Renton (1991).

Table 3.3 – Results of Finite Element Analysis on Rectangular Sections (ν= 0.01)

L/*d*	*b*/*d*	Moment of Inertia (L^4)		Form Factor		
		Actual	FEA	Cowper	Renton	FEA
2	0.25	3333.3	3330.7	1.199	1.200	1.196
	0.50	416.7	416.3	1.199	1.200	1.196
	1.0	52.1	52.1	1.199	1.200	1.197
	2.0	6.51	6.48	1.199	1.200	1.196
3	0.25	3333.3	3330.7	1.199	1.200	1.199
	0.50	416.7	416.3	1.199	1.200	1.199
	1.0	52.1	52.0	1.199	1.200	1.198
	2.0	6.51	6.48	1.199	1.200	1.198
4	0.25	3333.3	3330.7	1.199	1.200	1.198
	0.50	416.7	416.3	1.199	1.200	1.199
	1.0	52.1	52.0	1.199	1.200	1.199
	2.0	6.51	6.48	1.199	1.200	1.198

Table 3.4 – Results of Finite Element Analysis on Rectangular Sections (v=0.3)

L/*d*	*b*/*d*	Moment of Inertia (L^4)		Form Factor		
		Actual	FEA	Cowper	Renton	FEA
2	0.25	3333.3	3331.0	1.177	1.200	1.196
	0.50	416.7	416.3	1.177	1.201	1.196
	1.0	52.1	52.0	1.177	1.207	1.202
	2.0	6.51	6.60	1.177	1.275	1.209
3	0.25	3333.3	3330.6	1.177	1.200	1.199
	0.50	416.7	416.3	1.177	1.201	1.199
	1.0	52.1	52.0	1.177	1.207	1.205
	2.0	6.51	6.53	1.177	1.275	1.230
4	0.25	3333.3	3330.7	1.177	1.200	1.198
	0.50	416.7	416.3	1.177	1.201	1.200
	1.0	52.2	52.0	1.177	1.207	1.206
	2.0	6.51	6.50	1.177	1.275	1.248

As shown in Table 3.4 where Poisson's ratio is 0.3, the finite element analysis was again able to recover the moment of inertia almost exactly. The form factors produced by Cowper's formula and Renton's formula are somewhat different; in Cowper's expression the form factor decreases with increased Poisson's ratio, and in Renton's expression the form factor increases with Poisson's ratio. The finite element analysis follows the trend predicted by Renton's expression and the agreement is particularly good when the span-to-depth ratio was 4.0.

The fact that the finite element analysis method as applied to rectangular sections is able to recover moments of inertia exactly and form factors with very good accuracy (as compared to Renton) indicates that the method should be applicable to wide flange sections as well. The other main conclusions drawn from the analysis are that Timoshenko's form factor

of 1.5 is not valid and that a form factor of 1.2 is sufficiently accurate for analysis of rectangular sections with depth equal to or greater than width.

Chapter 4 Wide Flange Sections

Due to disparity in the values of shear area reported by the various expressions in the literature, it is imperative to perform a three-dimensional finite element analysis to ascertain the "exact" shear area. As stated earlier, values of shear area are "exact" within the limits of finite element analysis. The following sections describe the development of the model for finite element analysis about the strong and the weak axis, the analysis procedure and the results of the analysis.

4.1 Strong Axis Model for Finite Element Analysis

The wide flange sections were modeled about the strong axis using eight-node solid elements in SAP2000 v7.44 (CSI, 2002). Only half of the cross-section of the beams was modeled to increase computational efficiency and permit higher mesh density across the model. Beams were oriented such that the beam length extended in the X direction, the cross-section strong axis was along the Y direction and the weak axis was along the Z direction. The applicable boundary conditions are as follows:

- Restraints were placed in the Y direction at the plane where the beams were cut in half. This set of restraints ensured that the half model behaved like the full model.
- Restraints were placed at the support end in the X direction at all nodes. Only the node along the horizontal neutral axis of the cross-section lying in the plane of

symmetry of the model is restrained in the Y direction. All the nodes on the horizontal neutral axis of the cross-section are restrained in the Z direction.

This set of restraints ensured that the cross-section was free to expand and contract due to Poisson's effects, but behaved like a fixed connection for the loads applied. It is important to note that the fixed end restraints just described had to be coupled with applied support forces to accurately create the fixed condition. The above procedure was adopted due to the presence of tension field action in some beams as explained in Chapter 3. The models of wide flange sections developed did not include the fillets found in the rolled sections. The fillets serve the purpose of reducing the stress concentration at the region of the web-flange interface. It will be established that neglecting the fillets in the model does not affect the calculation in an appreciable manner. The half models of the cantilever beams were generated by a special auxiliary program. The program was configured to create the input files for SAP2000 using the input data provided.

4.1.1 Element Discretization

In each of the cantilever half models, there were three types of elements with regard to geometry. They were web, flange, and union elements as labeled in Figure 4.1. The element dimensions for the model were determined as follows:

1) The number of nodes in the web was chosen. Typically, this was either two or three nodes, which would mean one or two elements respectively. $dYw = 0.5t_w$ if one

element is used through the width of web or $dYw = 0.25t_w$ if two elements are used through the width of the web.

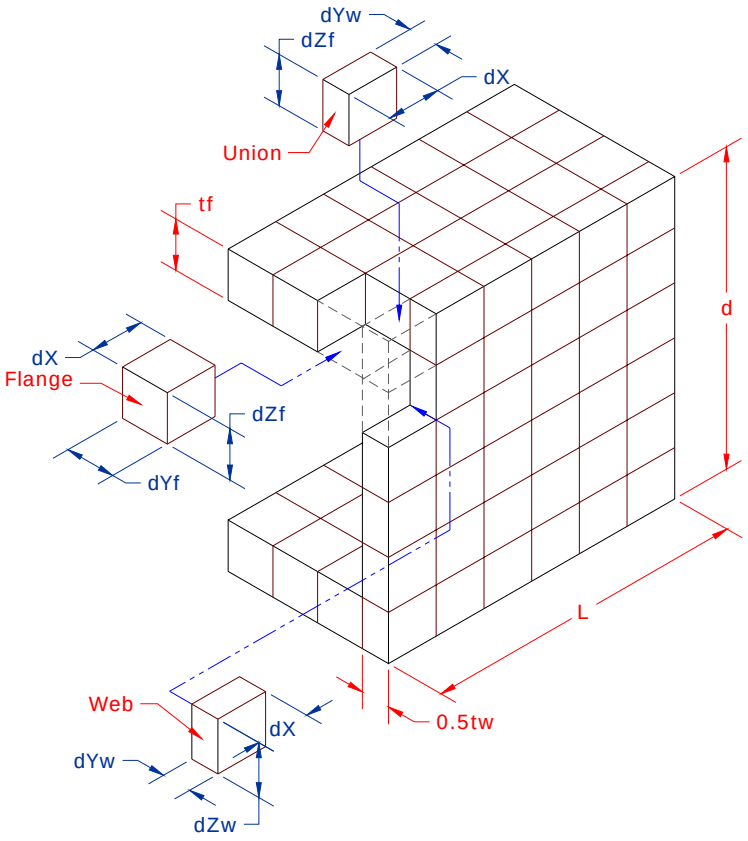

Figure 4.1 – Element discretization for wide flange section

2) The number of elements in the X direction, or along the length L, was determined. At this point, the user is allowed to input a desired maximum aspect ratio, which is defined as the ratio of the largest dimension of the element to the smallest dimension. The maximum number of elements allowed along the length was 999.

$$numX = \left\langle \frac{L}{AR \cdot dYw} \right\rangle Rounded\_to\_nearest\_whole\_number,$$

where *numX* is the number of elements in the X direction and *AR* is a specified maximum aspect ratio.

Then, $dX = \frac{L}{numX}$

Note that *dX* is the same for all elements.

3) The height of the web element was determined such that an even number of elements in the web would be obtained. This was done so that the origin of the system could be located in the middle of the web at the interface of two elements. This is desirable over the option of having the origin at the center of an element.

$$dZw = \left\langle 2\left(\frac{d - 2t_f}{2dX} \right) \right\rangle Rounded\_to\_nearest\_whole\_number$$

4) The height of the elements in the flanges was determined. The equations for the number and size are as follows:

$$numZf = \left\langle \frac{t_f}{dX} \right\rangle Rounded\_to\_nearest\_whole\_number \geq 1$$

$$dZf = \frac{t_f}{numZ}$$

The number of elements is limited by the fact that there has to be at least one element though the thickness of the flange.

5) The final elemental dimension is *dYf*. This is the width of an element in the flange, which is not part of the union of the web and the flange. The equations for the number and size of the elements are as follows:

$$numYf = \left\langle \frac{\frac{b_f}{2} - \frac{t_w}{2}}{dX} \right\rangle Rounded\_to\_nearest\_whole\_number$$

$$dYf = \frac{\frac{b_f}{2} - \frac{t_w}{2}}{numYf}$$

4.1.2 Note on Specified and Resultant Aspect Ratios:

In the determination of element sizes, there were essentially two significant aspect ratio quantities. The first is the specified aspect ratio. This was a user defined quantity which only applied to web elements and applied only to the Y dimension of the web element. In other words, the web elements could be smaller in the Y direction than in the X and Z direction by a specified aspect ratio. The specified aspect ratio was never higher than 1.9. In most cases, it was less than 1.6. The second type of aspect ratio is called, for the sake of discussion, the resultant aspect ratio. The resultant aspect ratios are all the aspect ratios other than the specified aspect ratio. In most situations, the resultant aspect ratios were approximately one. In all three types of geometry, the resultant aspect ratios in cross-sections

tended to be greater than one when the flanges or web were thin. It is important to note however, that even when the resultant aspect ratios exceeded one, they were typically less than 1.2. In a very few cases, the aspect ratio climbed to 1.4.

4.1.3 Influence of Aspect Ratio on Shear Area

It must be mentioned, that the specified aspect ratios did influence the shear area values calculated by finite element analysis. However, the influence was minimal when the aspect ratios were monitored and kept within limits. The influence of specified aspect ratio for three different cross-sections is provided in the Figures 4.2 – 4.4.

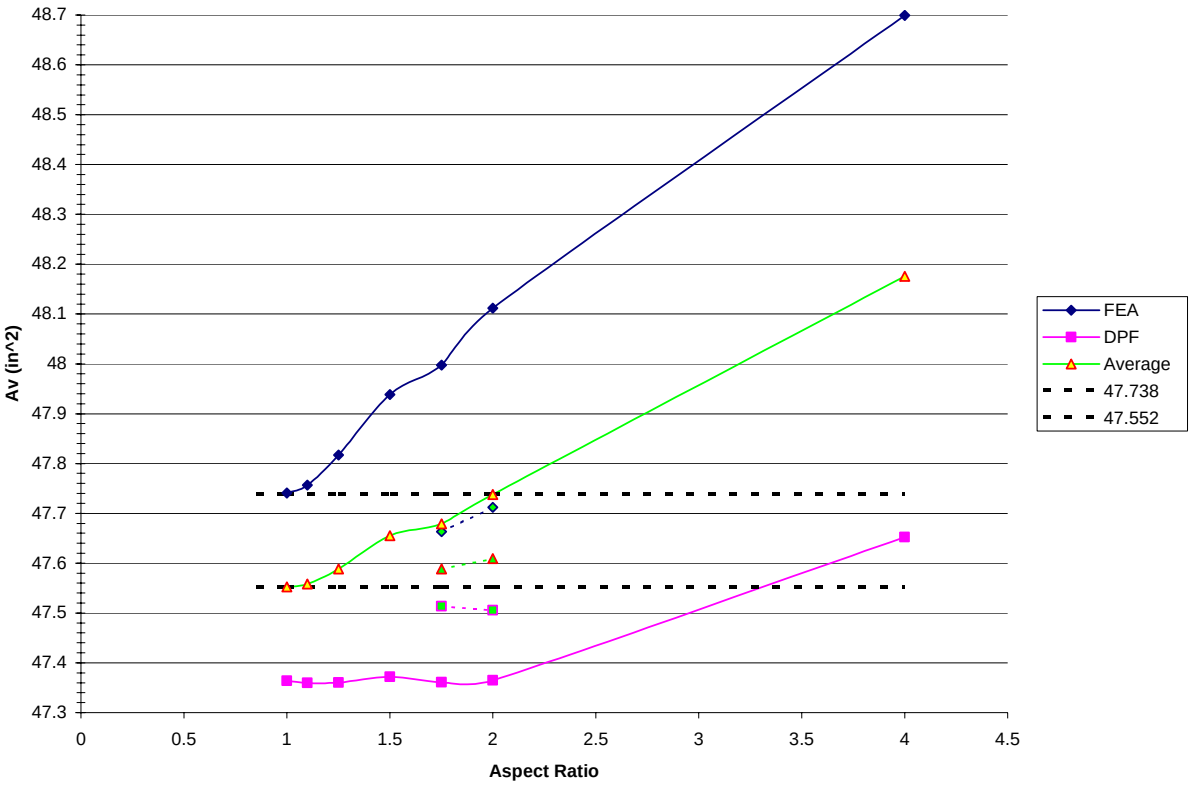

Figure 4.2 – W14x605 -- Shear area values for various specified aspect ratios

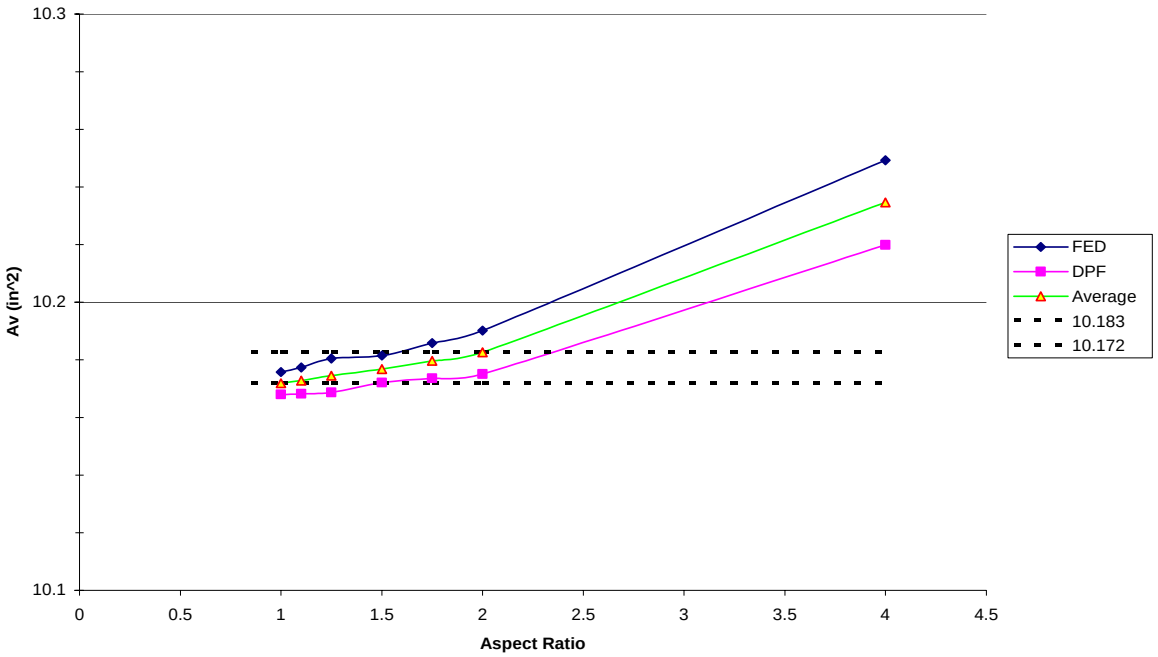

Figure 4.3 – W18x106 Shear area values for various specified aspect ratios

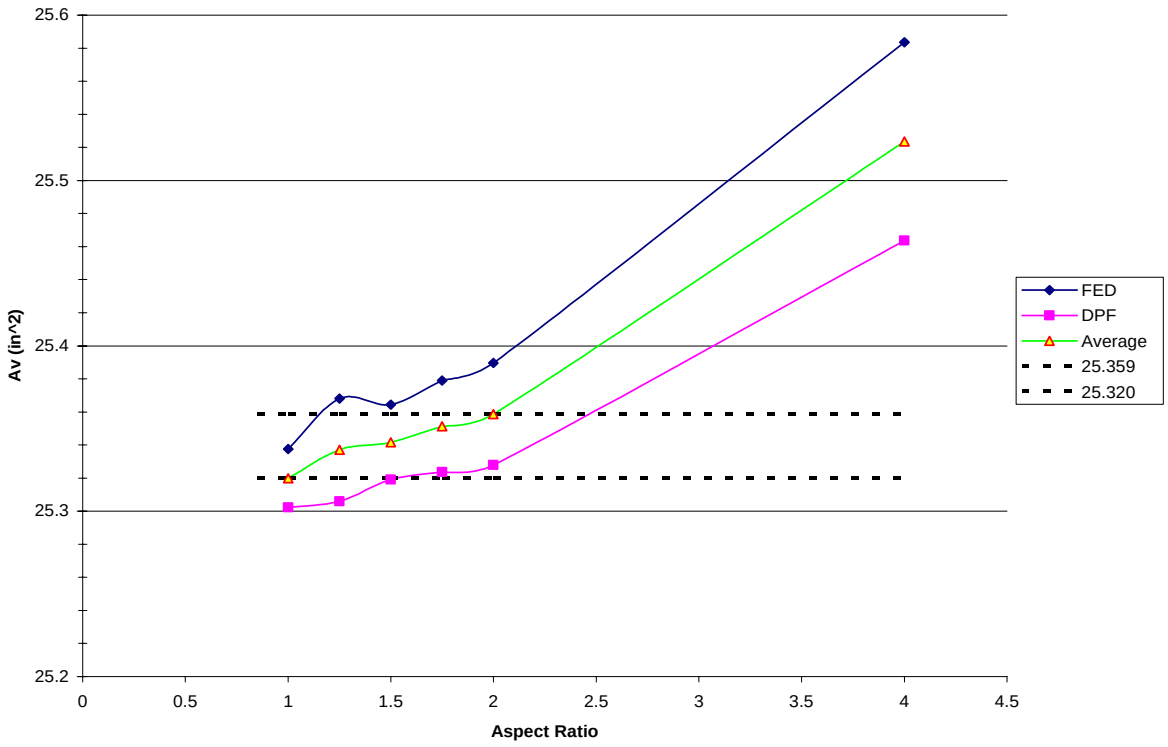

Figure 4.4 – W24x250 Shear area values for various specified aspect ratios

For all three of the cross-sections shown in Figures 4.2 – 4.4, the results from both the Finite Element Displacement method and the Displacement Participation Factor method are

plotted. Also included in the figures is the average of the FED and DPF methods. The average values were considered to be the true shear areas. Also included in the figure are lines which represent the average shear area values for specified aspect ratios of both one and two. The limits of one and two were chosen because the specified aspect ratios used throughout the actual analyses were limited to 1.9 as a maximum and one as a minimum.

It is clear from the above figures that the specified aspect ratio affects shear area determination. Ideally, those shear area values calculated with specified aspect ratios of approximately one will be the most accurate. However such a conclusion cannot be presumed. Hence it was decided that a better approach would be to minimize shear area variation caused by the specified aspect ratios. If the variation is minimized to negligible proportions, then the resulting shear area values would effectively be independent of specified aspect ratios.

Not only were the shear area values dependent on specified aspect ratios, they were also dependent on size of the element used in the model. This is best illustrated in Figure 4.2. In Figure 4.2, two sets of data are plotted. The first is represented with solid lines. All of the finite element models solved in this set had two elements through the thickness of the web. Thus the *Y* dimension of the element in the web was 0.65 inch. This resulted in elements that were approximately 0.65 inch cubes when the specified aspect ratio was one, and 1.25 inches in the *X* and *Z* direction when the specified aspect ratio was two. The difference in shear area values calculated using the specified aspect ratios of one and two was approximately 0.19 in^2. It was felt that such variance was excessive and so several other models were created and

solved, hence the broken line set of data. In the broken line set of data the number of elements through the thickness of the web was increased to four. This resulted in elements that were approximately half the sizes of those used in the first set. By increasing the number of elements in the web and thereby reducing the sizes of the elements, the shear area values approached those calculated when the specified aspect ratio was closer to one. In a similar manner, the amount of variance between the cross-sections was influenced by element sizes. Table 4.1 summarizes this phenomenon.

Table 4.1 – Summary of Aspect Ratio and Element size Variation related to Shear Area Variation

Section	Cubic Element Size (in.)		A_v Variation between Aspect Ratios of 1 and 2 (in^2)
	Aspect Ratio = 1	***Aspect Ratio = 2***	
W14x605	0.65	1.25	0.186
W18x106	0.29	0.59	0.011
W24x250	0.51	1.00	0.039

As one might expect, Table 4.1 shows that the element sizes increase by a factor of approximately two when the specified aspect ratio is increased from one to two. Moreover, from Table 4.1, it is clear that the element size has a significant impact on the variation in shear area calculation. For these analyses, higher degrees of discretization resulted in increased accuracy. By examining the effects of specified aspect ratio and element size on shear area calculation, conditions were established whereby error would be minimized. Those conditions were essentially twofold. Firstly, they sought to keep specified aspect ratios as

close to one as possible and always below two. Secondly, they sought to keep element sizes smaller than approximately 0.75 in. The models created for analysis satisfied both these conditions.

4.1.4 Load distribution

In wide flange beams, shear stress due to an applied load is not uniform throughout the section. It is assumed to be governed by the equation:

$$\tau = \frac{VQ}{It} \quad \text{..... (4.1)}$$

where V = Shear force

$Q = \int y \cdot dA$ = First moment of area

I = Moment of inertia with respect to the axis of loading

t = Width of the member at the location that the shear stress is calculated

A shear stress diagram for a wide flange section is parabolic in shape. However, since t has two different values, b_f and t_w, the shape of the shear stress diagram is discontinuous at the interface of the flange and web. An example of a shear stress diagram is presented in Figure 4.5. This stress distribution is valid only along the centerline of the section. The above distribution gives some value of stress at the interface of the web and flange. Also stresses are reported at the lower edge of the top flange and upper edge of the bottom flange. This is fictitious as there cannot be any stress on the lower and the upper edges of the top and bottom flanges. This is due to the fact that they are free surfaces and hence cannot have any shear stress under a transverse load. This is explained in detail in Popov (1976) and Ugural (1991).

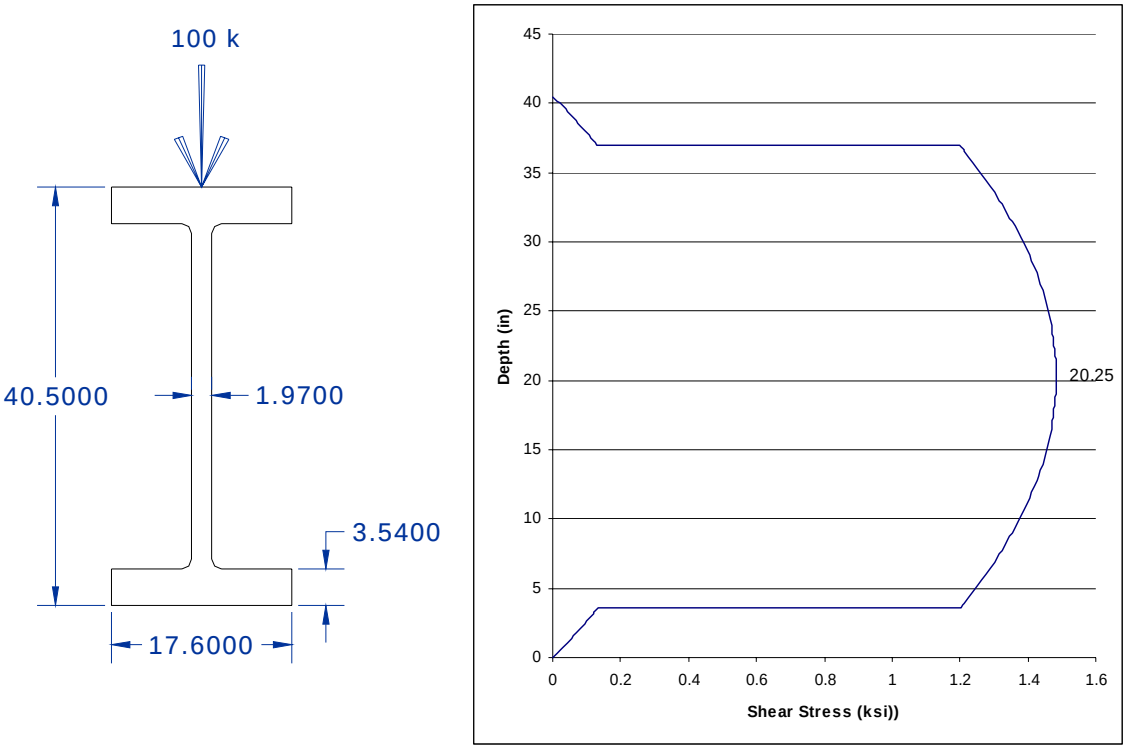

Figure 4.5 – Shear stress diagram for a W36x650 subjected to a 100 kip load

Since the actual shear stress in a wide flange section does not look like what is shown in Figure 4.5, the method of load application was modified to better reflect the actual stress distribution. Based on the stress distribution provided in Popov (1976) and Ugural (1991), a linear approximation of the shear stress was created. The linearized shear stress distribution is shown in Figure 4.6.

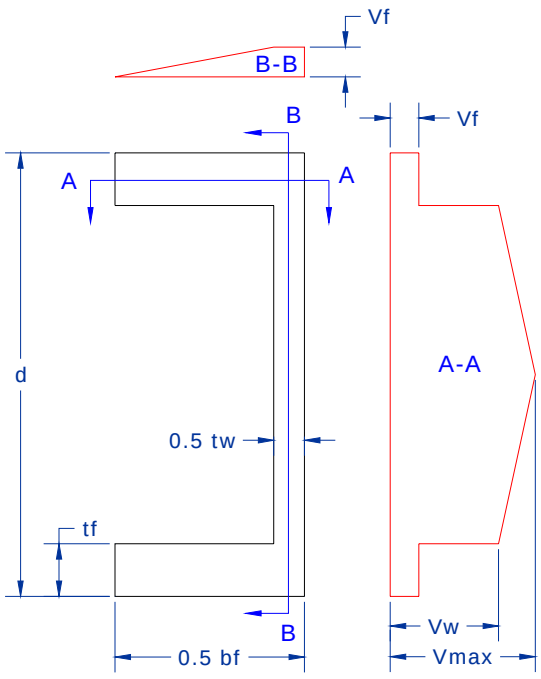

Figure 4.6 – Linearized approximation of shear stress in half model wide flange section

In the above diagram, two of the force values, V_f and V_w, were determined from equation 4.1. They are derived as follows:

$$Q_{\max-flange} = \left(\frac{d}{2} - \frac{t_f}{2}\right)\frac{b_f}{2}t_f \quad \text{..... (4.2)}$$

$$\tau_f = \frac{VQ_{\max-flange}}{I(0.5b_f)} \quad \text{..... (4.3)}$$

$$\tau_w = \frac{VQ_{\max-flange}}{I(0.5t_w)} \quad \text{..... (4.4)}$$

4.1.5 Effect of Fillets on Moment of Inertia

The models for finite element analysis did not include the fillets at the web-flange interface. This was due to the difficulty in modeling the fillets along with the model. Hence the models were run without the fillets. Table 4.2 shows the values of moments of inertia for various sections analyzed. The moments of inertia with and without fillets are hand-calculated and compared with the moment of inertia calculated by finite element analysis of the models.

Table 4.2 – Moments of Inertia with and without Fillets for Wide Flange Section

Section	Tabulated (in^4) (inc. Fillets)	Calculated (in^4) (No Fillets)	DPF (in^4) (No Fillets)	% difference (Calc. vs DPF)
W36x650	48900	48813	48786	0.05
W36x328	22500	22264	22412	-0.66
W36x232	15000	14838	14838	0.00
W33x387	24300	24294	24284	0.04
W33x263	15900	15696	15691	0.03
W33x201	11600	11413	11409	0.04
W24x335	11900	11830	11821	0.08
W24x250	8490	8437	8432	0.07
W24x94	2700	2671	2670	0.01
W21x201	5310	5282	5277	0.09
W21x111	2670	2644	2641	0.10
W21x62	1330	1311	1311	0.01
W18x175	3450	3432	3429	0.11
W18x97	1750	1733	1731	0.12
W18x55	890	879	879	0.02
W14x730	14300	14305	14167	0.97
W14x398	6000	6006	5964	0.70
W14x90	999	983	977	0.61

As shown in the table, there is no significant difference in the values of moment inertia. Hence the absence of fillets does not affect the stiffness of the model. If the effect of the fillet on moment of inertia is so low, the effect of the fillet on shear area should be equally low, and therefore negligible. It is also evident from Table 4.2 that the DPF method is able to

recover the moment of inertia with less than 1.0 percent error in all situations. This validates the ability of the DPF method to recover a known quantity and provides confidence that the method can be used successfully to recover shear area and form factors for the wide flange sections.

4.2 Results of Analytical Expressions

For all sections and for all weights there appear to be significant differences between the analytical expressions, and the relative applicability of the empirical expressions appears to vary with both depth and weight. Figure 4.7 provides the values of shear area using different expressions for some of the W14, W24 and W36 sections. The largest dispersion among results produced by the various expressions occurs for the heavier sections, particularly for the heaviest W14s. It is also noted that there appears to be consistent agreement between the results computed from Cowper's expression and those obtained from the empirical equation when the effective depth is taken as the depth between the centers of the flanges. Table 4.3 provides the values of form factors due to different expressions for some sections.

It is interesting to note that a clear trend emerges from Cowper's expression. Figure 4.8 plots the relationship between Cowper's form factor and the dimensionless parameter m for all sections in the AISC database. Recall that m is equal to $\frac{2b_f t_f}{dt_w}$. It is remarkable, given the complexity of the expression, that the form factors fall on a nearly straight line.

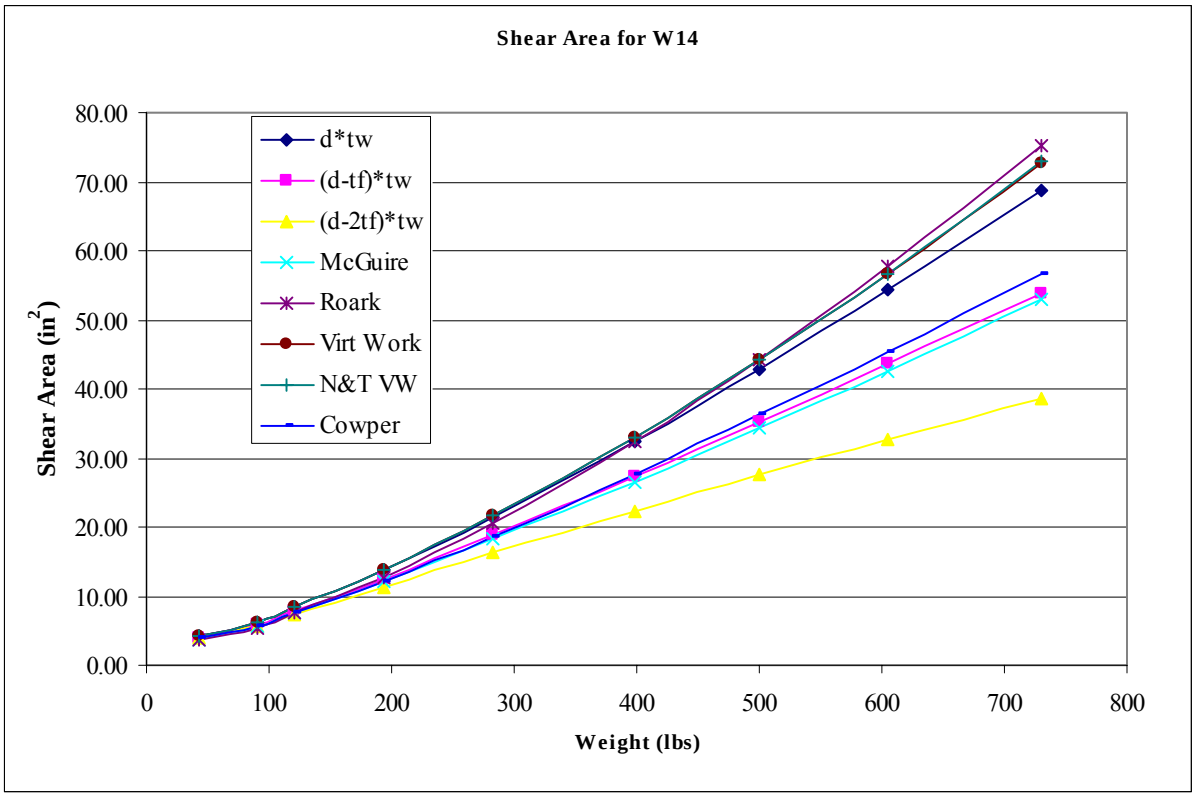

a) Shear area for W14 sections

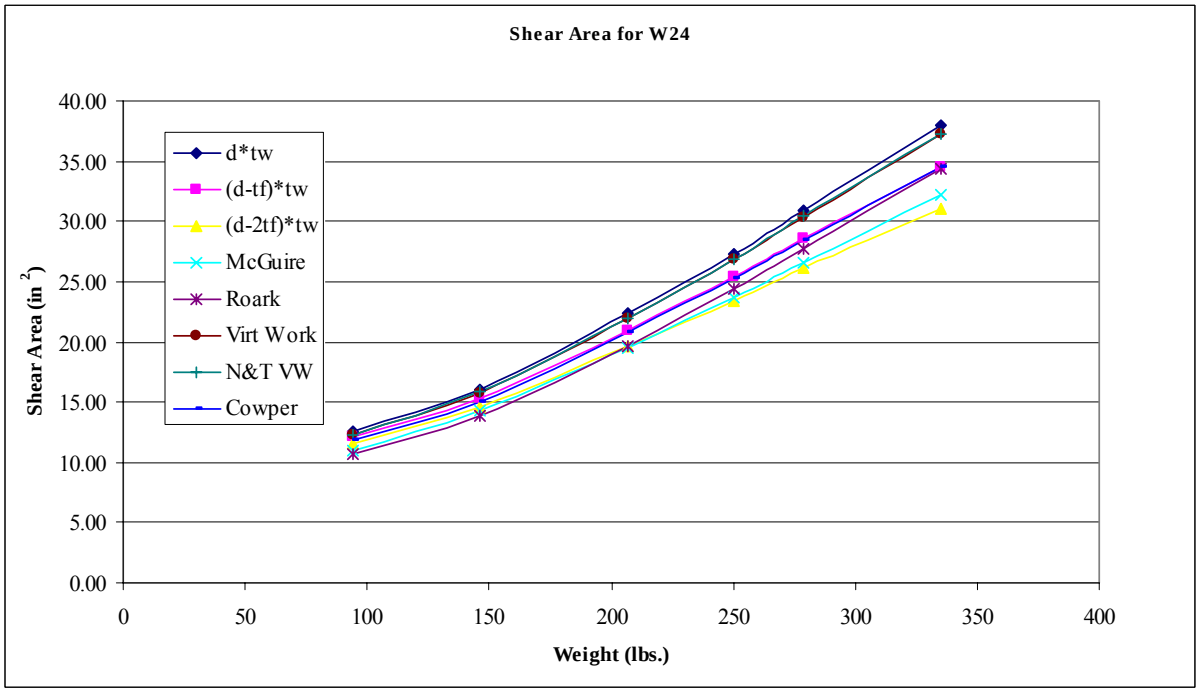

b) Shear area for W24 Section

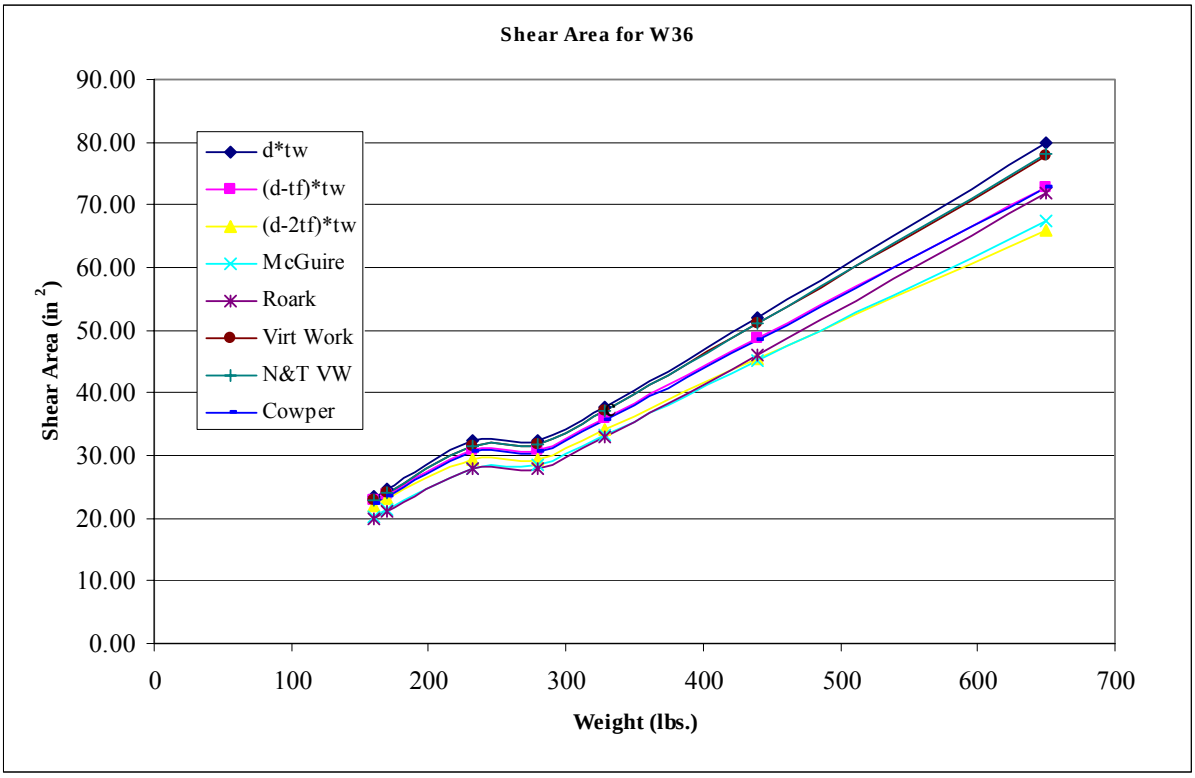

c) Shear area for W36 section

Figure 4.7 – Values of shear area for various sections using the different expressions

A trend line analysis of the data indicates that Cowper's form factor may be very accurately calculated using the following:

$$\kappa = 0.85 + 1.16m \quad \text{..... (4.5}a\text{)}$$

or

$$\kappa = 0.85 + 2.32\frac{b_f t_f}{dt_w} \quad \text{..... (4.5}b\text{)}$$

Table 4.3 – Variation of Form Factor values given by different expressions for some wide flange section

Section	Form Factor							
	N&T Virtual Work	N&T Simplified (Roark)	Timoshenko (McGuire)	Cowper (Pilkey, 1994)	Cowper Trend Line	Effective depth, d-2tf	Effective depth, d-tf	Effective depth, d
W14x730	2.9350	2.8470	4.0490	3.80	3.82	5.551	3.993	3.118
W24x250	2.7210	3.0090	3.0950	2.93	2.97	3.13	2.888	2.68
W36x135	1.8880	2.1760	2.1420	1.96	1.88	1.929	1.885	1.843

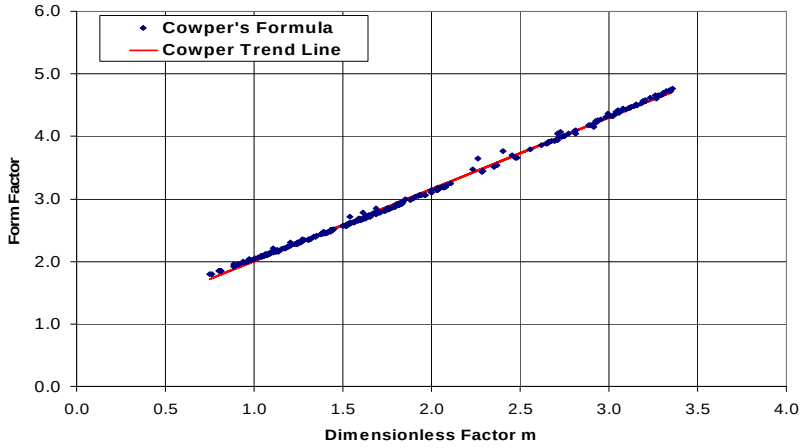

Figure 4.8 – Trend line analysis of Cowper form factors

Using equation 4.5, the form factors for the W14x730, W24x250 and W36x360 are 3.81, 2.97 and 1.88 respectively. These values shown in Table 4.3 are very consistent with those obtained from the full expression, which uses the much more complex formula.

4.3 Results of Strong Axis Finite Element Analysis

Several expressions have been presented for the form factor of wide flange sections, but it is not possible to assess the accuracy of any of them without obtaining an "exact" solution. Two different finite element analysis approaches were used to obtain such a solution. In one approach, the form factors were extracted using a virtual work analysis of the stress resultants computed from a finite element analysis of a three-dimensional cantilever beam. Appendix B provides details about the implementation of this method. The second finite analysis approach was exercised through a computer program available from Pilkey (2003). As discussed in Appendix B, the DPF approach is capable of reporting the section moment of inertia as well as the form factor. Since the moment of inertia is a known quantity for wide flange beams, the validity of the approach could be demonstrated if it were able to recover the moment of inertia.

Form factors computed using the DPF method are shown in Table 4.4. The portion of the form factor due to the web and the flange are provided, as are the actual values. As with all the previous solutions, the largest form factors are for the W14s, and the lowest form factors are for the W36s. Recalling that the lowest possible form factor is 1.2 (for a rectangular section), it is seen that the W14x90 is nearly four times more flexible in shear than a rectangle, while the W36x135 is only twice as flexible as the rectangle.

Table 4.4 – Form Factor Calculated from Finite Element Analysis

Section	Finite Element Analysis v=0.30			Pilkey v=0.30
	Web Contribution Value (%)	Flange Contribution Value (%)	Total	
W14x90	4.266 (89.2)	0.517 (10.8)	4.783	4.753
W14x398	3.496 (84.4)	0.646 (15.6)	4.142	4.128
W14x730	2.809 (80.1)	0.698 (19.9)	3.507	3.508
W24x94	2.244 (96.4)	0.084 (3.6)	2.328	2.314
W24x250	2.722 (94.0)	0.174 (6.0)	2.896	2.882
W24x335	2.621 (93.3)	0.188 (6.7)	2.809	2.795
W36x135	1.894 (96.9)	0.061 (3.1)	1.955	1.941
W36x328	2.564 (95.2)	0.130 (4.8)	2.694	2.680
W36x650	2.425 (93.8)	0.160 (6.2)	2.585	2.461

Table 4.5 – Form Factor Breakdown Calculated using Equation 2.15

	Section	Web Contribution Value (%)	Flange Contribution Value (%)	Total
Newlin & Trayer Virtual Work	W14x730	2.812 (95.8)	0.123 (4.2)	2.935
	W24x250	2.712 (99.7)	0.009 (0.3)	2.721
	W36x135	1.886 (99.9)	0.002 (0.1)	1.888

It is interesting to compare the results shown in Table 4.4 with those shown in Table 4.5, which provide the form factor breakdown for the virtual work solution based on shear stresses as determined from simple beam theory. Using the W14x730 as an example, the finite element analysis result from Table 4.4 indicates that the web portion of the form factor is 2.809, which is nearly identical to the web portion, 2.811, listed in Table 4.5. However, the finite element analysis computes a flange contribution of 0.698, while simple beam theory produced a flange contribution of only 0.123. Similarly, Table 4.4 indicates that the web contribution to the form factor for the W35x135 is 1.894, which is very close to 1.887 listed

in Table 4.5. In this case, however, the finite element analysis produced a flange contribution of 0.061, while the flange contribution from Table 4.5 is essentially zero.

The reason that the finite element analysis produces a higher flange contribution to the form factor than equation 2.15 may be seen from Figure 4.9. In this figure, the shear stress contours computed for the W14x730 section are shown. Plots of the actual shear stress from the finite element analysis and the shear stress from simple beam theory are given for the web and for the flange. For the web, the stresses from FEA and from simple beam theory are very consistent through almost the full depth between the flanges. A correlation of form factors for the web portions of the beam can be expected, therefore, because the stresses in this portion of the beam are nearly identical. On the other hand, there is almost no agreement between the stresses in the flange. Simple beam theory, which is based on equilibrium alone, predicts a uniform stress across the width of the flange at any depth. It also predicts the presence of shear stresses at the inner flange surface, which is impossible. Simple beam theory does, however, report the correct average stress across the flange. The finite element analysis predicts higher form factors for the flange portion of the section because the high intensity shear stresses at the flange-web intersection are squared in the form factor calculations. This may be seen in the most basic form of equation 2.12.

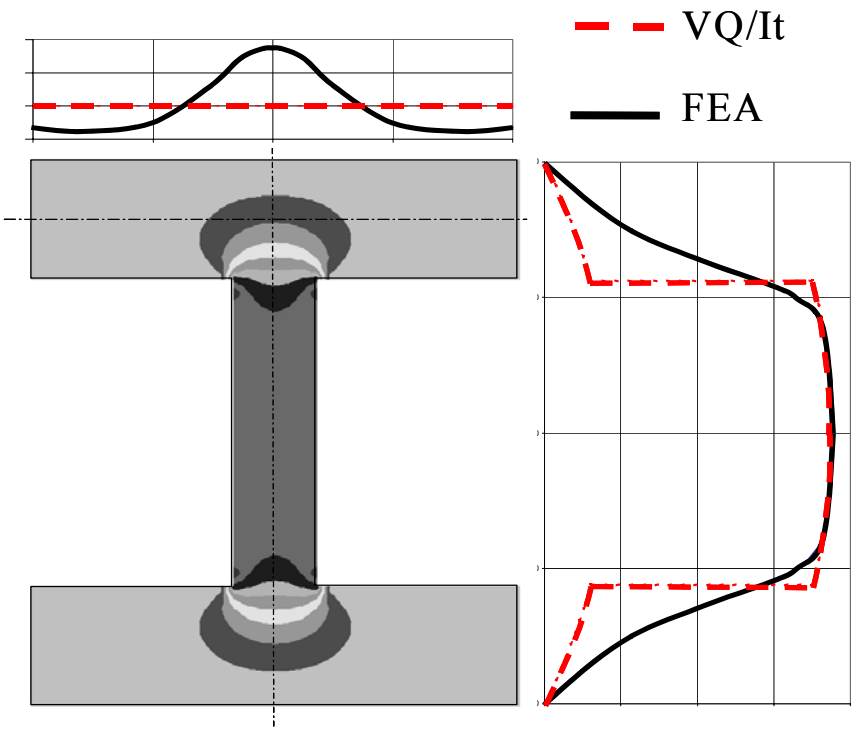

Figure 4.9 – Shear stresses in a wide flange section

Results using Pilkey's finite element analysis program are shown in Table 4.4. The program does not provide a breakdown of the flange and web component of the form factor. As is observed, the results are very consistent with those determined using the DPF approach. It is noted, however, that the DPF results indicate greater differences in the form factor when the analysis was run with Poisson's ratios of 0.3 and 0.01 than were obtained from Pilkey's program. In both cases, however, the effect of Poisson's ratio was negligible.

Given all the analytical expressions and finite element analysis results, it is clear that Cowper's analytical solution, provided by equation 2.18, provides the best correlation with the finite element analysis. It is clear that for all sections, except for the heavier W14s, that Cowper's expression provides an excellent match when compared to the finite element

analysis. The simple empirical formula provides a good match as well, but has the tendency to slightly underestimate the form factor in most cases, with the exception again being the heavier W14s.

Figure 4.10 shows form factors for all sections analyzed using the DPF method plotted against Cowper's dimensionless ratio *m*. Also shown in the plot is the trend line represented by equation 4.5. As may be seen, the trend line is highly accurate in most situations and is generally, but not always, conservative.

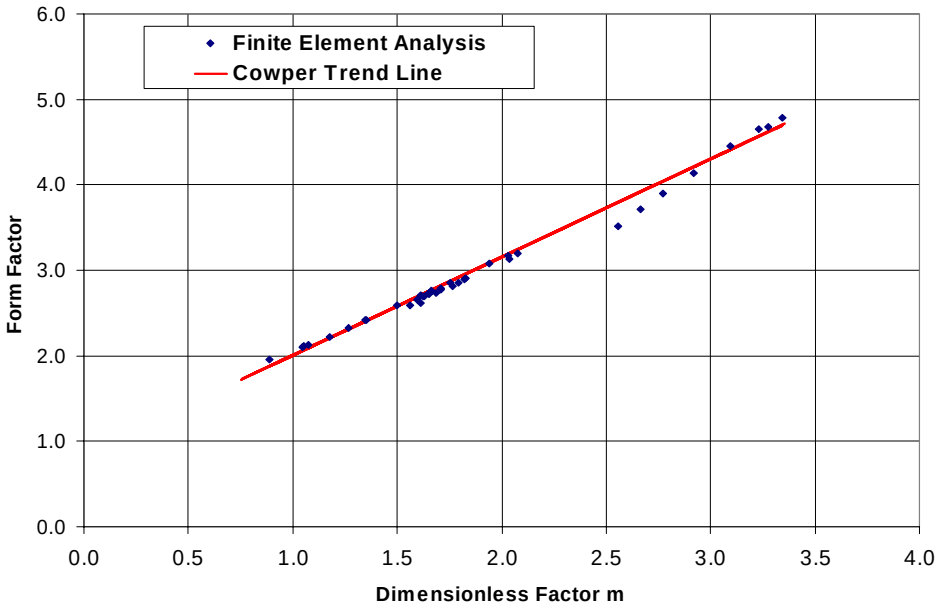

Figure 4.10 – Comparison of FEA results with Cowper trend line

4.4 Weak Axis Model for Finite Element Analysis

Wide flange sections were modeled about their weak axis to calculate the shear area about the weak axis. Finite element analysis is needed to calculate the value of shear area since there are no analytical expressions for it. It is surprising that there are no analytical expressions for the shear area of the section about the weak axis of wide flange sections. Also it will be shown that the finite element based solution by Pilkey (2003) is incorrect for calculating the form factors about the weak axis. It is, indeed, surprising that the program which calculated the values of form factors about the strong axis with high accuracy should fail to do so for the form factor about the weak axis. DPF analysis of the models indicates that the values shall be closer to 1.2 times the ratio of the gross area of the sections to the total area of the flanges. This is true for most sections since the wide flange sections essentially behave as two deep rectangles separated by a thin horizontal web. The following sections explain in detail the development of the model for finite element analysis and the results obtained from virtual work and finite element analysis.

4.4.1 Model for Finite Element Analysis

The models for weak axis analysis are built in a similar manner as those for strong axis models. The only difference is that there is an even number of elements across the depth of the web. This is the governing parameter for the model. The other dimensions of the elements are determined as described in the earlier section for strong axis model. The restraints at the support are the same as for strong axis model. Also, the procedure for analysis

is the same as for strong axis model. The loads are applied in a different manner since the shear stress distribution is different for the sections about the weak axis.

4.4.2 Load distribution for model about weak axis

The shear stress distribution about the weak axis is more simplified than the distribution about strong axis. It is similar to that of a rectangle with reduced shear stress along the width of the web. Figure 4.11 has the typical stress distribution for the wide flange section about the weak axis.

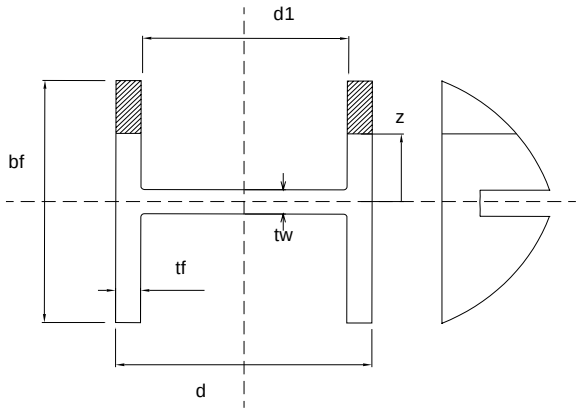

Figure 4.11 – Typical wide flange section about weak axis and shear stress distribution in flange

For the section shown in the above figure, the first moment of area is given by the following equation. When z is less than 0.5 t_w, the plane of interest is in the web, producing

$$Q_w(z) = 0.25t_f(b_f - t_w)(b_f + t_w) + 0.5d(0.5t_w - z)(0.5t_w + z) \quad \text{..... (4.6a)}$$

When z is greater than 0.5 t_w, the plane of interest is in the flanges, and

$$Q_f(z) = t_f(0.5b_f - z)(0.5b_f + z) \quad \text{(4.6b)}$$

Invoking equation 2.12, we get

$$\kappa = \left[\frac{2A}{I_y^{\,2}} \left[\int_0^{\frac{t_w}{2}} \frac{\left(0.25t_f(b_f - t_w)(b_f + t_w) + 0.5d(0.5t_w - z)(0.5t_w + z)\right)^2}{d^2} dz + \int_{\frac{t_w}{2}}^{\frac{b_f}{2}} \frac{(t_f(0.5b_f - z)(0.5b_f + z))^2}{4t_f^{\,2}} dz \right] \right] \quad \text{(4.7)}$$

where I_y = moment of inertia about the weak axis.

Using equation 4.7, the form factors for some of the wide flange sections were determined. The form factors obtained from Pilkey (2003) were compared with the values from virtual work and those obtained by the finite element analysis. Table 4.6 provides the form factors from virtual work, DPF analysis and Pilkey (2003).

4.5 Results of Weak Axis Finite Element Analysis

Pilkey (2003) provides a finite element based solution based on the theory of elasticity. The values are presented in Table 4.6 along with the values obtained from the finite element analysis and virtual work. The values were calculated for *L/d* ratio of 3, with Poisson's ratio set to 0.3. It can be seen that the Pilkey values are wrong by a big margin for the W14 sections and gradually converge towards the DPF values as the section size increases

to W36. Still, the least difference is about 7%, which is not very encouraging. Due to this reason, Pilkey (2003) shall not be considered for form factors about the weak axis of wide flange sections.

The DPF values are, also, not very close to the values given by virtual work. But the difference in these values is lower than the difference from Pilkey values and nearly constant for all sections. This leads to the recommendation of the DPF values for use in weak axis of wide flange section. Also, the DPF values for the weak axis of the sections are plotted against the dimensionless parameter *m* from the Cowper expression. This is done to examine the possibility of developing a simplified expression for the form factor about the weak axis.

Table 4.6 – Comparison of form factors about weak axis of wide flange section

Section	DPF	VW	Pilkey	1.2 A_G/A_f
W14x90	1.55	1.46	3.51	1.54
W14x398	1.41	1.29	4.13	1.48
W14x730	1.32	1.21	4.75	1.46
W24x94	2.16	1.88	2.80	2.09
W24x250	1.77	1.55	2.88	1.76
W24x335	1.72	1.49	2.31	1.76
W36x135	2.56	2.28	2.46	2.51
W36x280	1.94	1.72	2.68	1.89
W36x650	1.79	1.52	1.94	1.84

Table 4.7 provides the values of various sections calculated using the DPF method, Virtual Work and the empirical formula. Observing the table, we find that the form factor values reduce as the sections become bigger. This can be attributed to the behavior of the sections as two rectangles connected by a thin web which does not influence the stress distribution significantly. It is found that the empirical formula $1.2\ A_G/A_f$ gives very good answers for

form factors about the weak axis. The correlation between the empirical formula and the DPF values increases for increasing sizes as also for increasing weights of a given size.

Table 4.7 – Form Factors about Weak Axis of various wide flange sections

Section	Weight	DPF	VW	1.2 A_G/A_f
W40	593	1.88	1.60	1.93
	503	1.94	1.65	1.95
	431	1.98	1.70	1.97
	372	2.00	1.74	1.97
	324	2.02	1.76	1.96
	235	2.18	1.91	2.17
W36	650	1.79	1.52	1.83
	439	1.87	1.62	1.86
	328	1.91	1.68	1.87
	280	1.94	1.72	1.88
	170	2.34	2.04	2.25
	160	2.36	2.07	2.28
	135	2.56	2.28	2.49
W24	335	1.72	1.49	1.76
	279	1.76	1.53	1.76
	250	1.77	1.55	1.76
	207	1.80	1.59	1.78
	104	1.99	1.79	1.91
	94	2.16	1.88	2.08
	76	2.26	2.00	2.17
W18	175	1.70	1.50	1.70
	130	1.74	1.55	1.71
	97	1.81	1.63	1.76
	76	1.84	1.67	1.77
	71	2.04	1.80	2.01
	55	2.10	1.86	2.03
	46	2.27	1.98	2.20
W14	730	1.32	1.21	1.46
	605	1.34	1.23	1.47
	283	1.45	1.33	1.49
	193	1.49	1.38	1.50
	120	1.54	1.44	1.52
	90	1.55	1.46	1.52
	68	1.68	1.53	1.63
	43	1.82	1.64	1.75

Figure 4.12 presents the plot of the form factors from the DPF method with respect to the dimensionless parameter *m* equal to $\frac{2b_f t_f}{dt_w}$ from Cowper's expression.

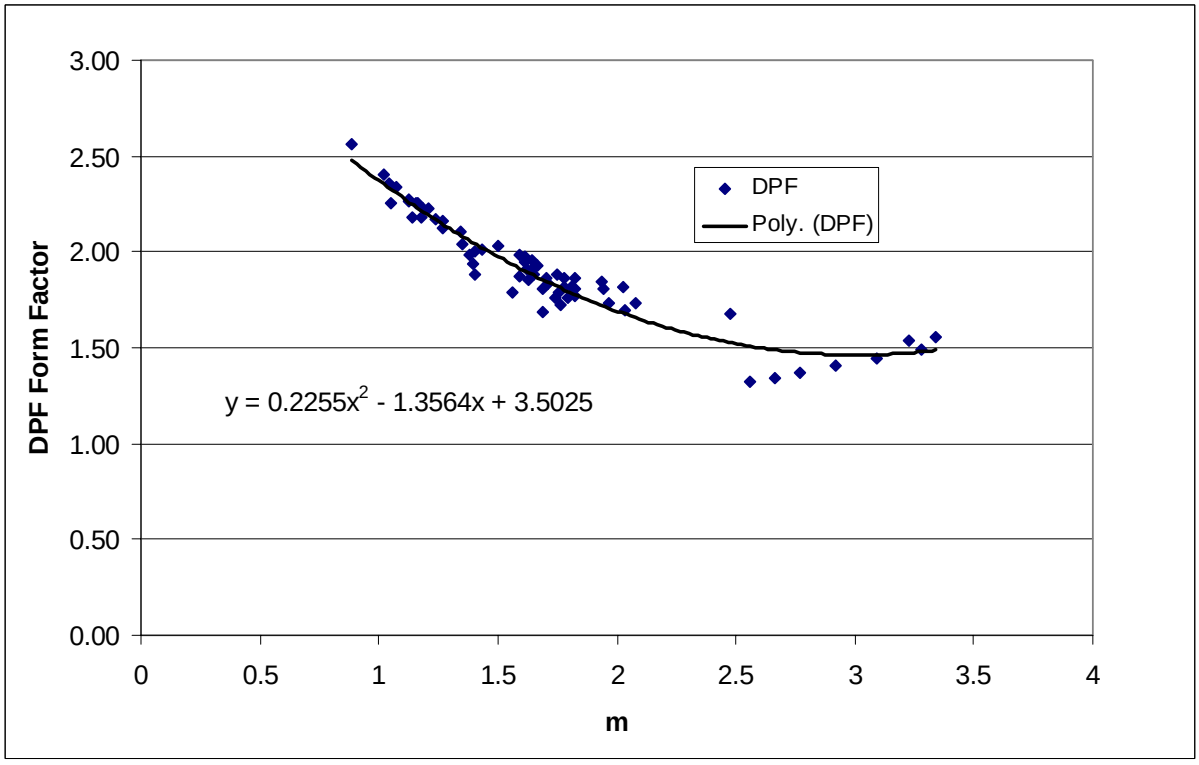

Figure 4.12 – Trend line analysis of DPF values and m

Based on Figure 4.12, the following simplified equation is obtained for the form factor of a wide flange section about the weak axis:

$$\kappa = 0.2255m^2 - 1.3564m + 3.5025 \quad \ldots\ldots\ldots\ldots\ldots\ldots\ldots\ldots\ldots\ldots \quad (4.8)$$

The trend line equation gives a good approximation of the form factor for most of the wide flange sections. It fails to provide satisfactory values for W14 sections. Also, the values from

the equation are not always conservative since some values are less than the DPF values by a good margin. Also it is advisable to use the empirical formula of $\kappa=1.2\ A_G/A_f$ for the form factor of wide flange sections about the weak axis.

Chapter 5 Analysis of Beam-Column Joint

Beam-column joints in steel moment-resisting frames are an excellent source of energy dissipation. But their behavior is not fully understood yet. This limits the ability to utilize their deformation capacity to dissipate energy. Knowledge of the deformation of beam-column joint allows for optimization of the drift in a frame for lateral loads. In this thesis, the term *beam-column (BC) joint* refers to the entire assembly at the intersection of the beam and the column. In addition to the column and the beam sections, doubler plates and continuity plates may be present in the joint. Doubler plates are steel plates placed parallel to the column web between the column flanges and held in place by fillet welds, full penetration welds and/or plug welds along the column flanges and column web. Continuity plates (also known as stiffeners) are steel plates placed horizontally across the column web and in line with the girder flanges. They are held in place with fillet welds or full penetration welds at the inside faces of the column flanges and along the column web. The *panel zone* (*PZ*) is the part of the column web forming the joint, including the doubler plate if present. Figure 5.1 shows a typical beam-column joint. A lot of research has been done in the past to model and analyze the behavior of the BC joint. The reader is referred to Downs (2002) for further background and details on the subject. This thesis will consider the beam-column joint to quantify the contribution of the individual components of the joint to the total drift of the sub-assembly.

5.1 Mathematical models for Panel Zone (PZ) Behavior

Various mathematical models have been proposed to model the beam-column joint and study the PZ behavior. Some of the models in use for modeling the joint (Downs, 2002) are:

1) Centerline model: In this model, the BC joint is treated as a point at the intersection of the beam and the column.
2) Rigid model: In this model, the physical extent of the PZ is considered to be completely rigid. This will exclude the strain energy sources in that region.
3) Flexible model: This model assumes that the beam column joint will have some rigidity. The PZ effects are included by determining the resultant shear forces and moments at the PZ interface and using virtual work to develop their contribution to the subassembly's displacement.

It is noted that all the above models consider only elastic deformations in the joint. There are two other models, namely the Krawinkler model and Scissors model, which include the inelastic effects in the PZ. But these are beyond the scope of this thesis and are not discussed. Detailed discussion about the modeling and analysis of beam-column joints in steel moment-resisting frames is available in Downs (2002).

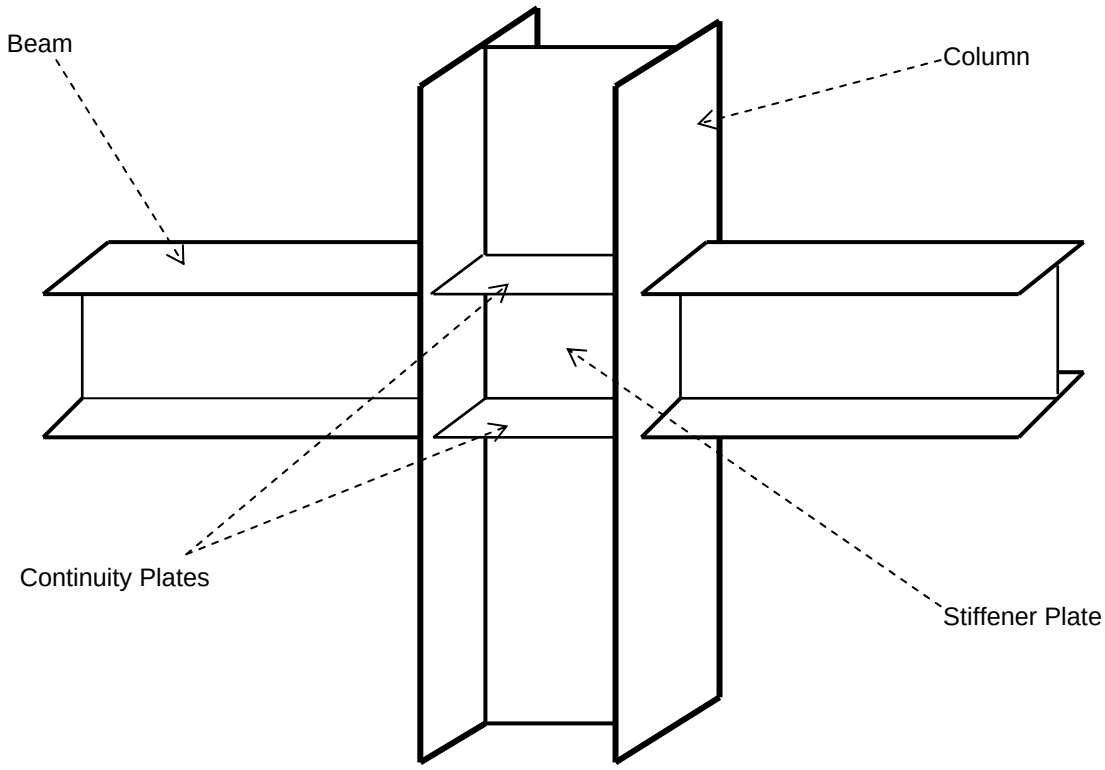

Figure 5.1 – Typical beam-column joint in steel moment resisting frames

5.2 Finite Element Model of Beam-Column Joint

The beam-column joint subassembly consisting of wide flange sections was modeled using the eight node solid elements. The finite element analysis software used is SAP2000. This was used for the linear static analysis. Modeling the beam column joint presented a lot of difficulties not present in the cantilever models of wide flange sections. The main hurdle was the mismatch of nodes of the elements at the interface, where the beam merges into the column. This necessitated the use of constraints to model the behavior adequately. But it was found that it would be easier to create a model when the beam and column sections were the same. Hence the beam and the column sections were the same for the rest of the analysis. Only half of the sub-assembly was modeled, using symmetry about the *XZ* plane, for

computational efficiency. This allowed the use of a finer mesh of solid elements. The nodes on the model were restrained to reflect the behavior of the sub-assembly. Figure 5.2 shows the typical deflected shape of the cruciform sub- assemblage. In Figure 5.2, δ is the drift of the sub-assembly.

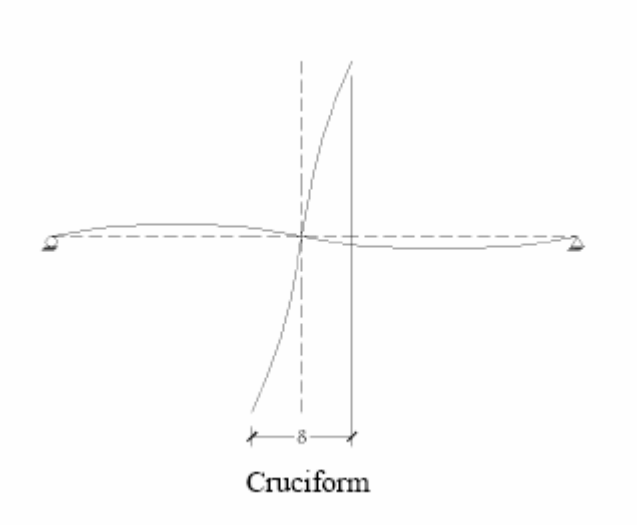

Figure 5.2 – Typical deflected shape of cruciform sub-assembly

Based on Figure 5.2, the following restraint conditions were used:

- The plane of symmetry of the model was restrained in the Y direction. This is necessary to prevent any lateral deformation of the model.
- The nodes on the neutral axis at left end of the girder were restrained in the X and Z direction. The nodes at the right end were restrained only in the Z direction to model the roller support condition.

The loads on the model were applied at the joints at the top and bottom of the column in the model. The loads were equal and opposite and applied uniformly over all the nodes. These loads were balanced at supports of the girder. The virtual loads were applied only at the top

and bottom of the column in the model. Figure 5.3 shows the model of a typical sub-assembly.

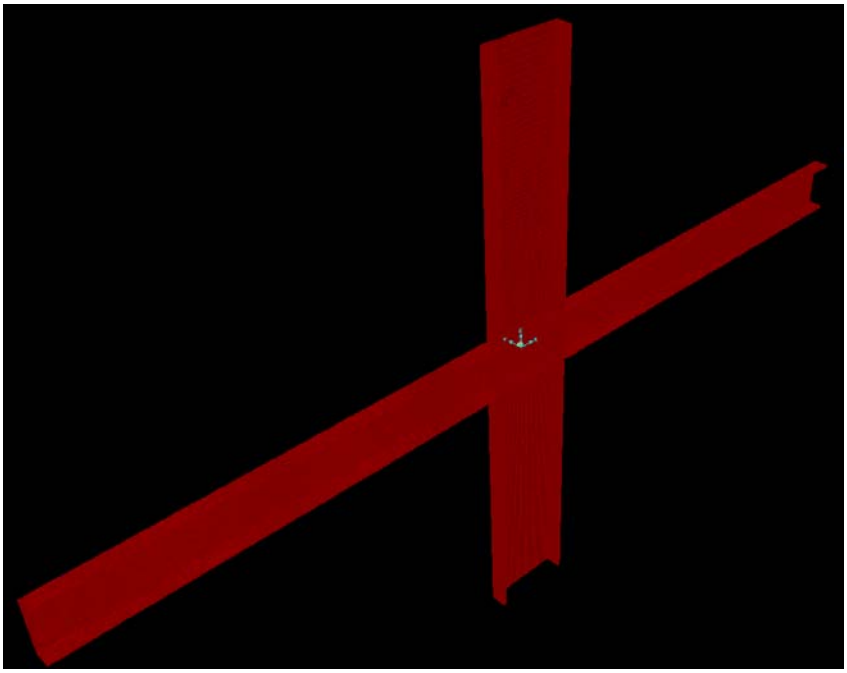

Figure 5.3 – Typical model of sub-assembly for finite element analysis

5.3 Analysis of Beam-Column Sub-assemblies

All the beam-column sub-assemblies were analyzed and the drift values calculated. The results of the analysis were not encouraging. The drift values obtained from the DPF analysis of the stresses did not match the drift values obtained from the displacements of the nodes at the top and bottom of the column. They were nearly 5% more than the values reported by FEA. This was perplexing as the DPF method was able to accurately recover the shear area and moments of inertia for wide flange sections previously. Correlating the values with those obtained using the formula in Downs (2002), further breakdown of the DPF values indicated that the bulk of the error is from the panel zone. This negates the whole purpose of

this exercise. Table 5.1 provides the values of drift calculated by the DPF method and the values calculated from the FEA analysis. All the models were subjected to a 500 kip load with *v=0.3*. The story height was 150 in. and the bay width was 240 in.

Table 5.1 – Comparison of DPF and FEA drift values for various Sub-assemblies

Beam Section	Column Section	DPF Drift (in.)	FEA Drift (in.)	(DPF/FEA)
W36x210	W36x210	5.566	5.155	7.97%
W24x250	W24x250	9.765	9.238	5.70%
W21x201	W21x201	13.765	13.178	4.45%
W14x90	W14x90	18.35	17.748	3.39%

Based on the values from Table 5.1, it was decided to construct a simple model of the sub-assembly. This was achieved using a rectangular section for the beam and the column and having unit (1.0) thickness. This model also had fillets at the beam-column interface to reduce the stress concentrations. The restraints and the loading procedure were the same as before. Figure 5.4 shows the elevation of the simplified model of the subassembly.

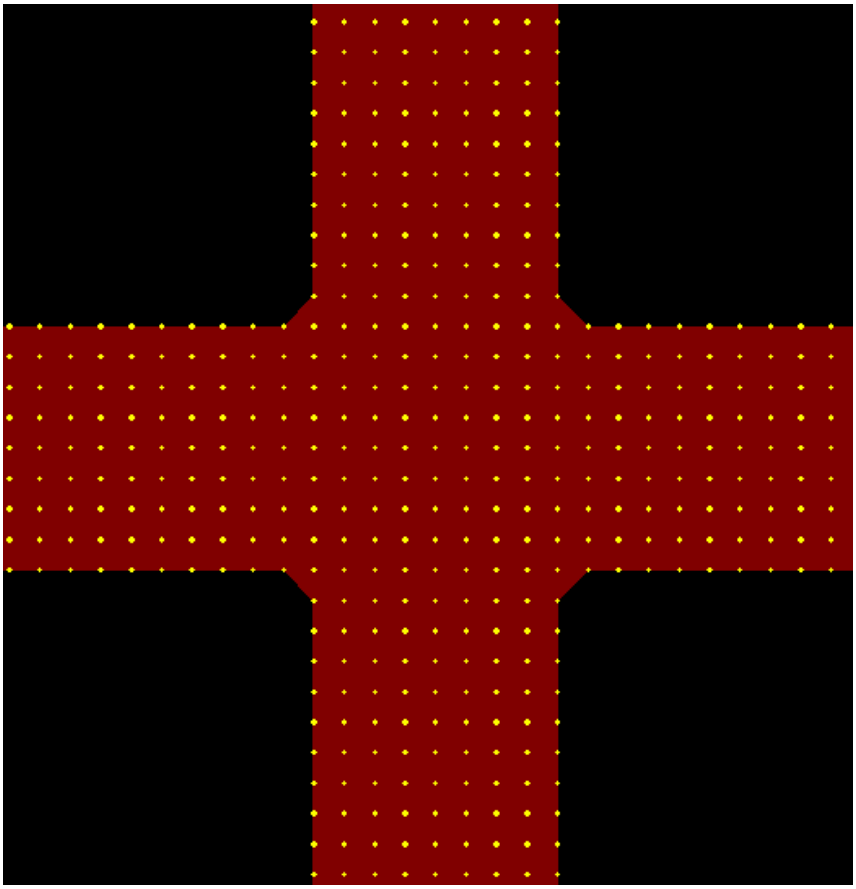

Figure 5.4 – Simplified model of the sub-assembly

Even with this modification and simplification, the drift values were no better. The error was stuck at ~5%. This leads one to believe that the error might be caused by the methodology adopted for modeling the sub-assembly. Another reason for this error could be the inadequacy of the software to generate and analyze such complex models.

Chapter 6 Conclusions and Recommendations

6.1 Summary of Results

For rectangular sections, the form factor consists of two terms, one representing simple beam theory and the other representing the effect of warping of the section. The portion of the form factor based on simple beam theory is exactly 1.2 regardless of the material and the width to depth ratio of the section. The term associated with warping depends on the Poisson's ratio, and should, according to the theory of elasticity, increase with increasing width to depth ratios.

Cowper's expression for the form factor of rectangular sections produces 1.2 when Poisson's ratio is zero, and decreases slightly for larger values of Poisson's ratio. The sectional width to depth ratio does not enter into Cowper's expression. Both of these trends are contrary to the solution, which uses shear stresses predicted by Timoshenko and Goodier's theory of elasticity.

Renton's solution for the form factor for rectangular sections is based on Timoshenko and Goodier's theory of elasticity formulation. Renton's form factor is exactly 1.2 when Poisson's ratio is zero, and converges to 1.2 for sections that have width to depth ratios less than unity. Renton's expression for form factor produces values significantly greater than 1.2 when the section width is much greater than the depth. Pilkey's finite element analysis program produces form factors similar to those predicted by Renton.

The DPF procedure produces form factors that are very comparable to those predicted by Renton and Pilkey, but only for sections that have a width less than 2.0 times the depth. When the width is greater than twice the depth, the finite element based solution indicates that the form factor remains at about 1.25, whereas Renton's solution predicts values that increase dramatically with width to depth ratio. Based on the information at hand, it is felt that the most accurate solution is provided by the finite element analysis.

For wide flange sections, there is a large difference in the effective shear area or form factor, depending on the analytical expression used. Timoshenko's solution, which is based on a physical interpretation of shear strains computed from simple beam theory, is not valid and should not be used. The virtual work based solution provided by Newlin and Trayer predicts reasonable form factors for very deep, slender sections, but not for stocky sections. This is due to the fact that the simple beam theory, on which the form factor is based, underestimates shear stresses that develop in the flange area just above and below the web. Newlin and Trayer's simplified expression produces inconsistent agreement with the finite element results and should not be used.

The form factor computed using Cowper expression is a function of Poisson's ratio, and as with Cowper's solution for rectangular section, the form factor decreases with increasing Poisson's ratio. As before, this is contrary to the theory of elasticity. It also contradicts the trend predicted from the solution using the DPF method. Because the effect of Poisson's ratio is negligibly small for wide flange beams, it is recommended that Cowper's equation be used with Poisson's ratio set to zero.

In using Cowper's expression, it was found that very good agreement with the finite element solution is obtained if the total depth of the beam, d, is used to calculate the dimensionless parameters m and n. This is contrary to the original paper, which indicates, by illustration, that the depth between the centers of the flanges should be used. When the above adjustments are made, Cowper's expression predicts form factors within 8% of those computed from finite element analysis, with the 8% error occurring only for the stockiest sections. The average error predicted over several dozen sections analyzed was less than 1%. An empirical expression for form factor ($\kappa = 0.85+1.16m$) produces excellent results over a wide range of sections analyzed.

The use of a simplified shear area equation, equal to the web thickness times the depth between the center of the flanges, produces form factors that are very close to those computed by the finite element analysis, with the exception again being the stockiest sections.

One of the most interesting observations from this work is that form factors for deep, slender sections are significantly less than those for very stocky sections. This indicates that for two sections with the same weight per unit length, the deep slender section is much more efficient in resisting shear force than the stocky section. The most shear efficient section of all is the deep rectangular beam, which has the minimum form factor and hence maximum shear stiffness.

With respect to the form factor about the weak axis, the solution by Pilkey (2003) is inaccurate and should not be used. The solution obtained using the DPF method should be

used, as it is close to the solution provided by virtual work. Also the empirical formula $\kappa=1.2\ A_G/A_f$ can be used as it provides answers very close to those calculated by the DPF method.

With regards to the beam-column sub-assemblies, the drift values for the beam-column joint had an average error of ~5% consistently. This negates the whole purpose of performing the finite element analysis. Even the use of increased mesh density and fillets around the PZ does not decrease the error. This leads one to believe that the error could be due to the manner in which the sub-assemblage is being modeled or the inadequacy of the software used to perform the analysis.

6.2 Recommendations for Future Research

The recommendations for further research are as follows:

1.) The value of form factor for rectangular sections with width more than twice the depth of the section should be investigated. The DPF analysis provides answers which do not increase significantly, but the theory of elasticity based solutions provide very different answers. This discrepancy should be addressed.

2.) The form factors for wide flange sections about the weak axis are inaccurately calculated by Pilkey (2003). This is surprising since the values about the strong axis are accurate. The procedure adopted by Pilkey for the weak axis should be investigated, as also should the stress distribution used in finite element analysis of the models about the weak axis. This should resolve the discrepancy.

3.) The behavior of the beam-column joint should be investigated, as the drift values obtained by DPF analysis do not match the values obtained by finite element analysis. This will help in determining the contributions of the PZ in shear and flexure more accurately. Also, it is recommended that the models be generated and analyzed using a more advanced finite element analysis package.

Nomenclature

P	Vertical load applied to the cantilever beam
L	Length of beam
b	Width of rectangular beam
b_f	Flange width of wide flange beam
d	Total depth of beam
d_1	Depth between centers of flanges of wide flange beam
t_f	Flange thickness of wide flange beam
t_w	Web thickness of wide flange beam
d	Vertical deflection at end of beam
d_ε	Deflection due to normal strains
d_γ	Deflection due to shear strains
A_v	Shear area
A	Cross sectional area
I	Moment of inertia
I_y	Moment of inertia about the weak axis
E	Modulus of elasticity
G	Shear modulus
κ	Form factor
Q	First moment of area
ε	Normal strain
γ	Shear strain
σ	Normal stress
τ	Shear stress
C	Constitutive matrix relating stress to strain
ν	Poisson's ratio
V	Volume
α	Distance of station a for calculation of DPF
β	Distance of station b for calculation of DPF

References

Charney, F. A. (1990). "Sources of elastic deformation in laterally loaded steel frame and tube structures," *Tall Buildings and Beyond – Proc. 4th World Congress, Council on Tall Buildings and Urban Habitat*, Lehigh University, Bethlehem, PA.,

Charney, F.A., Iyer, H**.**, Spears, P.W. (2005). "Computation of Major Axis Shear Deformations in Wide Flange Steel Girders and Columns", *Journal of Constructional Steel Research*, *Accepted for Publication.*

Cowper, G. R. (1966). "The shear coefficient in Timoshenko's beam theory," *J. Appl. Mech.*, **33**,335-340.

CSI (2002). *SAP2000: Integrated software for structural analysis and design*, v7.44, Computers and Structures, Inc. Berkeley, CA.

Downs, W. M. (2002). "Modeling and behavior of the beam/column joint regions of moment resisting frames," M.S. thesis, Department of Civil and Environmental Engineering, Virginia Tech, Blacksburg, VA.

Higdon, A., Ohlsen, E. H., Stiles, William B., Weese, John A., and Riley, William F. (1985). *Mechanics of materials*, John Wiley and Sons, New York, NY.

Love, A. E. H. (1944). *A treatise on the mathematical theory of elasticity*, Dover Publications, New York, NY.

McGuire, W., Gallagher, R., and Zieman, R. (2000). *Matrix structural analysis*, 2nd ed., John Wiley and Sons, New York, NY.

Newlin, J. A., and Trayer, G. W. (1924). "Deflection of beams with special reference to shear deformations," *Report No. 180*, Forest Products Laboratory, Department of Agriculture.

Pilkey, W. D. (1994). *Formulas for stress, strain, and structural matrices*, John Wiley and Sons, New York, NY.

Pilkey, W. D. (2003). *Analysis and design of elastic beams*, John Wiley and Sons, New York, NY.

Popov, E. P. (1976). *Mechanics of Materials*, Prentice-Hall Inc., Englewood Cliffs, NJ.

Renton, J. D. (1991). "Generalized beam theory applied to shear stiffness," *Int. J. Solids Struct*., **27**,1955-1967.

Schramm, U., Kitis, L., Kang, W., and Pilkey, W. D. (1994). "On the shear deformation coefficient in beam theory," *Fin. Elem. in Anal. & Design*, **16**,141-162.

Timoshenko, S. P. (1940). *Strength of materials*, Part I, D. Van Nostrand Company, Inc., New York, NY.

Timoshenko, S. P., and Goodier, J. N. (1970). *Theory of Elasticity*, McGraw Hill, New York, NY.

Ugural, A. C. (1991). *Mechanics of Materials*, McGraw Hill, Inc., New York, NY.

Young, W.C., and Budynas, R.G. (2002). *Formulas for Stress and Strain*, 7th ed., McGraw Hill, New York, NY.

Appendix A – Finite Element Displacement Method (FED) for Calculating Shear Area and Moment of Inertia

In this method, the analytical models shown in Figure A1 were utilized. The top of the figure shows the idealized one-dimensional beam from which theoretical displacements are computed, and the bottom shows a profile of the finite element model from which the "exact" displacements were computed. The theoretical and exact displacements were computed at the centerline of the beam at stations ***a*** and ***b.*** These interior points were chosen to eliminate end effects in the finite element model. In most of the analyses, these points were at least the depth of the beam away from the support or the free end.

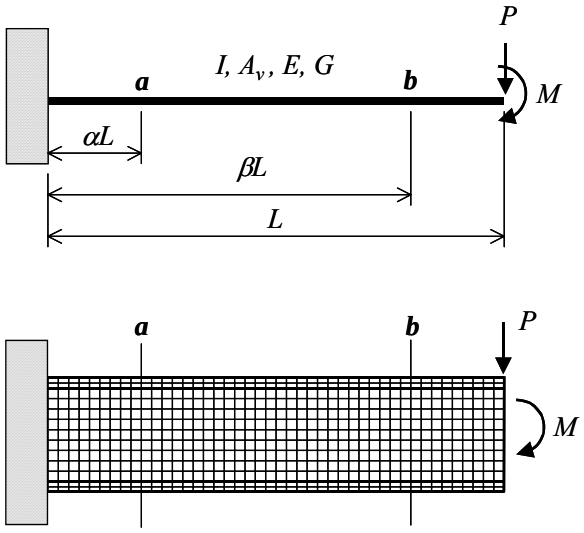

Figure A1 – Idealized cantilever beam (top) and finite element model (bottom) used for analysis

The idealized beam is first loaded with a concentrated moment *M* at the free end. Under this loading, shear deformations do not influence the displacements at ***a*** and ***b***. These theoretical displacements are computed as follows:

$$\delta_{aF,M} = \frac{M\alpha^2 L^2}{2EI} \quad \text{..... (A1)}$$

$$\delta_{bF,M} = \frac{M\beta^2 L^2}{2EI} \quad \text{..... (A2)}$$

In equation A1 the subscript *aF,M* refers to the Flexural deflection at point ***a*** due to the applied moment *M*. Subsequent subscripts have similar meanings. Note that the moment of inertia does not include the fillets and is therefore consistent with the finite element model.

The theoretical difference in flexural deflection between points ***a*** and ***b*** is

$$\Delta_{F,M} = \delta_{bF,M} - \delta_{aF,M} = \frac{ML^2}{2EI}(\beta^2 - \delta^2) \quad \text{..... (A3)}$$

If the finite element model is loaded as shown in Figure A1 and the displacements at ***a*** and ***b*** are computed as $\widetilde{\delta}_{aF,M}$ and $\widetilde{\delta}_{bF,M}$, respectively, the difference in deflection between the two points is $\widetilde{\Delta}_{F,M}$. Note that the tilde is used to represent the fact that these deflections come directly from the finite element model.

The displacement, $\Delta_{F,M}$, should theoretically be equal to the displacement from the finite element analysis, $\widetilde{\Delta}_{F,M}$. Using this and equation A3, the effective moment of inertia of the beam in the finite element analysis is given by equation A4, where now the tilde represents the fact that this is the moment of inertia from the finite element analysis, which will be

somewhat different from the moment of inertia computed from the section profile, absent the fillets.

$$\widetilde{I} = \frac{ML^2}{2E\widetilde{\Delta}_{F,M}}(\beta^2 - \delta^2) \quad \text{..... (A4)}$$

The difference is due to errors associated with the finite element analysis itself, including boundary effects, inherent element quality, and mesh density. There should be no error associated with the plane section assumption which is inherent in equation B4, because under the end moment load there are no shears, and hence no cross-sectional warping.

Next, consider the ideal beam of Figure A2 as subjected to the end load *P*. The flexural deflections at point ***a*** and ***b*** are

$$\delta_{aF,P} = \frac{PL^3\delta^2(3-\delta)}{6EI} \quad \text{..... (A5)}$$

and

$$\delta_{bF,P} = \frac{PL^3\beta^2(3-\beta)}{6EI} \quad \text{..... (A6)}$$

and the difference in flexural displacements between the two points is

$$\Delta_{F,P} = \delta_{bF,P} - \delta_{aF,P} = \frac{PL^3}{6EI}\left[\beta^2(3-\beta) - \alpha^2(3-\alpha)\right] \quad \text{..... (A7)}$$

The shear displacements at points ***a*** and ***b*** are computed as

$$\delta_{aV,P} = \frac{P\alpha L}{GA_v} \quad \text{..... (A8)}$$

$$\delta_{bV,P} = \frac{P\beta L}{GA_v} \quad \text{..... (A9)}$$

where the V in the subscript represents shear deformation. The difference in shear displacement between the two points is

$$\Delta_{V,P} = \delta_{bV,P} - \delta_{aV,P} = \frac{PL}{GA_v}(\beta - \alpha) \quad \text{..... (A10)}$$

Using equations A7 and A10, the total relative displacement between points ***a*** and ***b*** is

$$\Delta_{VF,P} = \Delta_{M,P} + \Delta_{V,P} = \frac{PL^3}{6EI}\left[\beta^2(3-\beta) - \alpha^2(3-\alpha)\right] + \frac{PL}{GA_v}(\beta - \alpha) \quad \text{..... (A11)}$$

If the total deflection, $\tilde{\Delta}_{VF,P}$, between points ***a*** and ***b*** is computed from the finite element analysis under load *P*, if it is assumed that this is equal to the theoretical displacement $\Delta_{VF,P}$ and if the effective moment of inertia $\tilde{I}$ computed on the basis of the finite element analysis under the load *M* is utilized, the effective shear area $\tilde{A}_v$ based on finite element analysis may be computed by rearranging terms in equation A11:

$$\widetilde{A}_v = \frac{PL(\beta - \alpha)}{G\left[\widetilde{\Delta}_{VF,P} - \frac{PL^3}{6E\widetilde{I}}\left[\beta^2(3-\beta) - \alpha^2(3-\delta)\right]\right]} \quad \text{..... (A12)}$$

It should be noted that in all of the analyses performed, the term $\widetilde{I}$ was within one percent of the value computed from the section geometry, not including the fillets.

Appendix B – Displacement Participation Factor (DPF) Method for Calculating Form Factor and Moment of Inertia

The DPF method is based the principle of virtual work. This method is adopted as it does not assume that plane sections remain plane under a shear load. Also using the virtual work method we can separately calculate the deflection caused in the beam due to normal and shear strains.

For calculation of the form factor, we use a cantilever beam of length L with load P at the tip and a moment M at the tip separately. The beam is rectangular in cross section with area A, moment of inertia I, modulus of elasticity E, Poisson's ratio *v* and shear modulus G. The following figure shows the typical beam for our analysis.

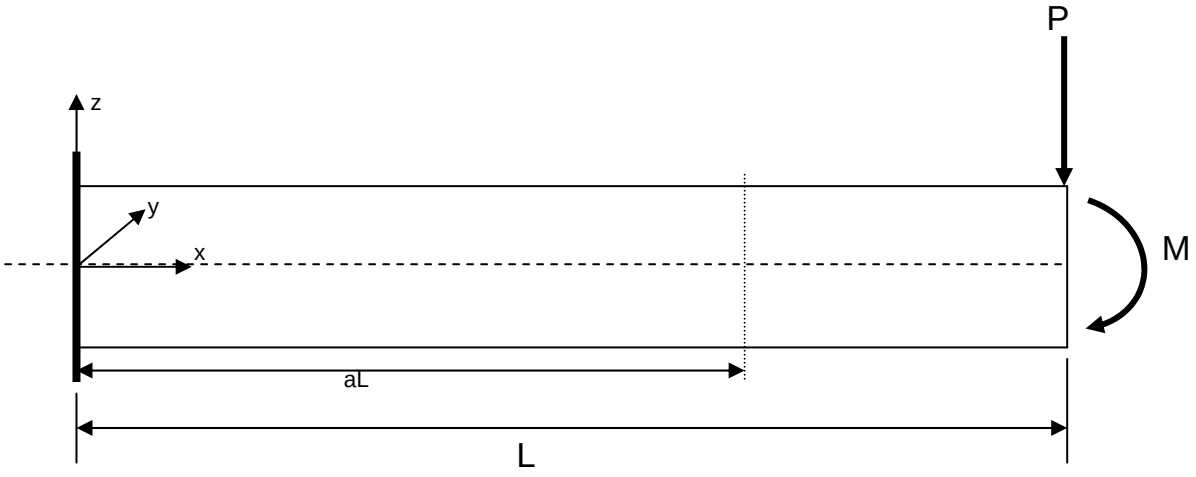

Figure B1 – Typical cantilever beam: orientation and loading

Only a portion of the beam, away from both ends of the beam, is considered for calculation of the moment of inertia and the form factor. This is necessary to eliminate any

adverse effects on the stresses due to proximity to the support and the load P. The beam is modeled with eight-node brick elements. Only half the beam section, symmetrical about the Y axis, is modeled for computational efficiency.

For calculation of moment of inertia of the section, a moment is applied at the tip of the beam. This produces deflections due to normal strains alone. Hence the deflection of the beam at distance *aL* from the support is given by

$$\delta_{a,M} = \frac{M(aL)^2}{2EI} \quad \text{..... (B1)}$$

The equation for the difference in deflection between two points *aL* and *bL* away from the support is given by

$$\delta_{ab,M} = \frac{ML^2(b^2 - a^2)}{2EI} \quad \text{..... (B2)}$$

For calculation of the form factor, a vertical load P is applied at the tip of the beam. The deflection produced at distance *aL* from the support is given by

$$\delta_{a,P} = \frac{P(aL)^3}{3EI} + \frac{kP(aL)}{GA} \quad \text{..... (B3)}$$

The equation for the difference in deflection between two points *aL* and *bL* away from the support is given by

$$\delta_{ab,P} = \frac{PL^3(b^3 - a^3)}{3EI} + \frac{kPL(b-a)}{GA} \quad \text{..... (B4)}$$

where k = form factor for the section. The second term in (B3) and (B4) is due to shear strains developed in the section due to load P. These are normally neglected in general practice, due to their relatively very low value.

For using the method of virtual work, we apply a unit virtual load at the point where the deflection is to be calculated. Then the equation for displacement is

$$\delta \times 1 = \int_V \hat{\sigma}^T \varepsilon \, d\, V \quad \text{..... (B5)}$$

where $\hat{\sigma}$ = stress vector due to unit virtual load ;

ε = strain vector due to real load P;

V = volume of the beam;

dV = volume of the differential element

The displacement δ under the real load can be split into two components: displacement due to flexural strains, δ_σ, and displacement due to shear strains, δ_τ. Thus

$$\delta = \delta_\sigma + \delta_\tau \quad \text{..... (B6)}$$

After completing the proper substitutions and simplification and discretizing the integral form of the equation in order to apply the finite element model, we have

$$\delta_\sigma = \frac{1}{E}\sum_{i=1}^{nels} \left\langle \hat{\sigma}_{xx,i} \quad \hat{\sigma}_{yy,i} \quad \hat{\sigma}_{zz,i} \right\rangle \begin{bmatrix} 1 & -\nu & -\nu \\ -\nu & 1 & -\nu \\ -\nu & -\nu & 1 \end{bmatrix} \begin{Bmatrix} \sigma_{xx,i} \\ \sigma_{yy,i} \\ \sigma_{zz,i} \end{Bmatrix} V_i \quad \text{..... (B7)}$$

and

$$\delta_\tau = \frac{1}{G}\sum_{i=1}^{nels}\left\langle \hat{\tau}_{xy,i} \quad \hat{\tau}_{yz,i} \quad \hat{\tau}_{zx,i} \right\rangle \begin{bmatrix} 1 & 0 & 0 \\ 0 & 1 & 0 \\ 0 & 0 & 1 \end{bmatrix} \begin{Bmatrix} \tau_{xy,i} \\ \tau_{yz,i} \\ \tau_{zx,i} \end{Bmatrix} V_i \quad \text{..... (B8)}$$

Since we consider only a certain portion of the beam, only the elements within that portion shall be considered.

The model has two load cases, virtual load A and virtual load B. These loads are applied at distances aL and bL from the support respectively. Now we fix the stations A1 and A2 at distances a_1L and a_2L respectively for virtual load A. The stations B1 and B2 are fixed at distances b_1L and b_2L from the support respectively for virtual load B. The load cases are illustrated in the figures below.

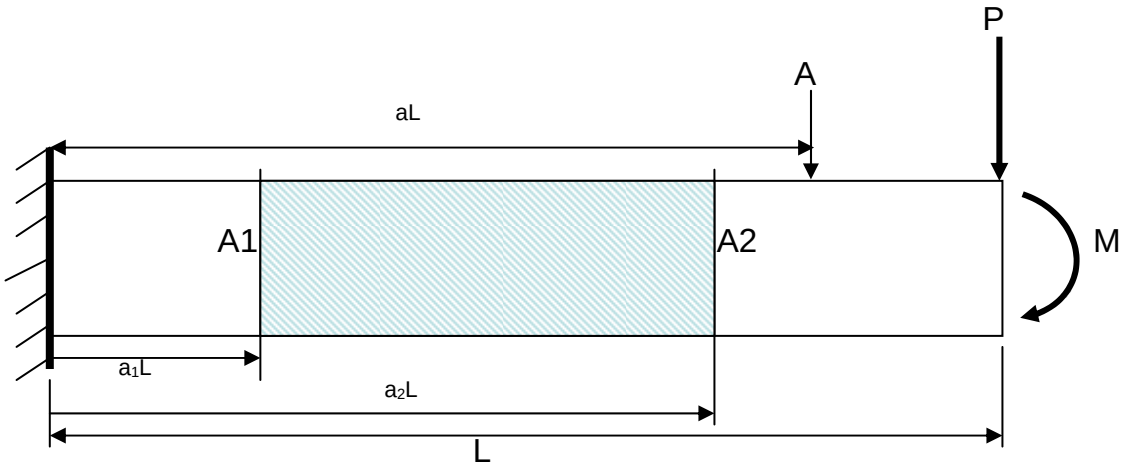

Figure B2 – Application of virtual load A

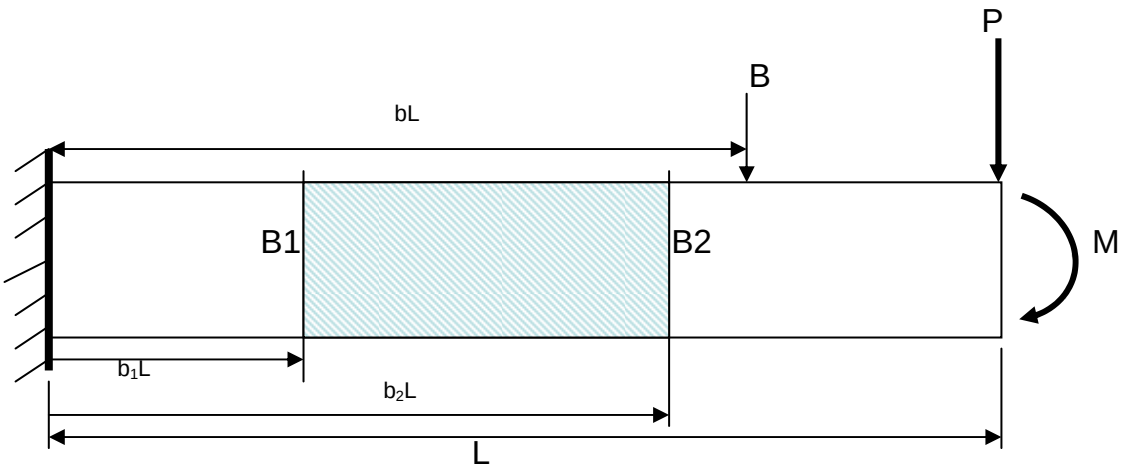

Figure B3 – Application of virtual load B

The distances *aL* and *bL* are specified in the input file itself. The stations A1, A2, B1 and B2 are selected during post-processing of the output file from the finite element analysis. The stations should be chosen so that they lie in regions of uniform stress due to real load P. For this purpose, it is advisable to view the stress profile for the beam along the span before deciding the location of the stations. Also, the stations are located some distance away from the virtual load as well, so as to eliminate any adverse effect due to the virtual stresses. This is not necessary, though, but is advisable for accurate calculation of the moment of inertia of the section.

The difference in deflection between stations A1 and A2 under moment M is calculated using equation (B7) over the elements between the stations. This gives us the flexural component of the deflection, $\delta_{A\sigma,M}$. We can equate this to equation (B2). Thus

$$\delta_{A\sigma,M} = \frac{ML^2(a_2^2 - a_1^2)}{2EI_A} \quad \text{..... (B9)}$$

Similarly, we can write the equation for virtual load B as

$$\delta_{B\sigma,M} = \frac{ML^2(b_2^2 - b_1^2)}{2EI_B} \quad \text{..... (B10)}$$

The values I_A and I_B are calculated from (B9) and (B10). Thus the moment of inertia of the section is the average of the two:

$$I_M = \frac{I_A + I_B}{2} \quad \text{..... (B11)}$$

Now the difference in deflection due to shear strains between A1 and A2 under the vertical load P, $\delta_{\tau A,P}$, is given by

$$\delta_{\tau A,P} = \frac{k_A PL(a_2 - a_1)}{GA} \quad \text{..... (B12)}$$

Similarly the equation for virtual load B is

$$\delta_{\tau B,P} = \frac{k_B PL(b_2 - b_1)}{GA} \quad \text{..... (B13)}$$

The values k_A and k_B are calculated from (B12) and (B13). The form factor k is calculated as

$$k = \frac{k_A + k_B}{2}$$

The moment of inertia is calculated as

$$\delta_{\sigma A,P} = \frac{PL^3(a_2^3 - a_1^3)}{EI_A} \quad \text{..... (B14)}$$

and

$$\delta_{\sigma B,P} = \frac{PL^3 (b_2{}^3 - b_1{}^3)}{EI_B} \quad \text{..... (B15)}$$

The moment of inertia is calculated as

$$I_P = \frac{I_A + I_B}{2} \quad \text{..... (B16)}$$

The values of moment of inertia from (B11) and (B16) should be equal. This ensures that the analysis performed is correct.

The above calculations are all done using an Excel Spreadsheet developed specifically for this purpose. The spreadsheet requires width and depth of section, span to depth ratio and the location of stations A1, A2, B1 and B2. In addition to this, it also requires the output file from the finite element analysis and text file with the discretization information. The spreadsheet automatically calculates the DPF's for each element and sums up the corresponding DPF. It then calculates the moment of inertia and the form factor for the section. It also calculates the stresses at the center and the edge of the section at the neutral axis at all stations. This is a good check to ensure that the selected stations lie in a region of uniform stress. The moment of inertia calculated by the spreadsheet should be checked with the hand-calculated value. If the amount of error is significant, then the stations should be located at different places. This process should be repeated till satisfactory values are obtained.

Vita

Hariharan Iyer was born to Shivkumar and Gowri Iyer on July 16, 1981 in Madras (now known as Chennai), the capital of the southern state of Tamil Nadu, India. His family moved to Bombay (now known as Mumbai), the capital of the western state of Maharashtra, in 1982. Growing up in Mumbai all his life, he completed his schooling in June 1999 and subsequently sought admission in Sardar Patel College of Engineering, Mumbai to study Civil Engineering. He completed the course requirements in June 2003 and was awarded the Bachelor of Engineering degree in Civil Engineering by the University of Mumbai. He proceeded to Virginia Polytechnic Institute and State University, Blacksburg, Virginia to begin his graduate studies in Fall 2003. He completed all the requirements for his course and was awarded the degree of Master of Science in Civil Engineering in May 2005.